

2

# NAVAL POSTGRADUATE SCHOOL

## Monterey, California

AD-A208 536



DTIC  
ELECTE  
JUN 06 1989  
S D cy D

## THESIS

DEVELOPMENT OF A SYSTEM MODEL AND  
LEAST MEAN SQUARE (LMS)  
FILTER FOR THE NAVAL POSTGRADUATE  
SCHOOL (NPS)  
INFRARED SEARCH AND TARGET DESIGNATION  
SYSTEM (IRSTD)

by

Michael Louis Gribaudo

March 1989

Thesis Advisor

Alfred W. Cooper

Approved for public release; distribution is unlimited.

89 6 05 121

Unclassified

security classification of this page

## REPORT DOCUMENTATION PAGE

1a Report Security Classification <b>Unclassified</b>		1b Restrictive Markings	
2a Security Classification Authority		3 Distribution Availability of Report <b>Approved for public release; distribution is unlimited.</b>	
2b Declassification Downgrading Schedule		5 Monitoring Organization Report Number(s)	
4 Performing Organization Report Number(s)		7a Name of Monitoring Organization <b>Naval Postgraduate School</b>	
6a Name of Performing Organization <b>Naval Postgraduate School</b>	6b Office Symbol (if applicable) <b>61</b>	7b Address (city, state, and ZIP code) <b>Monterey, CA 93943-5000</b>	
6c Address (city, state, and ZIP code) <b>Monterey, CA 93943-5000</b>		9 Procurement Instrument Identification Number	
8a Name of Funding Sponsoring Organization	8b Office Symbol (if applicable)	10 Source of Funding Numbers	
8c Address (city, state, and ZIP code)		Program Element No	Project No
		Task No	Work Unit Accession No
11 Title (include security classification) <b>DEVELOPMENT OF A SYSTEM MODEL AND LEAST MEAN SQUARE (LMS) FILTER FOR THE NAVAL POSTGRADUATE SCHOOL (NPS) INFRARED SEARCH AND TARGET DESIGNATION (IRSTD) SYSTEM</b>			
12 Personal Author(s) <b>Michael Louis Gribaudo</b>			
13a Type of Report <b>Master's Thesis</b>	13b Time Covered From To	14 Date of Report (year, month, day) <b>March 1989</b>	15 Page Count <b>108</b>
16 Supplementary Notation The views expressed in this thesis are those of the author and do not reflect the official policy or position of the Department of Defense or the U.S. Government.			
17 Cosati Codes		18 Subject Terms (continue on reverse if necessary and identify by block number)	
Field	Group	Subgroup	
		IRSTD, LMS filter, S/N ratio, Signal Processing	
19 Abstract (continue on reverse if necessary and identify by block number) <p>➤ A system model and a least mean square (LMS) filter for the Naval Postgraduate School (NPS) Infrared Search and Target Designation (IRSTD) system were developed.</p> <p>The system model was developed and run on the NPS IBM 3033 4381 mainframe computer network. The model simulated the effects of the optics and electronic processing equipment of the IRSTD system, and produced output data representative of the detector outputs of the system.</p> <p>The outputs of the IRSTD model were used to develop a digital filter based on the principle of least mean square optimization between an actual IRSTD detector output and a power series expansion representing a detector output containing both background clutter and a model target signal. It was determined that the raised cosine function served as the best model for IRSTD point and near-point targets. (0.1 mrad by 0.1 mrad to 1.5 mrad by 1.5 mrad), and a set of trial LMS filters were generated based on this model.</p> <p>After filtering both simulated and real data, consisting of simulated and real target signals embedded in simulated and real backgrounds, it was determined that an LMS filter generated from a raised cosine with a half-amplitude width of 0.9 mrad was optimal for point and near-point targets. The signal-to-noise ratios of all target and background combinations increased by a factor of approximately 30 for the simulated backgrounds, and approximately six for the real backgrounds, upon filtering the detector outputs with the optimal LMS filter. *</p> <p>It is believed that this filter should be incorporated into the NPS IRSTD system as an initial signal processing filter, and that the filtered outputs are appropriate for use as inputs to target detection and acquisition routines.</p>			
20 Distribution Availability of Abstract <input checked="" type="checkbox"/> unclassified unlimited <input type="checkbox"/> same as report <input type="checkbox"/> DTIC users		21 Abstract Security Classification <b>Unclassified</b>	
22a Name of Responsible Individual <b>Alfred W. Cooper</b>		22b Telephone (include Area code) <b>(408) 646-2452</b>	22c Office Symbol <b>61Cr</b>

DD FORM 1473-84 MAR

83 APR edition may be used until exhausted  
All other editions are obsolete

security classification of this page

Unclassified

Approved for public release; distribution is unlimited.

Development of a System Model and Least Mean Square (LMS)  
Filter for the Naval Postgraduate School (NPS)  
Infrared Search and Target Designation (IRSTD) System

by

Michael Louis Gribaudo  
Lieutenant, United States Navy  
B.S., University of Idaho, 1983

Submitted in partial fulfillment of the  
requirements for the degree of

MASTER OF SCIENCE IN PHYSICS


from the


NAVAL POSTGRADUATE SCHOOL  
March 1989

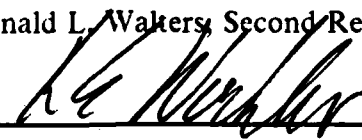
Author:


  
Michael Louis Gribaudo

Approved by:

  
Alfred W. Cooper, Thesis Advisor

  
Donald L. Walters, Second Reader

  
Karlheinz E. Woehler, Chairman,  
Department of Physics

  
Gordon E. Schacher,  
Dean of Science and Engineering

## ABSTRACT

A system model and a least mean square (LMS) filter for the Naval Postgraduate School (NPS) Infrared Search and Target Designation (IRSTD) system were developed.

The system model was developed and run on the NPS IBM 3033/4381 mainframe computer network. The model simulated the effects of the optics and electronic processing equipment of the IRSTD system, and produced output data representative of the detector outputs of the system.

The outputs of the IRSTD model were used to develop a digital filter based on the principle of least mean square optimization between an actual IRSTD detector output and a power series expansion representing a detector output containing both background clutter and a model target signal. It was determined that the raised cosine function served as the best model for IRSTD point and near-point targets, (0.1 mrad by 0.1 mrad to 1.5 mrad by 1.5 mrad), and a set of trial LMS filters were generated based on this model.

After filtering both simulated and real data, consisting of simulated and real target signals embedded in simulated and real backgrounds, it was determined that an LMS filter generated from a raised cosine with a half-amplitude width of 0.9 mrad was optimal for point and near-point targets. The signal-to-noise ratios of all target and background combinations increased by a factor of approximately 30 for the simulated backgrounds, and approximately six for the real backgrounds, upon filtering the detector outputs with the optimal LMS filter.

It is believed that this filter should be incorporated into the NPS IRSTD system as an initial signal processing filter, and that the filtered outputs are appropriate for use as inputs to target detection and acquisition routines.



Accession For	
NTIS CRA&I	<input checked="" type="checkbox"/>
DTIC TAB	<input type="checkbox"/>
Unannounced	<input type="checkbox"/>
Justification	
By	
Distribution /	
Availability Codes	
Dist	Avail and/or Special
A-1	

## TABLE OF CONTENTS

I. INTRODUCTION .....	1
A. GENERAL .....	1
B. PURPOSE AND ORGANIZATION OF THESIS .....	2
II. THE NPSIRSTD SYSTEM .....	4
A. SYSTEM DESCRIPTION AND SET-UP .....	4
B. SYSTEM SPECIFICATIONS .....	4
III. INFRARED BACKGROUNDS .....	6
A. THE NATURE OF INFRARED BACKGROUNDS .....	6
B. THE BACKGROUND MODEL .....	8
C. BACKGROUND MODEL OUTPUTS .....	11
IV. THEIRSTD MODEL .....	14
A. INTRODUCTION .....	14
B. FUNDAMENTAL COMPONENTS OF THE MODEL .....	14
1. The Object Plane .....	14
2. The Image Plane .....	15
3. The 1-D Detector Output .....	16
4. Noise and AC Coupling .....	17
C.IRSTD MODEL OUTPUTS .....	17
V. THE LMS FILTER .....	24
A. THEORY .....	24
B. FILTER DEVELOPMENT .....	29
C. TRIAL FILTERS .....	37
VI. FILTER OUTPUTS .....	41
A. SIGNAL-TO-NOISE RATIOS .....	41
B. ERROR ANALYSIS .....	42
C. FILTER OUTPUTS .....	44

1. Unfiltered Outputs .....	47
2. Filtered Outputs: Target Amplitude versus Noise Amplitude .....	49
3. Filtered Outputs: Multiple Targets .....	55
4. Filtered Outputs: Real Background and Target .....	55
 VII. CONCLUSIONS AND RECOMMENDATIONS .....	58
A. CONCLUSIONS .....	58
B. RECOMMENDATIONS .....	59
 APPENDIX A. FILTERED OUTPUTS: TARGET AMPLITUDE VERSUS NOISE AMPLITUDE .....	60
 APPENDIX B. FILTERED OUTPUTS: OPTIMAL LMS FILTERS .....	69
 APPENDIX C. BACKGROUND MODEL FORTRAN PROGRAM .....	79
 APPENDIX D. IRSTD MODEL FORTRAN PROGRAM .....	83
 APPENDIX E. FILTER OUTPUT FORTRAN PROGRAM .....	87
 LIST OF REFERENCES .....	94
 INITIAL DISTRIBUTION LIST .....	96

## LIST OF TABLES

Table 1.	LMS FILTER COEFFICIENTS .....	39
Table 2.	LMS FILTER COEFFICIENTS .....	40
Table 3.	VARIANCES OF ELEMENTS OF UNFILTERED AND FILTERED IRSTD OUTPUTS .....	44
Table 4.	S/N RATIOS FOR BKD I .....	45
Table 5.	S/N RATIOS FOR BKD II .....	45
Table 6.	S/N RATIOS FOR REAL BACKGROUND .....	45

## LIST OF FIGURES

Figure 1.	Amplitude Distribution of Background Radiance .....	7
Figure 2.	Amplitude Distribution; Radiance of Simulated Background I .....	12
Figure 3.	Amplitude Distribution; Radiance of Simulated Background II .....	13
Figure 4.	Detector Output; Simulated Background #1 (BKDI) .....	19
Figure 5.	Detector Output; Simulated Background #2 (BKDII) .....	19
Figure 6.	Detector Output; Real Background (BKDIII) .....	20
Figure 7.	Detector Output; Simulated Target #1 (TGTI) .....	20
Figure 8.	Detector Output; Simulated Target #2 (TGTH) .....	21
Figure 9.	Detector Output; Simulated Target #3 (TGTHH) .....	21
Figure 10.	Detector Output; Simulated Target #4 (TGTHV) .....	22
Figure 11.	Detector Output; Simulated Target #5 (TGTV) .....	22
Figure 12.	Detector Output; Real Target (Whip Antenna) (TGTVI) .....	23
Figure 13.	Magnitudes of the Spatial Frequency Distribution of BKDI .....	24
Figure 14.	Magnitudes of the Spatial Frequency Distribution of BKDIII .....	25
Figure 15.	Magnitudes of the Spatial Frequency Distribution of TGTH .....	25
Figure 16.	Magnitudes of the Spatial Frequency Distribution of TGTV .....	26
Figure 17.	Magnitudes of the Spatial Frequency Distribution of TGTVI .....	26
Figure 18.	TGTH and Raised Cosine with 0.31416 mrad Half-Amplitude Width ...	31
Figure 19.	TGTH and Raised Cosine with 0.41888 mrad Half-Amplitude Width ...	31
Figure 20.	TGTH and Raised Cosine with 0.52360 mrad Half-Amplitude Width ...	32
Figure 21.	TGTH and Raised Cosine with 0.62832 mrad Half-Amplitude Width ...	32
Figure 22.	TGTH and Raised Cosine with 0.73304 mrad Half-Amplitude Width ...	33
Figure 23.	TGTH and Raised Cosine with 0.83776 mrad Half-Amplitude Width ...	33
Figure 24.	TGTH and Raised Cosine with 0.94248 mrad Half-Amplitude Width ...	34
Figure 25.	TGTH and Raised Cosine with 1.0472 mrad Half-Amplitude Width ...	34
Figure 26.	Unfiltered Output; BKDI, TGTH .....	47
Figure 27.	Unfiltered Output; BKDII, TGTH .....	48
Figure 28.	Unfiltered Output; BKDIII, TGTVI .....	48
Figure 29.	Filtered Output; BKDI, TGTH, LMS6 .....	51
Figure 30.	Filtered Output; BKDI, TGTH, LMS9 .....	52
Figure 31.	Filtered Output; BKDI, TGTH, LMS12 .....	53



Figure 32. Filtered Output; BKDI, TGTI, LMS15 .....	54
Figure 33. Filtered Output; Multiple Targets .....	55
Figure 34. Filtered Output; Multiple Targets .....	56
Figure 35. Real Output .....	57
Figure 36. Filtered Output; BKDII, TGTI, LMS6 .....	61
Figure 37. Filtered Output; BKDII, TGTI, LMS9 .....	62
Figure 38. Filtered Output; BKDII, TGTI, LMS12 .....	63
Figure 39. Filtered Output; BKDII, TGTI, LMS15 .....	64
Figure 40. Filtered Output; BKDIII, TGTI, LMS1 .....	65
Figure 41. Filtered Output; BKDIII, TGTI, LMS3 .....	66
Figure 42. Filtered Output; BKDIII, TGTI, LMS5 .....	67
Figure 43. Filtered Output; BKDIII, TGTI, LMS7 .....	68
Figure 44. Filtered Output; BKDI, TGTI, LMS9 .....	69
Figure 45. Filtered Output; BKDI, TGTII, LMS9 .....	70
Figure 46. Filtered Output; BKDI, TGTIII, LMS9 .....	70
Figure 47. Filtered Output; BKDI, TGTIV, LMS9 .....	71
Figure 48. Filtered Output; BKDI, TGTV, LMS9 .....	71
Figure 49. Filtered Output; BKDI, TGTVI, LMS9 .....	72
Figure 50. Filtered Output; BKDII, TGTI, LMS9 .....	72
Figure 51. Filtered Output; BKDII, TGTII, LMS9 .....	73
Figure 52. Filtered Output; BKDII, TGTIII, LMS9 .....	73
Figure 53. Filtered Output; BKDII, TGTIV, LMS9 .....	74
Figure 54. Filtered Output; BKDII, TGTV, LMS9 .....	74
Figure 55. Filtered Output; BKDII, TGTVI, LMS9 .....	75
Figure 56. Filtered Output; BKDIII, TGTI, LMS3 .....	75
Figure 57. Filtered Output; BKDIII, TGTII, LMS3 .....	76
Figure 58. Filtered Output; BKDIII, TGTIII, LMS3 .....	76
Figure 59. Filtered Output; BKDIII, TGTIV, LMS3 .....	77
Figure 60. Filtered Output; BKDIII, TGTV, LMS3 .....	77
Figure 61. Filtered Output; BKDIII, TGTVI, LMS3 .....	78

## **ACKNOWLEDGMENTS**

This thesis is prepared in conjunction with research sponsored in part by the Naval Sea Systems Command, PMS-421, and funded by the Naval Postgraduate School.

## **I. INTRODUCTION**

### **A. GENERAL**

Several years after completion of at-sea trials in USS Kinkaid, the Advanced Development Model (ADM) of the SPAR Aerospace AN SAR-8 Infrared Search and Target Designation (IRSTD) system was transferred to the Naval Academic Center for Infrared Technology (NACIT) at the Naval Postgraduate School (NPS) in Monterey, California. NACIT received this system with the intention of using it in support of research in infrared physics, infrared technology, and infrared signal processing. Specific objectives of this research include:

- Collection and study of unfiltered infrared background scenes.
- Development of signal processing techniques for the rejection of background clutter.
- Development of target detection, acquisition, tracking, and classification techniques.

Since receiving the IRSTD system, NACIT personnel have accomplished a great deal of work involving the system installation, testing, and calibration. While installing the system in Spanagal Hall at NPS, a number of modifications were required to be made. Some of the more important modifications [Ref. 1] include:

- Removal of the Stable Platform and Stable Platform Control Console.
- Bypass of the Background Normalizer.
- Replacement of the Data Processing Unit with a MASSCOMP computer system of higher capacity.
- Replacement of the cryogenic engine and insulating vacuum assembly, leading to the removal of the inner germanium window of the system's optical subassembly (OSA).

Of these modifications, the cryogenic engine replacement had the most impact on the operation of the system. Removal of the germanium window changed the optical path of the system, thereby increasing the system's optical spot size. To correct for this effect, it was found [Refs. 1, 2] that a focal shift of the detector array by approximately 0.133 inches towards the reflecting mirror restored the modified system to a level of performance comparable to that of the original system.

Upon restoring the system to an acceptable level of performance, the relative responsivities of the individual detector elements were calibrated with their associated electronics. It was found [Ref. 2] that seven lead array detectors and eight lag array detectors were non-functional, and that three additional lag array detectors were performing at levels below standards. It was also found that the relative response amplitudes of the lag array detectors were a factor of 1.85 higher than the lead array detectors for the same calibration source. This difference was attributed to the use of different bandwidth filters for the two detector arrays.

As of January 1989, The system is in place in Spanagel Hall at NPS Monterey, and is ready to take and store data in the MASSCOMP computer. With these capabilities available, the NACIT research group can begin collecting infrared background data, and can also begin developing clutter rejection filters.

## **B. PURPOSE AND ORGANIZATION OF THESIS**

The purpose of this thesis is to develop a digital filter capable of extracting point and near-point targets from typical infrared background clutter scenes. The filter selected for this task is constructed using the principle of least-mean-square optimization, and is therefore known as an LMS filter [Ref. 3].

The text of this thesis describes the derivation of the LMS filter, and presents the results of its use on both simulated and real data. The thesis is organized as follows:

- Chapter II presents a brief description of the NPS IRSTD system, with particular emphasis on the system's specifications.
- Chapter III discusses the nature of infrared backgrounds, as compared to targets of interest to IRSTD signal processing, and also presents an infrared background simulation model.
- Chapter IV describes the development of an IRSTD simulation model, constructed to generate simulated IRSTD output signals for initial analysis of the LMS filter.
- Chapter V describes the development of an LMS filter for extracting targets of interest from infrared background scenes.
- Chapter VI presents the results of filtering both simulated and real infrared IRSTD data with the LMS filter.
- Chapter VII discusses the results of chapter VI and presents recommendations for further studies in this area.
- Appendix A presents plots of filtered outputs illustrating the increase in target and noise amplitude with increasing filter width.
- Appendix B presents plots of filtered outputs of all target and background combinations studied in this thesis, filtered with their proposed optimal LMS filters.

- Appendix C lists the background simulation model FORTRAN code.
- Appendix D lists the IRSTD simulation model FORTRAN code.
- Appendix E lists the LMS Filter FORTRAN code.

## **II. THE NPS IRSTD SYSTEM**

### **A. SYSTEM DESCRIPTION AND SET-UP**

The NPS IRSTD system is composed of four major subsystems. Since only a brief description of these subsystems will be presented in this thesis, the reader is directed to the system technical manual [Ref. 4], for a detailed description of the system.

A brief description of the function and set-up of the major subsystems and various peripheral components of the NPS IRSTD system follows:

- The Scanner Assembly, located on the roof of Spanagel Hall at NPS Monterey, houses the Optical Subassembly (OSA). The OSA consists of the system optics, the lead and lag detector arrays, and the cryogenics. As a unit, the Scanner Assembly physically rotates the OSA in complete 360 degree scans. The OSA, in turn, collects and responds to infrared radiation incident on the OSA aperture. Electronic signals from the detector arrays are then transmitted to the Data Conditioner Unit via the Buffer Power Unit.
- The Scanner Assembly Control Console (SACC), located on the seventh floor of Spanagel Hall, supplies power to, and controls, the Scanner Assembly and its associated electronic components. The SAAC controls parameters such as the Scanner Assembly scan rate.
- The Data Conditioner Unit (DCU), also located on the seventh floor of Spanagel Hall, receives signals from the OSA via the Buffer Power Unit. It is in the DCU that analog-to-digital conversion, multiplexing, and pre-processing of the detector outputs occurs.
- The MASSCOMP computer, located on the second floor of Spanagel Hall, receives digital detector output signals from the DCU for processing, display, and storage.

### **B. SYSTEM SPECIFICATIONS**

In order to proceed effectively with the development of an IRSTD model and the LMS filter, it is essential to know some of the IRSTD system's technical specifications. A short listing of the general specifications is presented below [Refs. 1, 2, and 4]:

- Number and type of detector elements - 90 indium antimonide (InSb) detector elements per array (2 arrays).
- Size of detector elements - 2.0 by 0.3 milliradians (0.3 milliradians along the scan dimension).
- OSA scan rate - variable (designed to operate at one-half revolution per second).
- DCU sampling rate - 10,000 8-bit samples per second; the 8-bit analog-to-digital converter will soon be replaced by a 12-bit converter. (This sampling rate corresponds to 0.10472 mrad per sample at one-half revolution per second.)
- Detector dwell time - approximately 3 samples per detector dwell.

- Optical spot size - approximately 0.7 mrad in diameter, based on the diameter of the blur spot of a point target at the detector array.
- System bandwidth filters - 3 to 5 micrometers.
- Optics - F 1 Schmidt catadioptric telescope.
- OSA aperture - 10 inch diameter with germanium aspheric corrector.
- Focusing mirror - 16.625 inch diameter aluminum spherical mirror.
- Coolant - liquid nitrogen, resulting in a detector operating temperature of 83K.

### III. INFRARED BACKGROUNDS

#### A. THE NATURE OF INFRARED BACKGROUNDS

Typical infrared backgrounds consist of scattered, reflected, or emitted infrared radiation from objects other than those sought by the system. These non-target objects include, but are not restricted to:

- the sun
- clouds
- precipitation
- sea spray
- land
- birds

The targets of interest, for the purpose of this thesis, are restricted to aircraft and missiles. Since the spatial extent of these targets is typically very small, they can be modeled as point, or near-point, targets.<sup>1</sup> It is therefore only necessary to consider how the spatial extent of these targets differs from the spatial extent of the background features.

The statistical properties of infrared backgrounds are available from previous studies [Ref. 6]. These studies show that a statistical model of background radiance can be regarded as a random set of two-dimensional pulses whose amplitudes can be described by either Gaussian or Poisson distributions, depending on the wavelength and type of infrared radiation, and whose pulse widths can be described by Poisson distributions.

In the 3-5 $\mu$ m region, the radiance received by the system is due to a combination of scattered sunlight and thermal radiation emitted from the background. Since the amplitude of the radiance of scattered sunlight obeys Poisson statistics, and the amplitude of the radiance of thermal radiation obeys Gaussian statistics, the amplitude of the

---

<sup>1</sup> For example, a typical jet aircraft engine has an exhaust nozzle with an area approximately 3600 cm<sup>2</sup> [Ref. 5], which corresponds to a diameter of approximately 68 cm. At a range of 10 kilometers (km) this source will subtend an angle of 0.068 milliradians (mrad), at 5 km it subtends 0.136 mrad, at 1 km it subtends 0.68 mrad, and at 500 meters it subtends 1.36 mrad. Therefore, typical air targets can be modeled as targets which subtend angles ranging from 0.1 to 1.5 mrad, where due to the sampling rate of the DCU a 0.1 mrad target is considered to be a point target.



radiance of the background in the  $3\text{-}5\mu\text{m}$  region should be describable by some combination of Gaussian and Poisson distributions [Ref. 6].

Figure 1 is a plot of the amplitude distribution of the radiance of a sky background in the  $3\text{-}5\mu\text{m}$  region, as determined by experimental observation [Ref. 6]. It is interesting to note that the influence of the scattered sunlight only slightly distorts the amplitude distribution from a true Gaussian form. Additionally, it should be noted that the mean value of the background radiance is greater than zero. However, the mean radiance can be changed to zero, or any other value, by adding or subtracting a constant from the individual radiances measured over the entire background. This is often desirable, when plotting background radiance over a region of space, because it can be used to change the offset of the plot while leaving all other statistical properties unaltered.

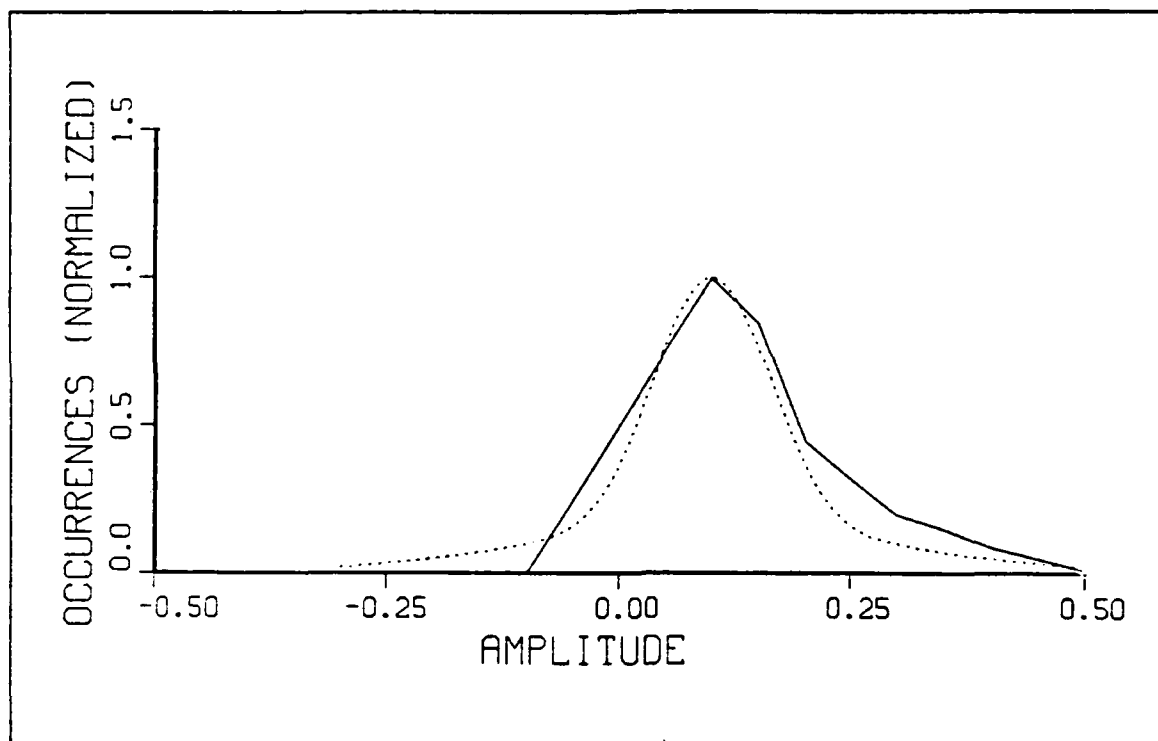


**Figure 1. Amplitude Distribution of Background Radiance:** Solid line, background radiance in the  $3\text{-}5\mu\text{m}$  region. Dotted line, Gaussian distribution overlaid for comparison. Radiance units normalized to a peak amplitude of  $\pm 0.5$ . [Ref. 6]

In the following section, the development of a background radiance distribution in the spatial domain will be presented. In order to simplify calculations, the amplitude distribution of the background radiance will be modeled as a Gaussian function, having a mean value of zero and a standard deviation ranging from 0.1 to 0.15. The backgrounds generated from this model will then be statistically analyzed to ensure that their radiance distributions are representative of the distribution shown in Figure 1 on page 7; then they will be used to simulate IR backgrounds for the purpose of evaluating the effectiveness of the proposed LMS filter.

## B. THE BACKGROUND MODEL

A background model for the 3-5 $\mu$ m region is developed using the statistical properties outlined in the previous section. The amplitude distribution of the background radiance can be described by the probability density function

$$P(B_{ij}) = \frac{1}{\sqrt{2\pi\sigma^2}} e^{-\frac{(B_{ij} - \bar{B})^2}{2\sigma^2}} \quad (3-1)$$

where  $B_{ij}$  is an element of the background radiance matrix  $\mathbf{B}$  which describes the radiance at given points in the background distribution,  $\bar{B}$  is the average radiance over the entire background, and  $\sigma^2$  is the variance of the radiance over the entire background.

Adjacent points in the background distribution are spatially correlated, with a correlation function of

$$L(r) = \sigma^2 e^{-\alpha r} \quad (3-2)$$

where  $\alpha^{-1}$  is the correlation length, and  $r$  is the distance between any two adjacent points.

Following the model developed by Ben-Yosef *et al.* [Ref. 7], the background radiance distribution can be generated directly in the space domain. This is accomplished by determining the conditional probability density function, which describes the probability of finding  $B_{ij}$  if the radiances of adjacent points are known.

As a first approximation,  $\bar{B}$  can be taken as zero, and the conditional probability density function for determining the radiance  $B_{ij}$ , from the radiance  $B_{ik}$  or  $B_{lj}$ , where  $k = j - 1$  and  $l = i - 1$ , can be written as

$$P(B_{ij} | B_{ik}) = \frac{1}{\sqrt{2\pi\sigma\beta_1}} e^{-\frac{(B_{ij} - ZB_{ik})^2}{2\sigma^2\beta_1^2}} \quad (3-3)$$

where

$$Z = e^{-\alpha} \quad (3-4)$$

and

$$\beta_1 = \sqrt{1 - Z^2} \quad (3-5)$$

Likewise, the conditional probability density function for determining the radiance  $B_{ij}$  from the radiances  $B_{ik}$  and  $B_{lj}$  is

$$P(B_{ij} | B_{ik}, B_{lj}) = \frac{1}{\sqrt{2\pi\sigma\beta_2}} e^{-\left(B_{ij} - \frac{ZB_{ik}}{(1+Z\sqrt{2})} - \frac{ZB_{lj}}{(1+Z\sqrt{2})}\right)^2 \frac{2\sigma^2\beta_2^2}{(1+Z\sqrt{2})^2}} \quad (3-6)$$

where

$$\beta_2 = \sqrt{\frac{(1 + Z\sqrt{2} - 2Z^2)}{(1 + Z\sqrt{2})}} \quad (3-7)$$

From Equation (3-3), it follows that given  $B_{ik}$ ,  $B_{ij}$  is normally distributed with a mean of

$$\langle B_{ij} \rangle = ZB_{ik} \quad (3-8)$$

and a standard deviation of  $\sigma\beta_1$ . Additionally, Equation (3-6) shows that given  $B_{ik}$  and  $B_{lj}$ ,  $B_{ij}$  is normally distributed with a mean of

$$\langle B_{ij} \rangle = \frac{Z}{1 + Z\sqrt{2}} (B_{ik} + B_{lj}) \quad (3-9)$$

and a standard deviation of  $\sigma\beta_2$ .

The background scene can therefore be generated using any normally distributed random number generation scheme. For this thesis, the International Mathematical and Statistical Libraries (IMSL) subroutine GGNML [Ref. 8] was used to generate a set of normally distributed random numbers, with a mean of zero and a standard deviation of one. The random numbers were then placed in all but the first element of a 4000 by 20 element matrix. The elements of this matrix can be represented as  $R_{ij}$ , with the index  $i$  ranging from one to 4000 and the index  $j$  ranging from one to 20.

The elements of the background scene ( $B_{ij}$ ) are then generated in a matrix of similar dimensions by first setting the value of the origin equal to zero; the average radiance  $\bar{B}$ . The remaining elements of the first row and first column are then determined using the results of Equation (3-3), and can be represented as

$$B_{i1} = \sigma\beta_1 R_{i1} + \langle B_{i1} \rangle \quad (2 \leq i \leq 4000) \quad (3-10)$$

for the first row, and

$$B_{1j} = \sigma\beta_1 R_{1j} + \langle B_{1j} \rangle \quad (2 \leq j \leq 20) \quad (3-11)$$

for the first column. From Equation (3-8), the mean values  $\langle B_{i1} \rangle$  and  $\langle B_{1j} \rangle$  represent

$$\langle B_{i1} \rangle = ZB_{k1} \quad (3-12)$$

and

$$\langle B_{1j} \rangle = ZB_{1l} \quad (3-13)$$

In a similar manner, the remaining elements of the background radiance distribution can be determined from the results of Equation (3-6) and are represented as

$$B_{ij} = \sigma\beta_2 R_{ij} + \langle B_{ij} \rangle \quad (3-14)$$

where  $2 \leq i \leq 4000$  and  $2 \leq j \leq 20$ . From Equation (3-9), the mean value  $\langle B_{ij} \rangle$  is represented by

$$\langle B_{ij} \rangle = \frac{Z}{(1 + Z\sqrt{2})} (B_{kj} + B_{il}) \quad (3-15)$$

It follows from this background generation scheme, that the resultant background radiance distribution for a background with  $\bar{B} = 0$  is dependent only on the two variables  $\sigma^2$  and  $\alpha^{-1}$ , and the random number generator seed which produces a different set of  $R_{ij}$  for each seed used. Additionally, a background distribution with  $\bar{B} \neq 0$  can be generated by adding the desired value of  $\bar{B}$  to each element of  $B_{ij}$ .

### C. BACKGROUND MODEL OUTPUTS

The background model was developed in FORTRAN code, to be run on the NPS IBM 3033.4381 mainframe computer network. The FORTRAN code for this model is attached as Appendix C.

For typical IR background scenes in the 3-5 $\mu$ m region, as determined by Itakura *et al.* [Ref. 6],  $\alpha^{-1} \approx 170.0$  mrad and  $\sigma$  varies as a function of cloud content. Figure 2 on page 12 is a plot of the amplitude distribution of the radiance of a simulated two-dimensional background generated with these statistics, and covering an area of approximately 2.1 mrad by 418.9 mrad. Likewise, Figure 3 on page 13 is a plot of the amplitude distribution of the radiance of a different simulated two-dimensional background covering the same area, but generated with a different random number generator seed and a different amplitude variance.

Both of these backgrounds have been chosen to be acceptable representations of infrared backgrounds in the 3-5 $\mu$ m region, because their amplitude distributions are similar to the experimentally determined amplitude distributions shown in Figure 1 on page 7. The similarity was determined on the basis that the amplitude distributions of the radiance of the simulated backgrounds generally conformed to the shape of the experimentally determined amplitude distribution of the radiance of an IR background in the 3-5 $\mu$ m region. This can be seen by comparing the solid and dotted plots in Figure 2 on page 12 and Figure 3 on page 13. These two backgrounds will be used in the following chapters to test the effectiveness of the LMS filters.

It is important to note that not all random number generator seeds produce acceptable backgrounds. In fact, approximately 50 different seeds were tested before the two backgrounds discussed above were generated. Since real backgrounds in the 3-5 $\mu$ m, as measured by Itakura *et al.* [Ref. 6], typically display the statistics illustrated in Figure 1 on page 7, simulated backgrounds not displaying a basic similarity to these statistics were considered unacceptable for the purpose of this thesis.

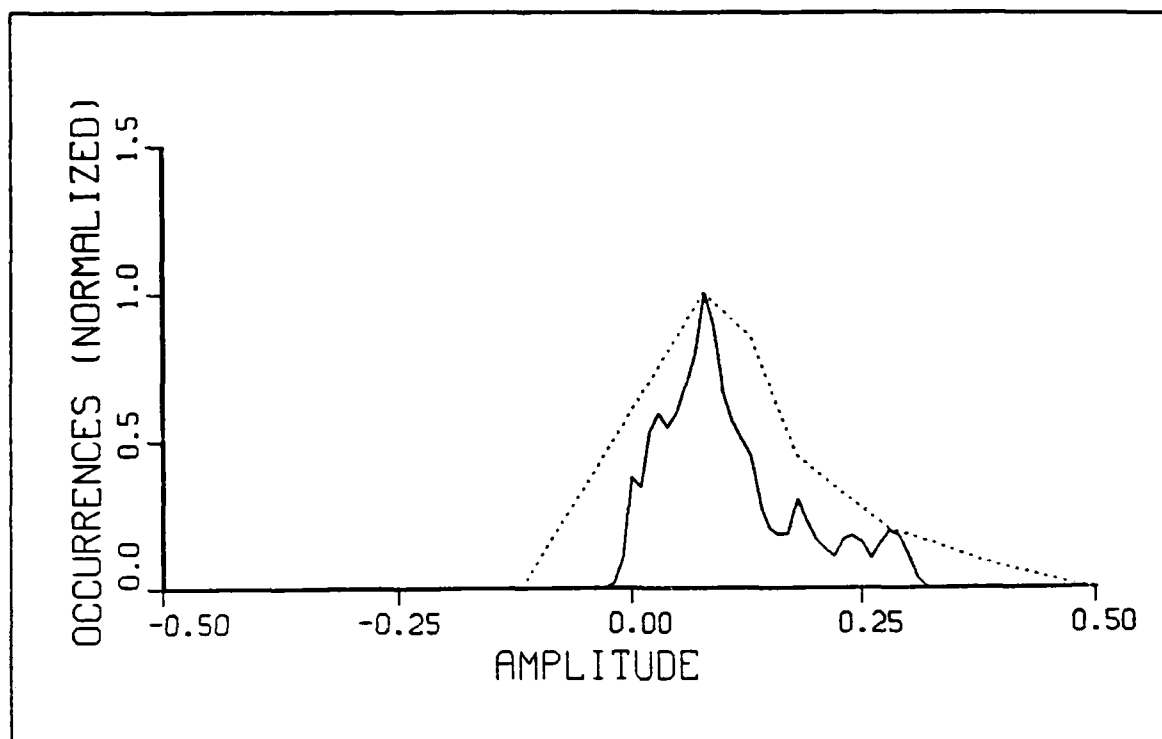


**Figure 2. Amplitude Distribution; Radiance of Simulated Background I:** Solid line, amplitude distribution of a simulated background generated with  $\alpha^{-1} = 170.0$  mrad,  $\sigma = 0.1$ , and random number seed = 356782367. Dotted line, experimentally determined amplitude distribution of an IR background in the  $3\text{-}5\mu\text{m}$  region [Ref. 6].

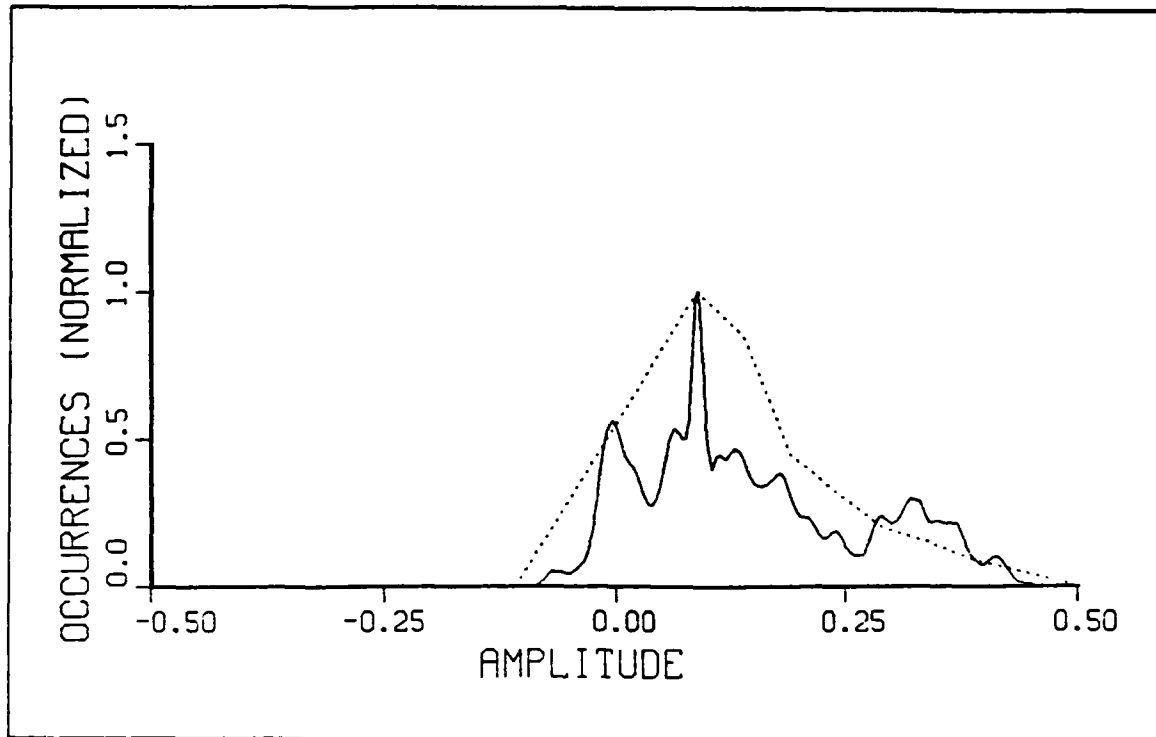


**Figure 3. Amplitude Distribution; Radiance of Simulated Background II:** Solid line, amplitude distribution of a simulated background generated with  $\alpha^{-1} = 170.0$  mrad,  $\sigma = 0.15$ , and random number seed = 414813567. Dotted line, experimentally determined amplitude distribution of an IR background in the  $3\text{-}5\mu\text{m}$  region [Ref. 6].

## **IV. THE IRSTD MODEL**

### **A. INTRODUCTION**

A number of analytic and computer simulated performance models have been developed for scanning electro-optical systems. These models have been used for predicting sensor performance, analyzing system transfer functions, and developing spatial filters.

The purpose of this chapter is to develop a computer simulated model which can be used to study the NPS Monterey IRSTD system. The model closely follows the analytic model presented by Scribner and Peters [Ref. 9].

In order to apply linear-system theory to this model, several constraints and assumptions are necessary. Specifically,

- the system must be linear through all optical processes,
- the system performance must be representable by an incoherent response function,
- the optical noise sources must be photon-additive,
- the imaging process must be spatially invariant,
- the system bandwidth must be narrow enough to allow for reducing spectrally dependent parameters to constants, and
- the background clutter must be stationary and Gaussian.

The simulation models one detector element, scanning horizontally across a rectangular object plane. Although this model represents only a small portion of the NPS IRSTD system, it can still be used to test and develop an LMS filter for enhancing the system signal-to-noise ratio.

### **B. FUNDAMENTAL COMPONENTS OF THE MODEL**

#### **1. The Object Plane**

The object plane is considered to be a two-dimensional radiance distribution, located an arbitrary distance from the IRSTD aperture. The radiance distribution contains information from both targets and background clutter, and can be represented by the function

$$O(x', y') = T(x', y') + B(x', y') \quad (4-1)$$



where  $\mathbf{T}(x', y')$  and  $\mathbf{B}(x', y')$  describe the target and background radiance distributions respectively. To simplify calculations with the object plane distribution, it is convenient to define an ideal object plane distribution function as

$$\mathbf{O}_i(x, y) = \mathbf{T}_i(x, y) + \mathbf{B}_i(x, y) \quad (4-2)$$

which describes the object plane distribution in the scale of the image plane.

The object plane power spectral density (PSD) is simply the 2-D Fourier transform of the ideal object plane distribution, and can be written as

$$\tilde{\mathbf{O}}_i(k_x, k_y) = F_{2D}\{\mathbf{O}_i(x, y)\} \quad (4-3)$$

## 2. The Image Plane

The object plane radiance distribution is mapped onto the image plane by the IRSTD system. This process can be represented as a 2-D convolution of the ideal object plane radiance distribution function  $\mathbf{O}_i(x, y)$  with the system point spread function  $\mathbf{P}_s(x, y)$ . The image plane radiance distribution function can therefore be written as

$$\mathbf{I}(x, y) = \mathbf{O}_i(x, y) ** \mathbf{P}_s(x, y) \quad (4-4)$$

where  $**$  represents the 2-D convolution. Additionally, by using the Convolution Theorem, the image plane PSD can be written as

$$\tilde{\mathbf{I}}(k_x, k_y) = F_{2D}\{\mathbf{I}(x, y)\} = \tilde{\mathbf{O}}_i(k_x, k_y) \cdot \tilde{\mathbf{P}}_s(k_x, k_y) \quad (4-5)$$

From analysis of the results of previous studies of the optical performance characteristics of the NPS IRSTD system [Ref. 10], it can be assumed that the system point spread function can be represented by the 2-D Gaussian function

$$\mathbf{P}_s(x, y) = \frac{1}{2\pi\sigma_0^2} e^{-(x^2 + y^2)/2\sigma_0^2} \quad (4-6)$$

where  $\sigma_0$  is the radius of the spot size of a point target in the focal plane. The system response function is the Fourier transform of the point spread function, and can be shown to be

$$\tilde{\mathbf{P}}_s(k_x, k_y) = e^{-2\sigma_0^2\pi^2(k_x^2 + k_y^2)} \quad (4-7)$$

### 3. The 1-D Detector Output

The detector can initially be considered to have a uniform response over a rectangular surface, with the dimensions  $a$  and  $b$  in the  $x$  and  $y$  directions respectively. The detector scans the image plane over the continuum of values  $\hat{x}$  on a scan line centered at  $\hat{y} = b/2$ . The detector output can then be expressed as

$$I_d(\hat{x}, \hat{y}) = \int_{(\hat{y} - \frac{b}{2})}^{(\hat{y} + \frac{b}{2})} \int_{(\hat{x} - \frac{a}{2})}^{(\hat{x} + \frac{a}{2})} I(x, y) dx dy \quad (4-8)$$

Taking the limits of integration over  $x$  into the integrand, we can write

$$I_d(\hat{x}, \hat{y}) = \int_{(\hat{y} - \frac{b}{2})}^{(\hat{y} + \frac{b}{2})} \left[ \int_{-\infty}^{\infty} I(x, y) \cdot D(\hat{x} - x, y) dx \right] dy \quad (4-9)$$

where  $D(\hat{x} - x, y)$  is the detector response function.

Since the inner integral in equation (4-9) is a 1-D convolution in the  $x$ -direction, we can write, using  $*$  to represent the 1-D convolution,

$$I_d(\hat{x}, \hat{y}) = \int_{(\hat{y} - \frac{b}{2})}^{(\hat{y} + \frac{b}{2})} I(\hat{x}, y) * D(\hat{x}, y) dy \quad (4-10)$$

where the continuum of values  $\hat{x}$  is identical to the continuum of values  $x$ , and the detector response function can be described by

$$D(x, y) = \left[ \text{Rect}\left(\frac{x}{a}\right) \cdot \text{Rect}\left(\frac{y}{b}\right) \right] \quad (4-11)$$

If the detector scans the image plane at a uniform speed  $\beta$ , the output can be expressed in terms of time, where  $x = \beta t$ . Additionally, if the detector responsivity  $\mathcal{R}$  is known, the detector output voltage can be written as

$$V(t) = \mathcal{R} \cdot I_d(\beta t, \hat{y}) \quad (4-12)$$

The detector output voltage can also be expressed in the electrical frequency domain as

$$\hat{V}(f) = F_{1D}\{\mathcal{R} \cdot I_d(\beta t, \hat{y})\} \quad (4-13)$$

#### 4. Noise and AC Coupling

One type of noise of particular interest in the IRSTD system is white noise. Considering this noise to be additive, the detector output can be expressed as

$$V'(t) = V(t) + N_w(t) \quad (4-14)$$

where  $N_w(t)$  describes the white noise, which can be represented by a uniformly distributed random variable.

Since the outputs are AC coupled, it is of interest to describe this coupling in the model. The AC coupled outputs can be expressed as [Ref. 10]

$$V_c(t) = V'(t) - \frac{Q_0}{C} e^{-t/RC} - \frac{1}{RC} V'(t) * e^{-t/RC} \quad (4-15)$$

where  $Q_0$  is the capacitor charge at  $t=0$ ,  $R$  is the resistance,  $C$  is the capacitance of the AC coupling circuit, and  $*$  again represents a 1-D convolution. As a first approximation,  $Q_0$  can be considered to be equal to zero; then

$$V_c(t) = V'(t) - \frac{1}{RC} V'(t) * e^{-t/RC} \quad (4-16)$$

approximately describes the output of the detector.

At this point, equation (4-16) describes the output of a generic scanning IR sensor system. By including parameters representative of the NPS IRSTD system, this model can be used to simulate IRSTD detector output data. These specific parameters will be introduced in the following section.

#### C. IRSTD MODEL OUTPUTS

This model was also developed in FORTRAN code, and run on the NPS IBM 3033 4381 computer. The FORTRAN code is attached as Appendix D. The program was developed to produce IRSTD output signals ranging in amplitude from -0.35 to 0.35. This was done because digital data from a 12-bit analog-to-digital (A/D) converter can be easily used to represent output signals ranging in amplitude from -0.4095 to 0.4095. Specific parameters used in the simulation include: detector width  $a = 0.3$  mrad,

detector height  $b = 2.0$  mrad, spot size radius  $\sigma_0 = 0.7$  mrad, and AC coupling constant  $RC = 1.3$ . These specific parameters were used to produce output data representative of real IRSTD output data. It must be emphasized that the model was not designed to, nor was it intended to, produce an "exact" replica of real IRSTD data.

Inserting backgrounds I and II into this IRSTD model, results in the detector outputs illustrated in Figure 4 on page 19 and Figure 5 on page 19. These two detector outputs will be used throughout this thesis, and will be referred to as BKDI and BKDII respectively.

For purposes of comparison, Figure 6 on page 20 is a real IRSTD background obtained from the NPS IRSTD system during system calibration, [Ref. 2]. This background contains information from a distant, uniform, partly-cloudy sky, with ambient atmospheric temperature of 52.5 degrees F and visibility of approximately 20 miles. Additionally, the data was digitized at  $100 \mu s$  per sample on a Nicolet digital oscilloscope, with the system scanning at  $\pi$  radians per second. This background will hereupon be referred to as BKDIII.

In addition to generating simulated IRSTD outputs of background distributions, this model was also used to generate simulated IRSTD outputs of various target signals. These simulated target signals were generated by inserting target signals of uniform amplitude and finite dimensions into an ideal object plane distribution, Equation (4-2), having a background distribution identically equal to zero.

To generate IRSTD outputs simulating point and near point targets, target signals of 0.10472 mrad by 0.10472 mrad, 0.31416 mrad by 0.31416 mrad, 0.52360 mrad by 0.52360 mrad, 1.0472 mrad by 1.0472 mrad, and 1.5708 mrad by 1.5708 mrad were used. The simulated IRSTD detector outputs of these five targets are illustrated in Figure 7 on page 20, Figure 8 on page 21, Figure 9 on page 21, Figure 10 on page 22, and Figure 11 on page 22.

To show how well the model represents the IRSTD system, these model detector outputs of simulated targets can be compared to the detector output of a whip antenna taken by the NPS IRSTD system, Figure 12 on page 23. These five simulated targets and one real target will be used throughout this thesis, and will be referred to as TGTI, TGTII, TGTIII, TGTIV, TGTV, and TGTVI respectively.

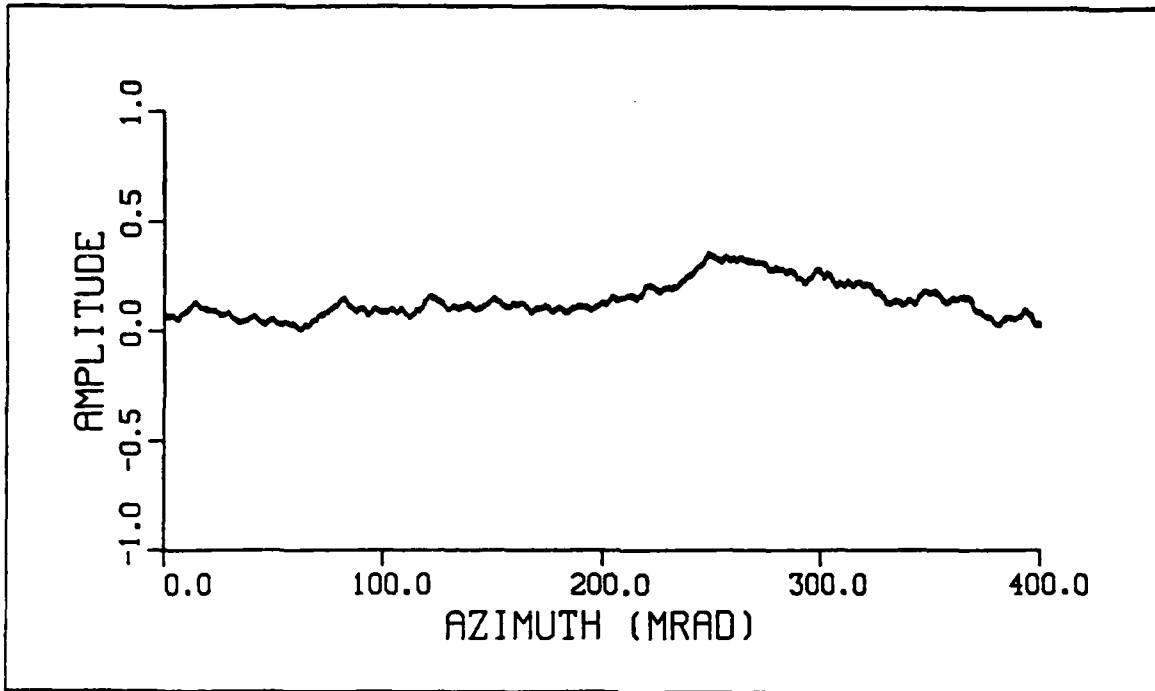


Figure 4. Detector Output; Simulated Background #1 (BKDI)

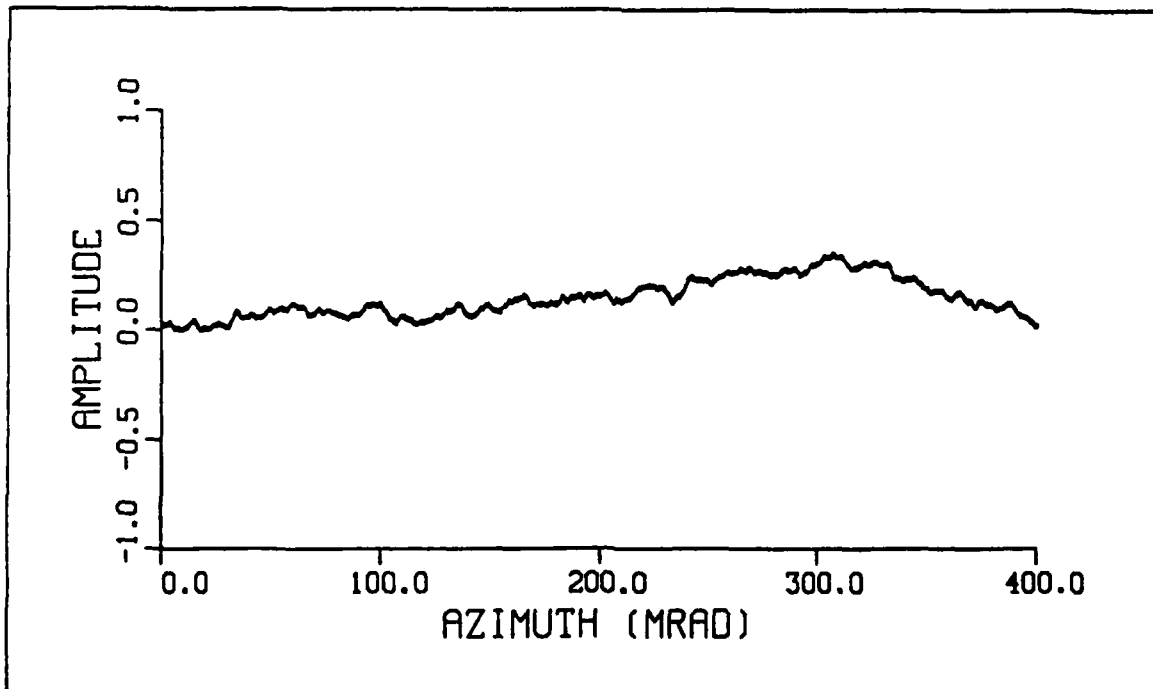


Figure 5. Detector Output; Simulated Background #2 (BKDII)

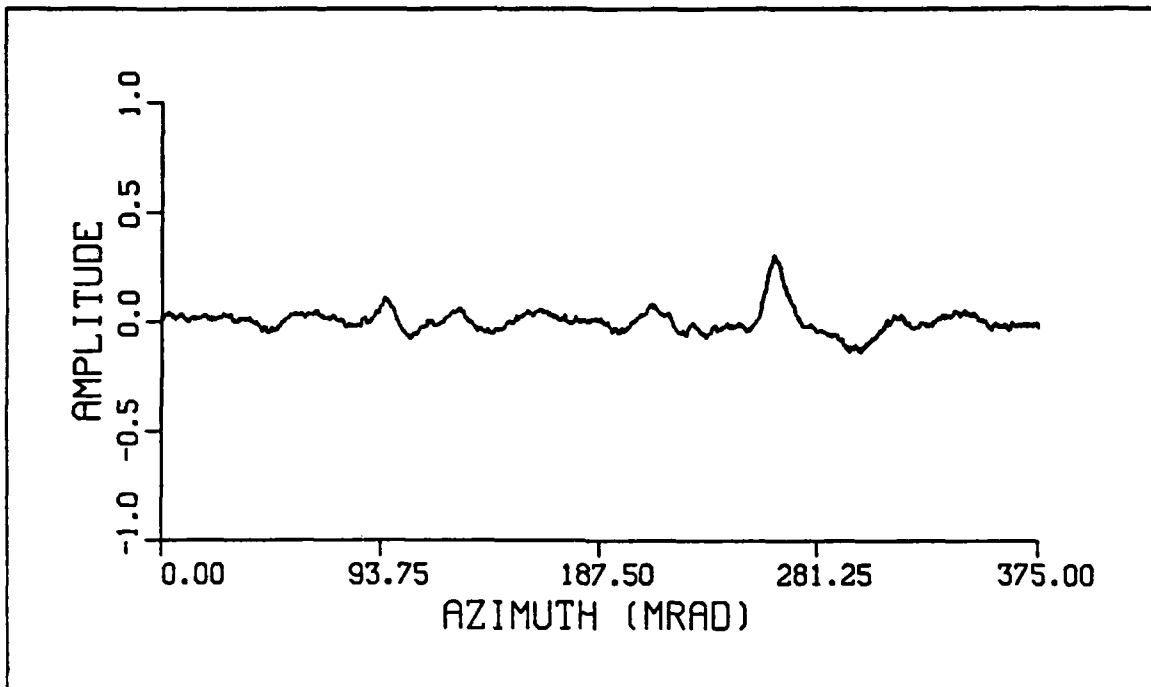


Figure 6. Detector Output; Real Background (BKDIII)

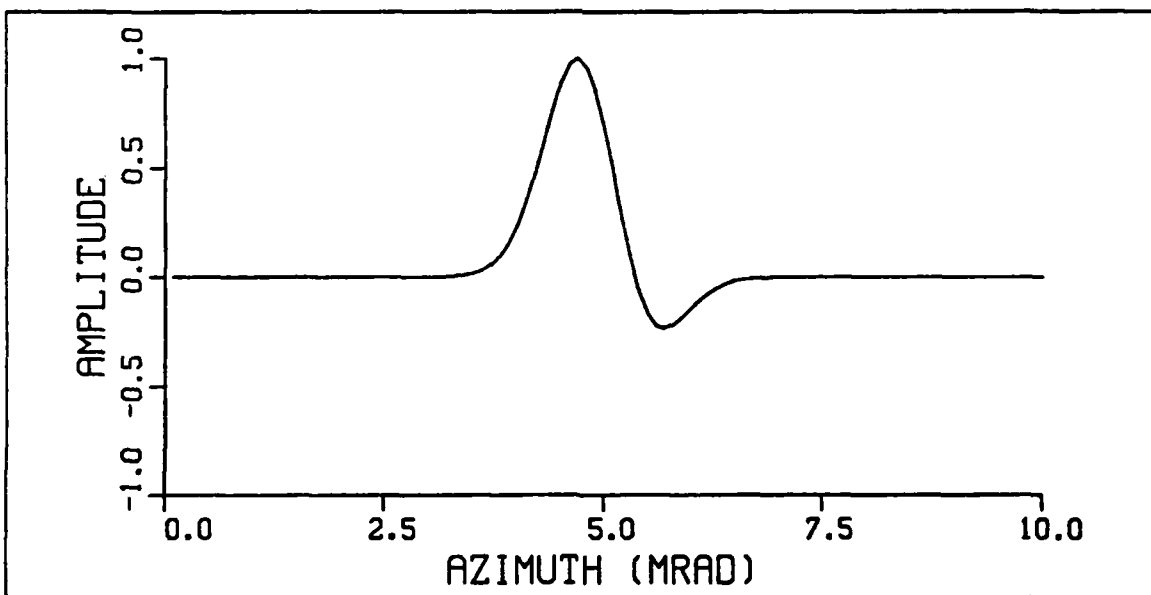
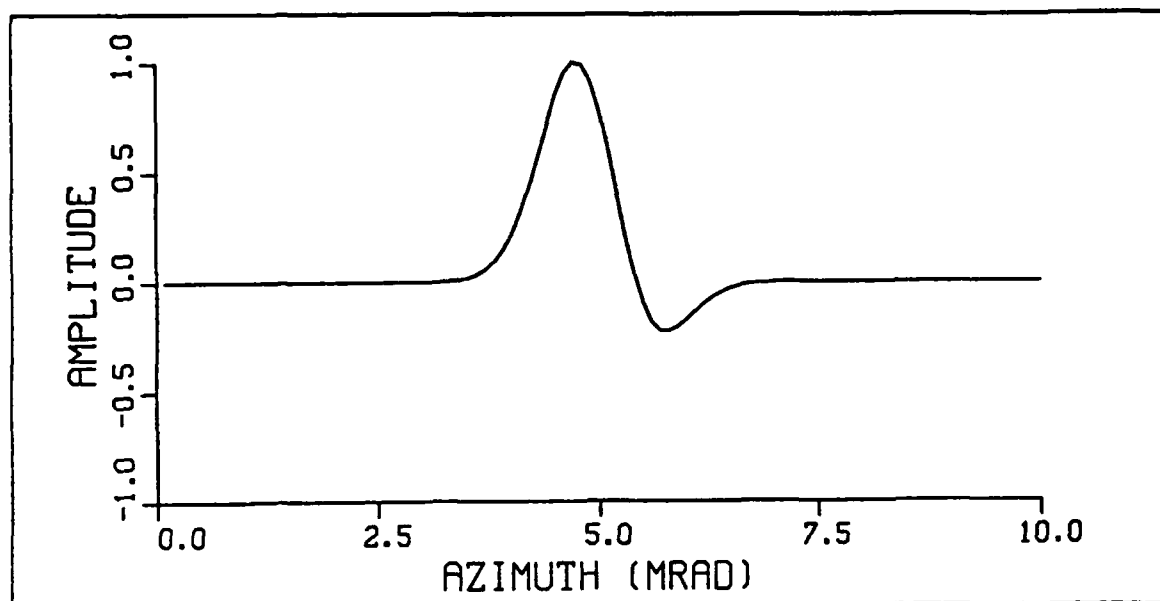
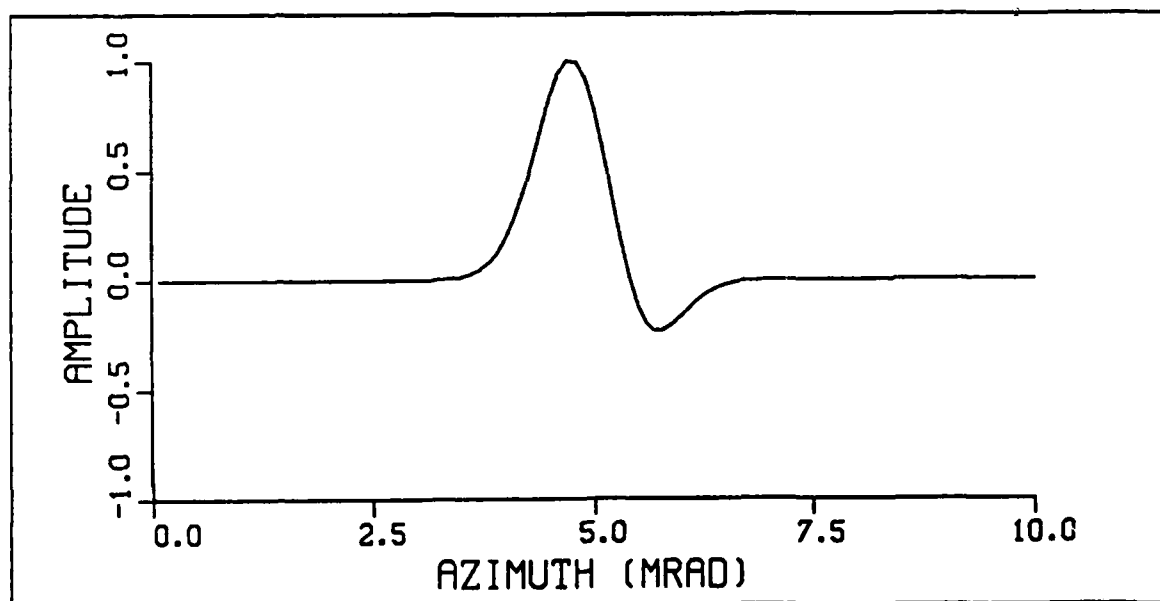


Figure 7. Detector Output; Simulated Target #1 (TGTI): Target dimensions are 0.10472 mrad by 0.10472 mrad.



**Figure 8. Detector Output; Simulated Target #2 (TGTII):** Target dimensions are 0.31416 mrad by 0.31416 mrad.



**Figure 9. Detector Output; Simulated Target #3 (TGTIII):** Target dimensions are 0.52360 mrad by 0.52360 mrad.

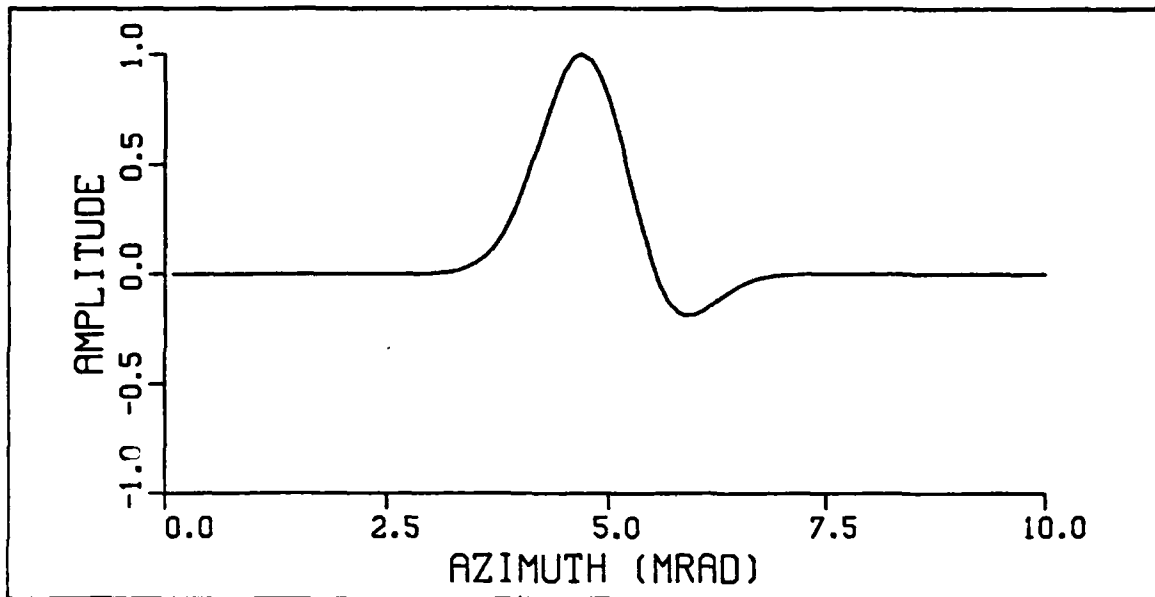


Figure 10. Detector Output; Simulated Target #4 (TGTIV): Target dimensions are 1.0472 mrad by 1.0472 mrad.

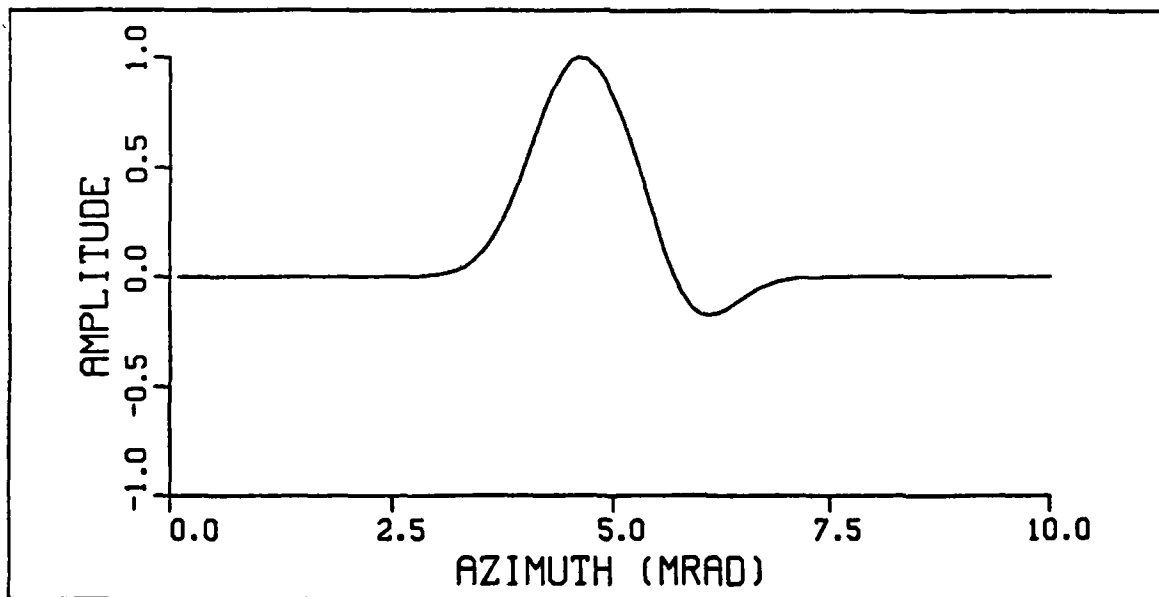


Figure 11. Detector Output; Simulated Target #5 (TGTIV): Target dimensions are 1.5708 mrad by 1.5708 mrad.



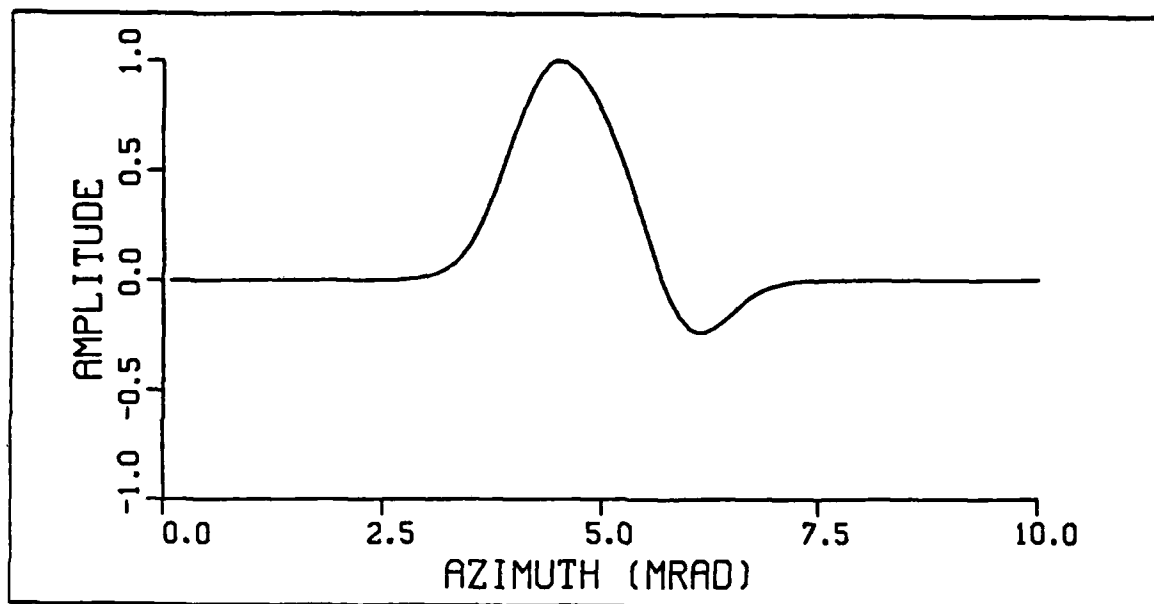


Figure 12. Detector Output; Real Target (Whip Antenna) (TGTVI)

## V. THE LMS FILTER

### A. THEORY

As previously discussed, the spatial extent of background clutter sources is typically much greater than the spatial extent of targets [Ref. 3]. This can be shown by comparing the frequency content of the spatial frequency distributions of the backgrounds and targets. Figure 13 through Figure 17 on page 26 are plots of the magnitudes of the spatial frequency distributions of BKDI, BKDII, TGTI, TGTV, and TGTVI respectively. These figures clearly illustrate that both the simulated and real background distributions are of predominantly lower frequency content, and hence larger spatial extent, than the target signals.

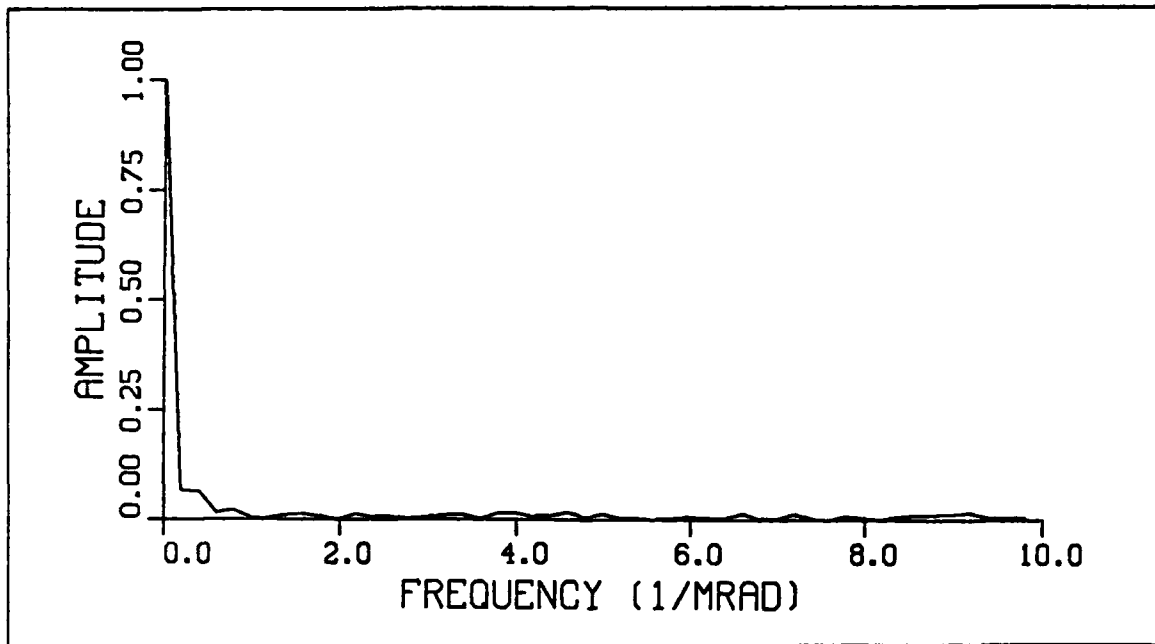


Figure 13. Magnitudes of the Spatial Frequency Distribution of BKDI

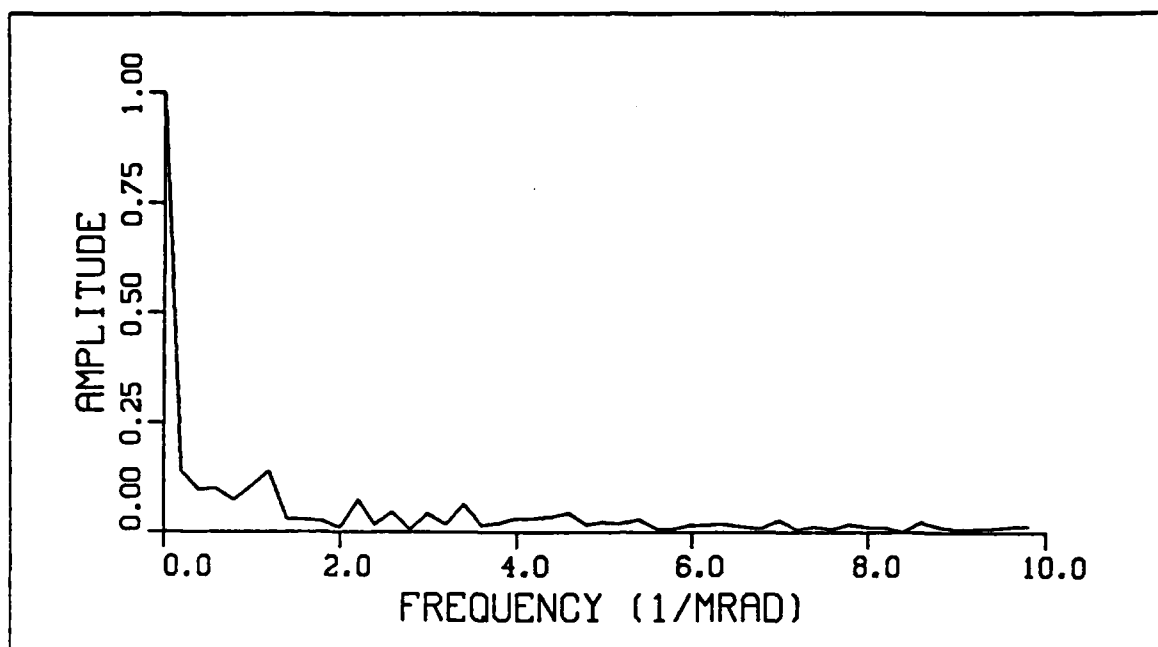


Figure 14. Magnitudes of the Spatial Frequency Distribution of BKDIII

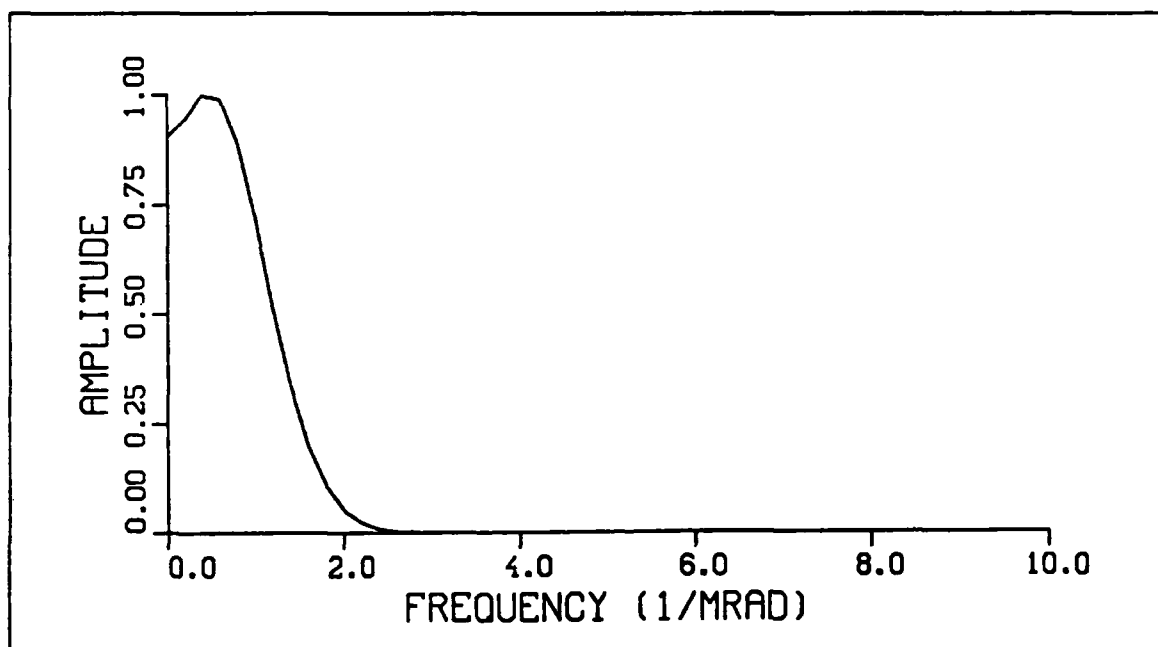


Figure 15. Magnitudes of the Spatial Frequency Distribution of TGTI

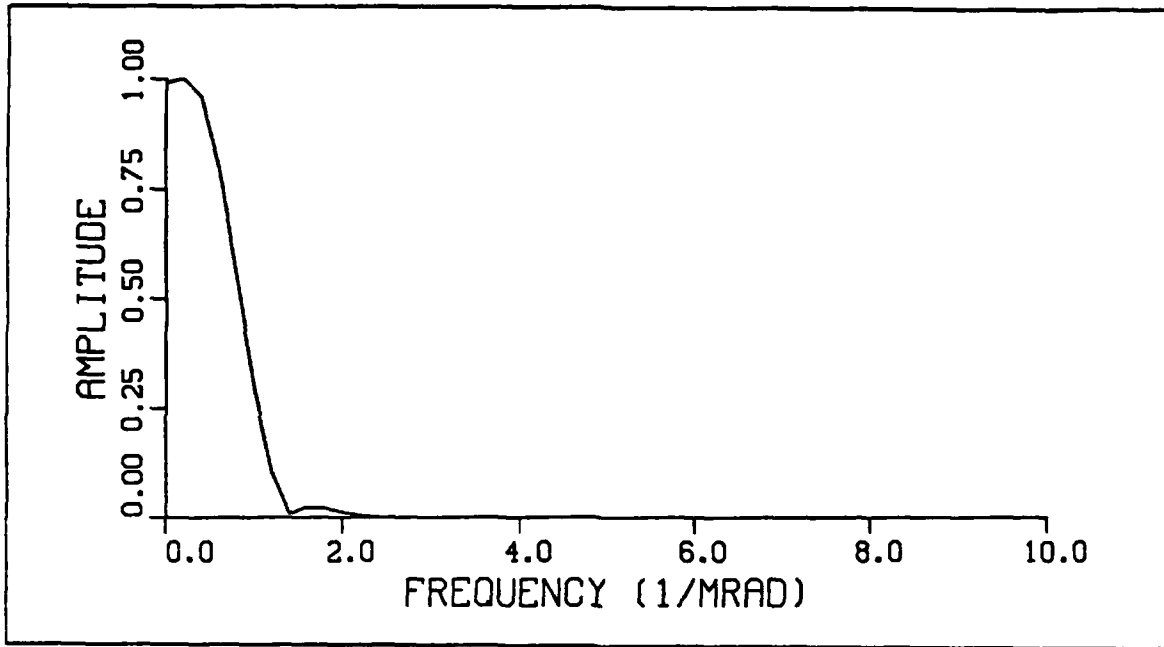


Figure 16. Magnitudes of the Spatial Frequency Distribution of TGTV

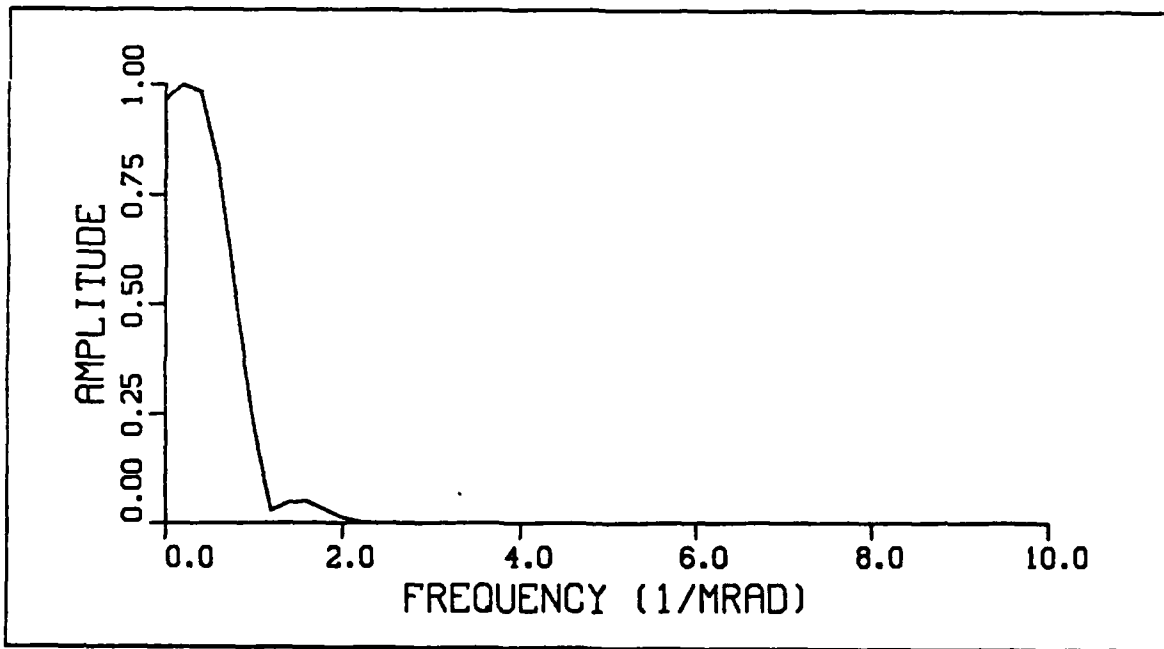


Figure 17. Magnitudes of the Spatial Frequency Distribution of TGTVI

A filter which has been shown to be very effective under these conditions, can be developed using the principle of least-mean-square (LMS) optimization [Ref. 3]. The response of such a filter can be determined by minimizing the difference between the received signal and a function which approximates the presence of both target and background. The most crucial step in this technique is selecting the proper function for estimating the target signal and background.

The model signal which best estimates the presence of both target and background clutter can be expressed as a weighted sum of anticipated target and an expansion series of low frequency noise expanded about the center of the target signal

$$x(t) = a s(t) + b_0 + b_1 \tau + b_2 \tau^2 + \dots \quad (5-1)$$

where  $s(t)$  is the model target signal,  $\tau$  is time measured from the center of  $s(t)$ , and  $a$ ,  $b_0$ ,  $b_1$ ,  $b_2$ ,  $\dots$  are weighting coefficients specifying the amount each component of the series contributes to the signal.

Defining the function  $v(t)$  as an actual signal output from the IRSTD system, the presence of a target at a given test time  $t_0$  can be tested for by minimizing the squared sum

$$F(t_0) = \int_{-t_d}^{t_d} dt [v(t_0 - t) - x(t)]^2 \quad (5-2)$$

where  $t_d$  is the half-amplitude width of the model target signal  $s(t)$ .

Since the coefficient  $a$ , in Equation (5-1), describes the amount of target present in  $v(t)$  at  $t = t_0$ , it can be considered to be the time dependent output of an optimum target detection LMS filter. To simplify the minimization of equation (5-2), it is convenient to truncate equation (5-1). If we consider removing only DC offset and linear noise from the received signal, equation (5-2) can be rewritten as

$$F(t_0) = \int_{-t_d}^{t_d} dt [v(t_0 - t) - a s(t) - b_0 - b_1 \tau]^2 \quad (5-3)$$

Differentiating equation (5-3) with respect to the coefficients  $a$ ,  $b_0$ , and  $b_1$ , and setting each derivative equal to zero, leads to the equations

$$\frac{\partial F}{\partial a} = \langle sv \rangle - a \langle s^2 \rangle - b_0 \langle s \rangle - b_1 \langle s\tau \rangle = 0 \quad (5-4)$$

$$\frac{\partial F}{\partial b_0} = \langle v \rangle - a \langle s \rangle - b_0 - b_1 \langle \tau^2 \rangle = 0 \quad (5-5)$$

$$\frac{\partial F}{\partial b_1} = \langle vt \rangle - a \langle s\tau \rangle - b_0 \langle \tau \rangle - b_1 \langle \tau^2 \rangle = 0 \quad (5-6)$$

where  $\langle \rangle$  denotes the time average over the interval  $-t_d \leq t \leq t_d$ . Equations (5-4), (5-5), and (5-6) can be written in matrix form as

$$\begin{bmatrix} \langle s^2 \rangle & \langle s \rangle & \langle s\tau \rangle \\ \langle s \rangle & 1 & \langle \tau \rangle \\ \langle s\tau \rangle & \langle \tau \rangle & \langle \tau^2 \rangle \end{bmatrix} \begin{bmatrix} a \\ b_0 \\ b_1 \end{bmatrix} = \begin{bmatrix} \langle sv \rangle \\ \langle v \rangle \\ \langle v\tau \rangle \end{bmatrix} \quad (5-7)$$

or, since  $\langle s\tau \rangle = 0$  and  $\langle \tau \rangle = 0$  for symmetric target signals

$$\begin{bmatrix} a \\ b_0 \\ b_1 \end{bmatrix} = \begin{bmatrix} \langle s^2 \rangle & \langle s \rangle & 0 \\ \langle s \rangle & 1 & 0 \\ 0 & 0 & \langle \tau^2 \rangle \end{bmatrix}^{-1} \begin{bmatrix} \langle sv \rangle \\ \langle v \rangle \\ \langle v\tau \rangle \end{bmatrix} \quad (5-8)$$

Then, since the inverse of the  $3 \times 3$  matrix in Equation (5-8) can be described by the proportionality

$$\begin{bmatrix} \langle s^2 \rangle & \langle s \rangle & 0 \\ \langle s \rangle & 1 & 0 \\ 0 & 0 & \langle \tau^2 \rangle \end{bmatrix}^{-1} \propto \begin{bmatrix} \langle \tau^2 \rangle & -\langle s \rangle \langle \tau^2 \rangle & 0 \\ -\langle s \rangle \langle \tau^2 \rangle & \langle s^2 \rangle \langle \tau^2 \rangle & 0 \\ 0 & 0 & \langle s^2 \rangle - \langle s \rangle^2 \end{bmatrix}$$

Equation (5-8) can be rewritten as

$$\begin{bmatrix} a \\ b_0 \\ b_1 \end{bmatrix} \propto \begin{bmatrix} \langle \tau^2 \rangle & -\langle s \rangle \langle \tau^2 \rangle & 0 \\ -\langle s \rangle \langle \tau^2 \rangle & \langle s^2 \rangle \langle \tau^2 \rangle & 0 \\ 0 & 0 & \langle s^2 \rangle - \langle s \rangle^2 \end{bmatrix} \begin{bmatrix} \langle sv \rangle \\ \langle v \rangle \\ \langle v\tau \rangle \end{bmatrix} \quad (5-9)$$

Solving for  $a$  results in the expression

$$a \propto \langle \tau^2 \rangle \langle sv \rangle - \langle \tau^2 \rangle \langle s \rangle \langle v \rangle \quad (5-10)$$

Rewriting the time averages in integral form, and recognizing that dividing the right side of Equation (5-10) by  $\langle \tau^2 \rangle$  will not destroy the proportionality, leads to

$$a \propto \frac{t_d^2}{3} \int_{-t_d}^{t_d} dt s(t) v(t_0 - t) - \frac{t_d^2}{3} \int_{-t_d}^{t_d} dt s(t) \int_{-t_d}^{t_d} dt v(t_0 - t)$$

This expression can be simplified to

$$a \propto \frac{t_d^2}{3} \int_{-t_d}^{t_d} dt [s(t) - \langle s \rangle] v(t_0 - t)$$

or

$$a \propto \frac{t_d^2}{3} \int_{-t_d}^{t_d} dt h(t) v(t_0 - t) \quad (5-11)$$

where  $h(t)$  is the LMS filter function

$$h(t) = s(t) - \langle s \rangle \quad (5-12)$$

## B. FILTER DEVELOPMENT

In this section, an LMS filter will be developed for extracting target signals from IRSTD outputs. This is accomplished by properly modeling IRSTD target signals, and generating the filter function from equation (5-12).

As previously mentioned, the most crucial step in this filtering technique is choosing the proper function to model target signals. In order to use equation (5-12) to develop this filter, the target signal must be modeled as a symmetric function. Referring back to the target signals illustrated in Chapter IV, it is clear that these signals are not symmetric. However, upon closer inspection, it can be seen that each target signal is approximately symmetric over a small region about its maximum amplitude.

Four functions which have the potential of modeling this symmetric region of the target signal are: a raised cosine function, a parabolic function, a Gaussian function, and a Sinc function ( $\text{Sinc}(x) = \frac{\sin(\pi x)}{(\pi x)}$ ). Upon initial investigation, the parabolic, Gaussian, and Sinc functions were ruled out, because the parabolic function would not fit the top region of the target signals, and the Gaussian and Sinc functions would not

fit the sides of the target signals. The raised cosine function, however, modeled the target signals remarkably well, over a range near the peak of the signals, and was selected as an appropriate function for modeling them.

Figure 18 on page 31, through Figure 25 on page 34 display how raised cosine functions of half-amplitude widths ranging from 0.31416 to 1.04728 mrad can be used to model TGTI. It can be seen from these figures that the raised cosine functions of half-amplitude widths ranging from 0.31416 to 0.94248 mrad model the leading edge, or rise, of the target signal remarkably well. However, raised cosine functions with half-amplitude widths greater than 0.62832 mrad begin to deviate substantially from the trailing edge, or fall, of the target signal.

Similarly, upon investigating how well raised cosine functions model TGTII through TGTVI, it was found that raised cosine functions of half-amplitude widths ranging from 0.31416 to 0.94248 mrad also modeled the leading edges of these target signals remarkably well. However, raised cosine functions with half-amplitude widths greater than 0.62832 mrad begin to deviate substantially from the trailing edge of TGTII and TGTIII, functions with half-amplitude widths greater than 0.73304 mrad begin to deviate substantially from the trailing edge of TGTIV, and functions with half-amplitude widths greater than 0.83776 mrad begin to deviate substantially from the trailing edge of TGTV and TGTVI.

From this analysis, it can be concluded that the symmetric portion of the target signals can be modeled as a raised cosine function

$$\begin{aligned} s(t) &= 1 + \cos\pi\left(\frac{t}{t_d}\right) & -t_d \leq t \leq t_d \\ &= 0 & \text{elsewhere} \end{aligned} \quad (5-13)$$

where  $t_d$  is the half-amplitude width of the signal, also referred to as the signal dwell time.

It should be noted that  $t_d$  can be expressed in terms of either time or azimuth. Unless otherwise specified, it will always be expressed in terms of azimuth, with units of mrad, throughout the remainder of this thesis.



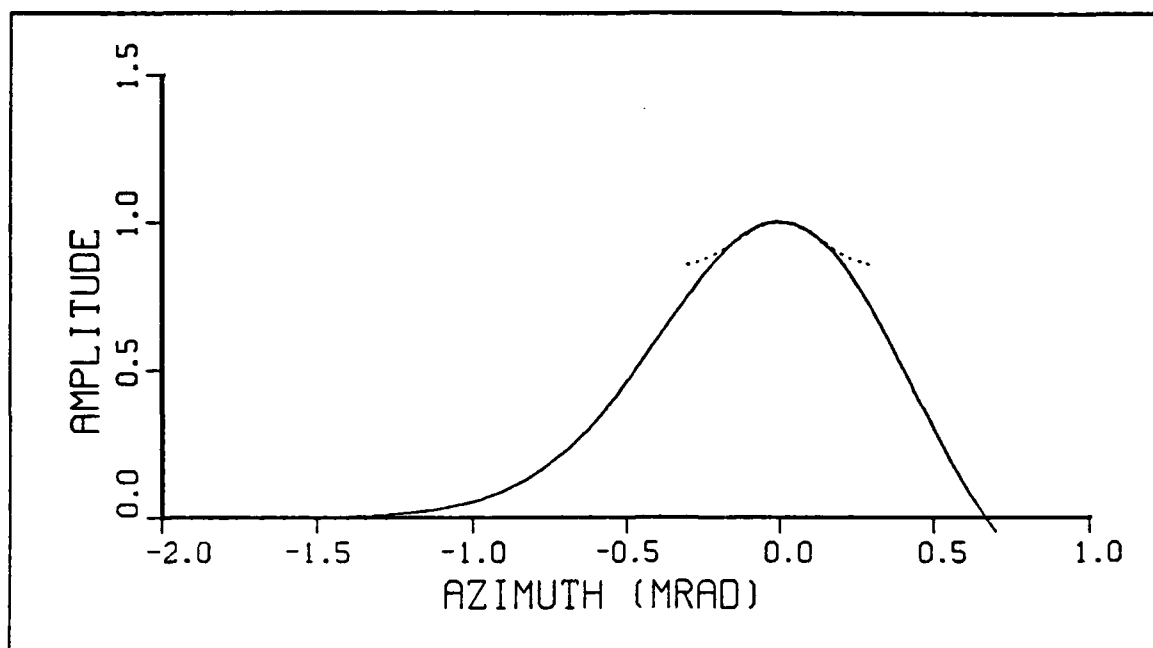


Figure 18. TGTI and Raised Cosine with 0.31416 mrad Half-Amplitude Width

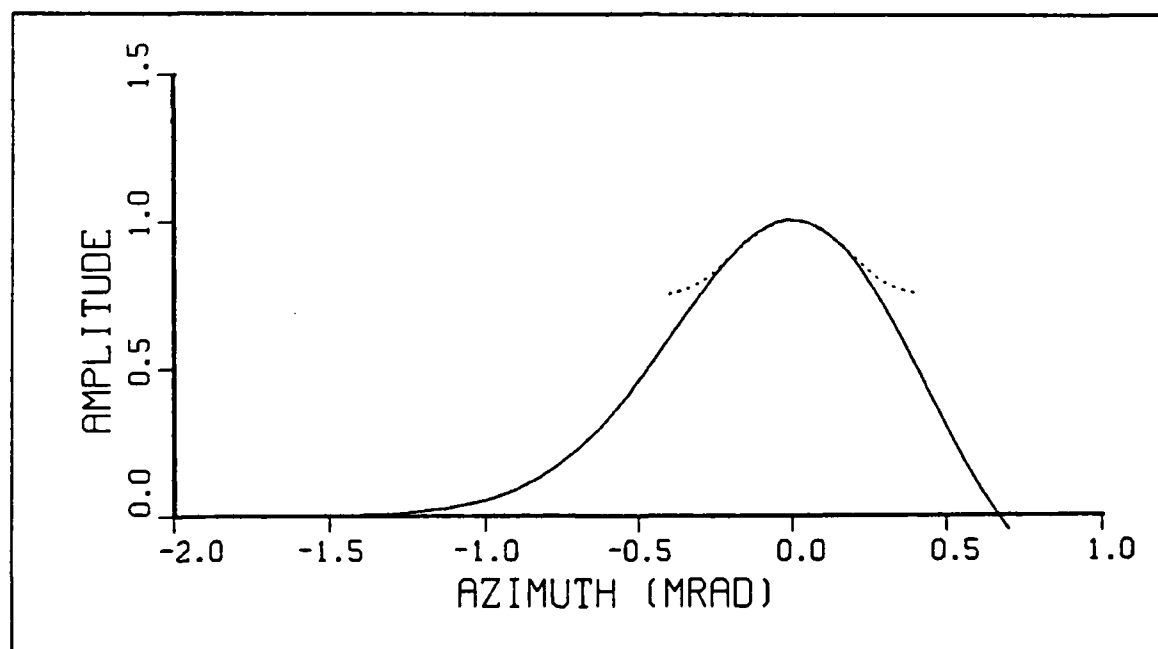


Figure 19. TGTI and Raised Cosine with 0.41888 mrad Half-Amplitude Width

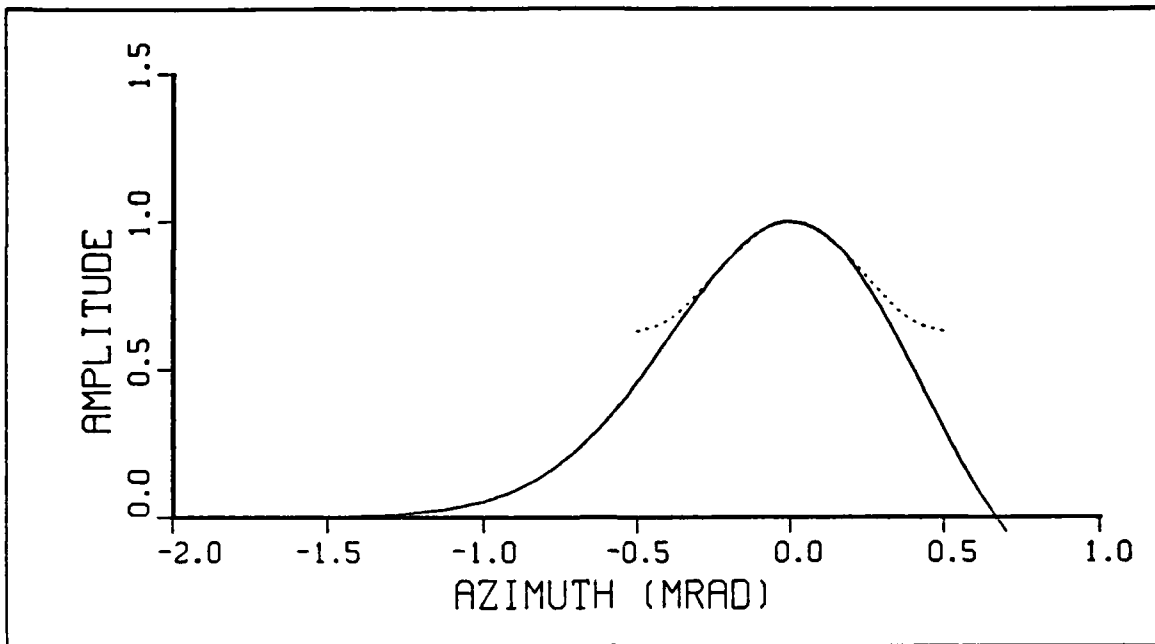


Figure 20. TGTI and Raised Cosine with 0.52360 mrad Half-Amplitude Width

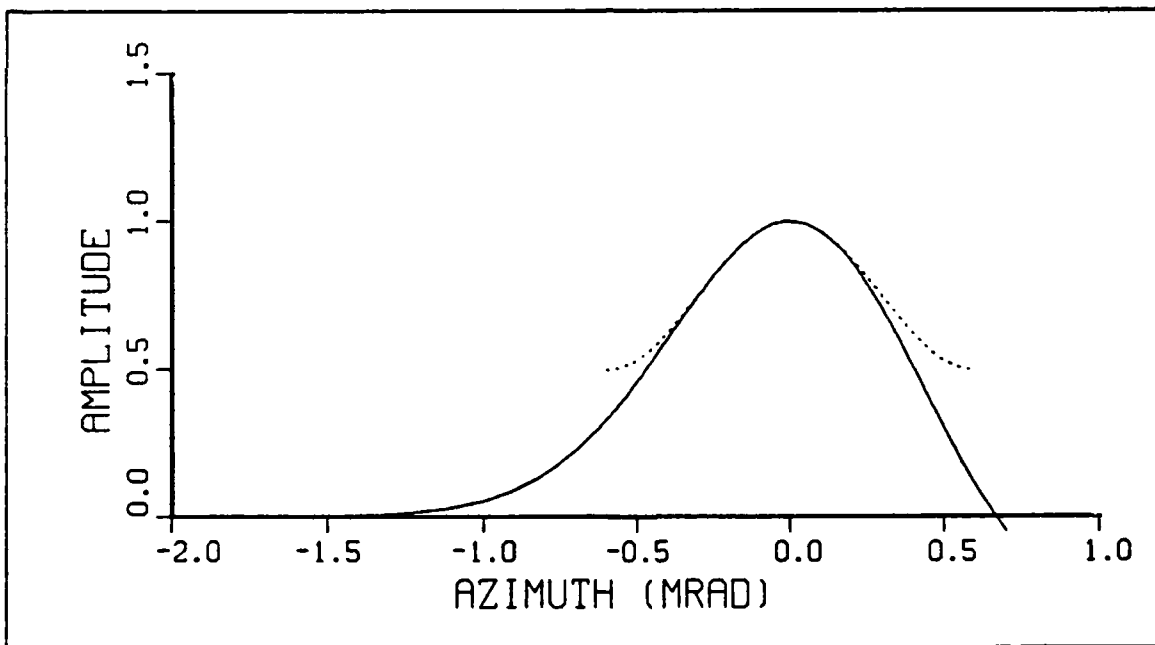


Figure 21. TGTI and Raised Cosine with 0.62832 mrad Half-Amplitude Width

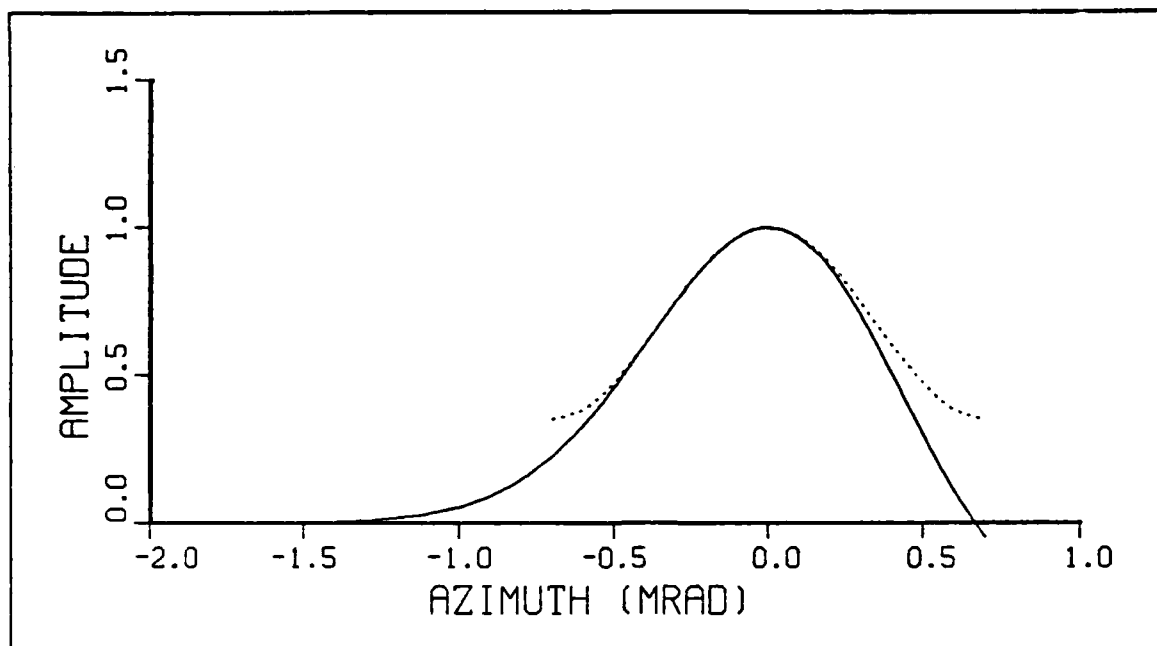


Figure 22. TGTI and Raised Cosine with 0.73304 mrad Half-Amplitude Width

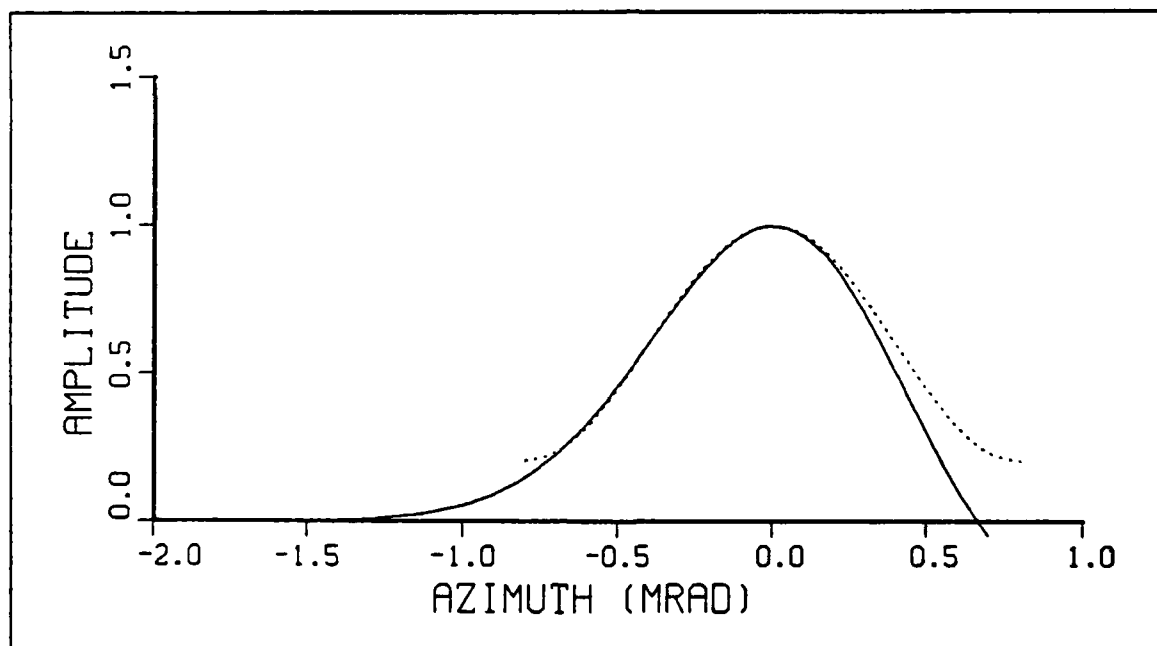


Figure 23. TGTI and Raised Cosine with 0.83776 mrad Half-Amplitude Width

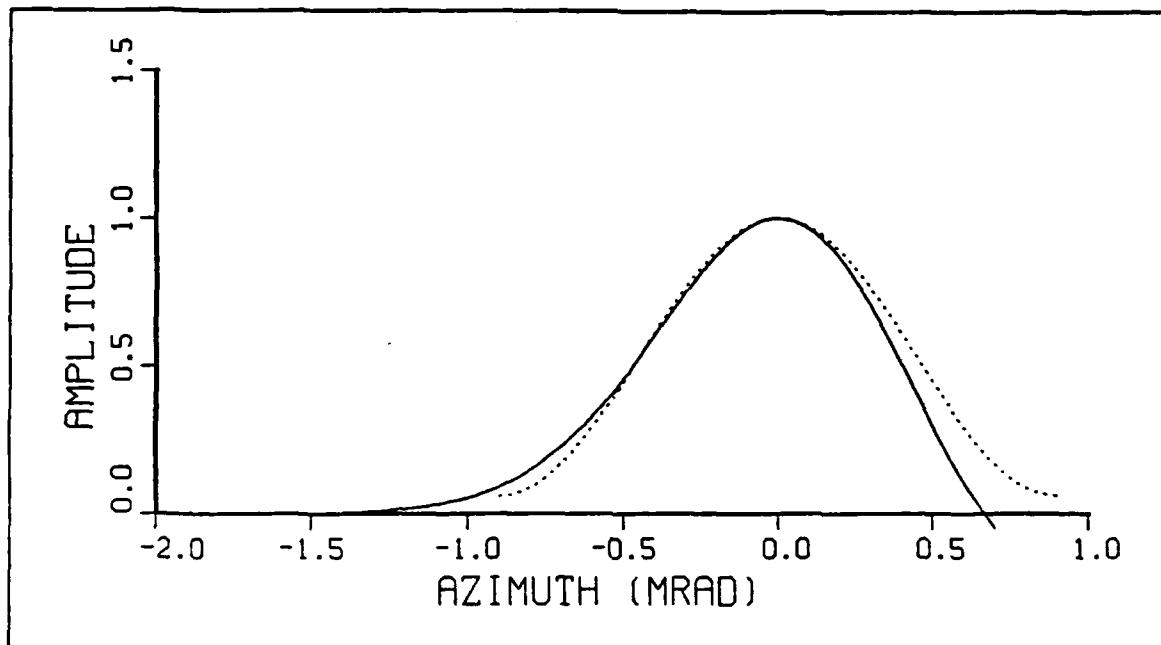


Figure 24. TGTI and Raised Cosine with 0.94248 mrad Half-Amplitude Width

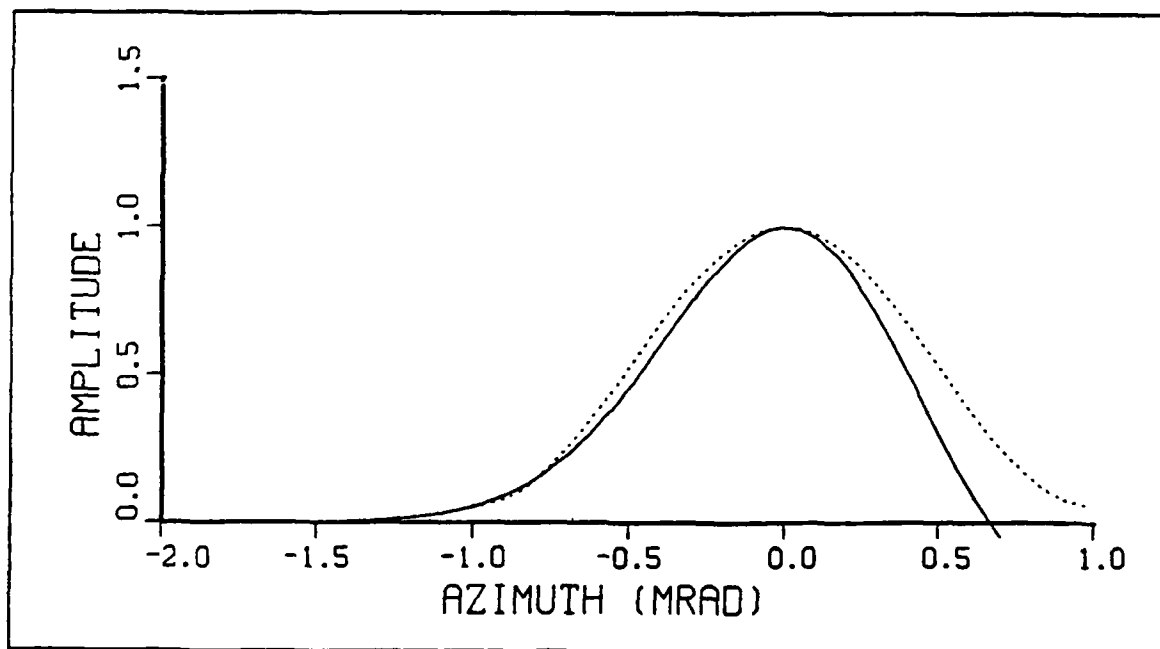


Figure 25. TGTI and Raised Cosine with 1.0472 mrad Half-Amplitude Width

Substituting equation (5-13) into equation (5-12) gives

$$h(t) = \begin{cases} \cos\pi(\frac{t}{t_d}) & -t_d \leq t \leq t_d \\ 0 & \text{elsewhere} \end{cases} \quad (5-14)$$

where  $\langle 1 + \cos\pi(\frac{t}{t_d}) \rangle = 1$ .

Since the output signals of the IRSTD system are digitized, it is necessary to express the filter in digital form. This can be accomplished by expressing  $s(t)$  in the form of a vector, whose components are

$$S_n = \frac{1}{2} \left[ 1 + \cos\pi n(\frac{t_s}{t_d}) \right] \quad (5-15)$$

where

$$n = 0, \pm 1, \pm 2, \dots \pm \frac{t_d}{t_s} \quad (5-16)$$

and  $t_s$  is the sampling time of the IRSTD. It should be noted that, if  $\frac{t_d}{t_s}$  is non-integer, the maximum value of  $n$  will assume the value of the integer which is closest to and less than  $\frac{t_d}{t_s}$ . For example, if  $\frac{t_d}{t_s} = 3.2$ ;  $n = 0, \pm 1, \pm 2, \pm 3$ .

To illustrate this vector representation for  $\frac{t_d}{t_s} = 3$ , it is clear that

$$S_n = \frac{1}{2} \left[ 1 + \cos\pi \frac{n}{3} \right] \quad n = (-3, -2, -1, 0, 1, 2, 3) \quad (5-17)$$

or in matrix form

$$\mathbf{S} = \frac{1}{2} \begin{bmatrix} 0.000 \\ 0.500 \\ 1.500 \\ 2.000 \\ 1.500 \\ 0.500 \\ 0.000 \end{bmatrix} = \begin{bmatrix} 0.000 \\ 0.250 \\ 0.750 \\ 1.000 \\ 0.750 \\ 0.250 \\ 0.000 \end{bmatrix} \quad (5-18)$$

The vector representation of the filter can then be written, from equation (5-12), as

$$\mathbf{H} = \frac{1}{|\mathbf{S}_{\max} - \langle \mathbf{S} \rangle|} [\mathbf{S} - \langle \mathbf{S} \rangle] \quad (5-19)$$

where the factor  $\frac{1}{|S_{\max} - \langle S \rangle|}$  is a normalization constant. To continue the example for  $\frac{t_d}{t_s} = 3$ , the LMS filter coefficients become

$$\mathbf{H} = \frac{1}{0.571} \begin{bmatrix} -0.429 \\ -0.179 \\ 0.321 \\ 0.571 \\ 0.321 \\ -0.179 \\ -0.429 \end{bmatrix} = \begin{bmatrix} -0.750 \\ -0.312 \\ 0.562 \\ 1.000 \\ 0.562 \\ -0.312 \\ -0.750 \end{bmatrix} \quad (5-20)$$

This example LMS filter  $\mathbf{H}$  is symmetric with zero mean, making it appropriate for extracting symmetric target signals from received signals digitized with a sampling time of  $t_s = 3t_d$ , and containing linear noise of spatial extent much greater than  $t_d$ .

When the limits of integration are changed to investigate the presence of target signals over all time, the coefficient  $a$  becomes time dependent, and equation (5-12) can be rewritten as

$$a(t_0) \simeq \frac{t_d^2}{3} \int_{-\infty}^{\infty} dt h(t) v(t_0 - t) \quad (5-21)$$

which is the convolution of  $v(t)$  with  $h(t)$ . In matrix form, equation (5-21) can be rewritten as

$$\mathbf{A} \simeq \mathbf{H} * \mathbf{V} \quad (5-22)$$

Therefore, the output array,  $\mathbf{A}$ , can be determined by digitally convolving the IRSTD output signal,  $\mathbf{V}$ , with the digital LMS filter,  $\mathbf{H}$ . It should be emphasized that the output array,  $\mathbf{A}$ , is the vector, or digital, representation of the time dependent expansion series coefficient  $a$ , which describes the amount of target present in  $\mathbf{V}$ .

For large IRSTD output arrays,  $\mathbf{V}$ , digital convolution can be costly with respect to computer processing time. It is therefore convenient to take advantage of the Convolution Theorem, and rewrite equation (5-22) as

$$\mathbf{A} = \mathbf{F}_{1D}^{-1} \{ \tilde{\mathbf{H}} \cdot \tilde{\mathbf{V}} \} \quad (5-23)$$

where  $\tilde{H}$  and  $\tilde{V}$  are the Fourier transforms of  $H$  and  $V$  respectively,  $F_{ID}^{-1}$  represents the 1D inverse Fourier transform, and  $\tilde{H}$  is commonly referred to as the filter transfer function.

In order to accomplish the spatial frequency domain multiplication of equation (5-23), it is first necessary to place the coefficients of the LMS filter in an array of the same dimensions as  $V$ . This is done by centering the coefficients in an empty array, and letting all of the remaining elements of the array be zero.

A set of trial filters, for filtering both simulated and real IRSTD data, will be generated in the following section. The resultant filtered outputs will be presented and discussed in the following chapters.

### C. TRIAL FILTERS

As previously discussed, a raised cosine function can be considered an appropriate model for specific portions of TGTI through TGTVI. To see how well this function does model the targets, a set of 15 trial LMS filters were developed from raised cosine functions with half-amplitude widths ranging from 0.10472 to 1.5708 mrad.

Using the methods outlined in the previous section, the coefficients of these trial filters were determined, and were used to filter both simulated and real IRSTD output data with the objective of seeing which filters yield the best signal-to-noise (S/N) ratio increase for each target. It is important to note that even though these filters were designed for extracting targets with specific signal half-amplitude widths, they are much more general in nature. Since the targets under investigation were sampled at 0.10472 mrad per sample, these filters are actually capable of extracting any targets with signals having 1 through 15 samples per half amplitude width. In light of this, these filters will hereupon be referred to as LMS1 through LMS15 respectively.

The coefficients of LMS1 through LMS8 are listed in Table 1 on page 39, and the coefficients of LMS9 through LMS15 are listed in Table 2 on page 40. The coefficients of a particular filter can be obtained from these tables by reading down the columns under the appropriate heading for the desired filter. The coefficients were rounded-off to the third significant digit to the right of the decimal for ease in illustration. However, the coefficients used in the filtering process were generated by the NPS IBM 3033/4381 computer and represented by 32-bit words, thereby increasing their precision substantially.

Additionally, it should be noted that by using these LMS filters on TGTI through TGTVI, an inherent thresholding takes place during the filtering process. This thresholding can be seen by referring back to Figure 18 on page 31 through Figure 25 on page 34, where the target signals can be considered to be thresholded at the base of the raised cosine functions during the filtering process. Therefore, as the filter width increases, a greater portion of target signal becomes available for filtering. This combination of filtering and thresholding, during the filtering process, can generate serious problems in that the probability of thresholding out target signals increases as the width of the raised cosine function decreases. It will therefore be necessary to weigh this factor when determining which filter is optimal, by considering both the noise reduction capability and half-amplitude width of the filters.

Before proceeding to the next chapter, a discussion of the real background, BKDIII, is necessary. As previously mentioned, both the IRSTD model and the IRSTD DCU sample data at 0.10472 mrad per sample. However, the real background was sampled by the Nicolet digital oscilloscope at 0.31416 mrad per sample, or one third the system sampling rate.

In order to embed the targets into BKDIII, it was necessary to sample them at the same rate as the background. This was accomplished by altering the sampling rate of the IRSTD model, and generating new targets sampled at 0.31416 mrad per sample. Analysis of these modified target signals showed that the same raised cosine functions used to model the simulated targets can be used to model the modified targets as well. However, since the increased sampling time reduces  $\frac{t_d}{t_s}$  by a factor of three, the LMS filters will not have the same effect on BKDIII as they do on BKDI and BKDII. Specifically, if LMS9 is determined to be the optimal filter for TGTI in BKDI and BKDII, LMS3 can be expected to be optimal for TGTI in BKDIII.



**Table 1. LMS FILTER COEFFICIENTS**

Azimuth (mrad)	LMS Filter							
	LMS1	LMS2	LMS3	LMS4	LMS5	LMS6	LMS7	LMS8
-8 $t_s$	0.000	0.000	0.000	0.000	0.000	0.000	0.000	-0.889
-7 $t_s$	0.000	0.000	0.000	0.000	0.000	0.000	-0.875	-0.817
-6 $t_s$	0.000	0.000	0.000	0.000	0.000	-0.857	-0.782	-0.612
-5 $t_s$	0.000	0.000	0.000	0.000	-0.833	-0.733	-0.522	-0.306
-4 $t_s$	0.000	0.000	0.000	-0.800	-0.658	-0.393	-0.146	0.056
-3 $t_s$	0.000	0.000	-0.750	-0.536	-0.200	0.071	0.271	0.417
-2 $t_s$	0.000	-0.667	-0.312	0.100	0.367	0.536	0.647	0.723
-1 $t_s$	-0.500	0.167	0.563	0.736	0.825	0.876	0.907	0.928
0 $t_s$	1.000	1.000	1.000	1.000	1.000	1.000	1.000	1.000
1 $t_s$	-0.500	0.167	0.563	0.736	0.825	0.876	0.907	0.928
2 $t_s$	0.000	-0.667	-0.312	0.100	0.367	0.536	0.647	0.723
3 $t_s$	0.000	0.000	-0.750	-0.536	-0.200	0.071	0.271	0.417
4 $t_s$	0.000	0.000	0.000	-0.800	-0.658	-0.393	-0.146	0.056
5 $t_s$	0.000	0.000	0.000	0.000	-0.833	-0.733	-0.522	-0.306
6 $t_s$	0.000	0.000	0.000	0.000	0.000	-0.857	-0.782	-0.612
7 $t_s$	0.000	0.000	0.000	0.000	0.000	0.000	-0.875	-0.817
8 $t_s$	0.000	0.000	0.000	0.000	0.000	0.000	0.000	-0.889

**Table 2. LMS FILTER COEFFICIENTS**

Azimuth (mrad)	LMS Filter						
	LMS9	LMS10	LMS11	LMS12	LMS13	LMS14	LMS15
-15 $t_z$	0.000	0.000	0.000	0.000	0.000	0.000	-0.937
-14 $t_z$	0.000	0.000	0.000	0.000	0.000	-0.933	-0.916
-13 $t_z$	0.000	0.000	0.000	0.000	-0.929	-0.909	-0.854
-12 $t_z$	0.000	0.000	0.000	-0.923	-0.901	-0.838	-0.752
-11 $t_z$	0.000	0.000	-0.917	-0.890	-0.818	-0.722	-0.617
-10 $t_z$	0.000	-0.909	-0.878	-0.794	-0.686	-0.569	-0.453
-9 $t_z$	-0.900	-0.862	-0.765	-0.641	-0.512	-0.386	-0.268
-8 $t_z$	-0.843	-0.727	-0.586	-0.442	-0.306	-0.182	-0.070
-7 $t_z$	-0.678	-0.516	-0.356	-0.210	-0.081	0.033	0.133
-6 $t_z$	-0.425	-0.250	-0.095	0.038	0.152	0.248	0.331
-5 $t_z$	-0.115	0.045	0.178	0.287	0.378	0.453	0.516
-4 $t_z$	0.215	0.340	0.440	0.519	0.583	0.636	0.679
-3 $t_z$	0.525	0.607	0.669	0.718	0.757	0.789	0.815
-2 $t_z$	0.778	0.818	0.848	0.871	0.890	0.904	0.916
-1 $t_z$	0.943	0.953	0.961	0.967	0.972	0.976	0.979
0 $t_z$	1.000	1.000	1.000	1.000	1.000	1.000	1.000
1 $t_z$	0.943	0.953	0.961	0.967	0.972	0.976	0.979
2 $t_z$	0.778	0.818	0.848	0.871	0.890	0.904	0.916
3 $t_z$	0.525	0.607	0.669	0.718	0.757	0.789	0.815
4 $t_z$	0.215	0.340	0.440	0.519	0.583	0.636	0.679
5 $t_z$	-0.115	0.045	0.178	0.287	0.378	0.453	0.516
6 $t_z$	-0.425	-0.250	-0.095	0.038	0.152	0.248	0.331
7 $t_z$	-0.678	-0.516	-0.356	-0.210	-0.081	0.033	0.133
8 $t_z$	-0.843	-0.727	-0.586	-0.442	-0.306	-0.182	-0.070
9 $t_z$	-0.900	-0.862	-0.765	-0.641	-0.512	-0.386	-0.268
10 $t_z$	0.000	-0.909	-0.878	-0.794	-0.686	-0.569	-0.453
11 $t_z$	0.000	0.000	-0.917	-0.890	-0.818	-0.722	-0.617
12 $t_z$	0.000	0.000	0.000	-0.923	-0.901	-0.838	-0.752
13 $t_z$	0.000	0.000	0.000	0.000	-0.929	-0.909	-0.854
14 $t_z$	0.000	0.000	0.000	0.000	0.000	-0.933	-0.916
15 $t_z$	0.000	0.000	0.000	0.000	0.000	0.000	-0.937

## VI. FILTER OUTPUTS

The 15 trial LMS filters (LMS1 through LMS15), introduced and developed in the previous chapter, were used to filter both simulated and real IRSTD outputs. The following sections summarize the effectiveness of these filters, and illustrate filtered outputs of selected LMS filters.

### A. SIGNAL-TO-NOISE RATIOS

In order to quantitatively analyze the effectiveness of the LMS filters, it is necessary to determine the signal-to-noise (S/N) ratio of both the filtered and unfiltered outputs. Since the convolution of the filter with the IRSTD output is performed in the spatial frequency domain, it is convenient to determine the S/N ratio in this domain also.

The S/N ratio of the filtered detector outputs can be represented by the expression

$$(S/N)_F = \frac{\sum_{i=0}^n (\tilde{H}_i \cdot \tilde{T}_i)}{\left[ \sum_{i=0}^n (\tilde{H}_i \cdot \tilde{B}_i)^2 \right]^{1/2}} \quad (6-1)$$

where  $\tilde{T}_i$  are the elements of the target spatial frequency distribution,  $\tilde{B}_i$  are the elements of the background spatial frequency distribution, and the index  $i$  ranges over all of the  $N$  elements in the IRSTD output array.

It is important to note that for analysis of the S/N ratios of the unfiltered IRSTD data, no filter is being used. Therefore, the elements of the filter transfer function,  $\tilde{H}_i$ , are all equal to one, and Equation (6-1) can be rewritten as

$$(S/N)_U = \frac{\sum_{i=0}^n \tilde{T}_i}{\left[ \sum_{i=0}^n \tilde{B}_i^2 \right]^{1,2}} \quad (6-2)$$

for the unfiltered IRSTD data.

## B. ERROR ANALYSIS

In order to obtain some degree of confidence in the filtered outputs, it is essential to study the types of errors, or uncertainty, which are inherent in computer simulations and calculations. Two of the most important sources of uncertainty, which are applicable to this thesis, are quantization and roundoff.

Quantization error occurs during A/D conversion, where digital quantities can only be represented to a fixed and finite precision. The effect of this limitation to finite quantities is that the representation of all physical and simulated signals must be viewed as corrupted by noise. The variance of this noise can be represented by the expression [Ref. 11]

$$\sigma_q^2 = \frac{1}{12} 2^{-2b} \quad (6-3)$$

where  $b$  is the number of bits being used to represent the magnitude of the digital data.

Roundoff error is introduced by rounding off the least significant figure kept, in order to represent digital quantities in a fixed and finite form. The effect of this error must be viewed as an addition of a noise term, with a variance which can be represented by the expression [Ref. 11]

$$\sigma_r^2 = \frac{1}{12} 10^{-2d} \quad (6-4)$$

where  $d$  is the number of base ten significant digits to the right of the decimal point remaining after roundoff.

The effects of quantization and roundoff errors on the filtered outputs can be determined by considering the noise amplification effects of digital filters. Specifically, if the variance of the elements of the unfiltered signal ( $\sigma_u^2$ ) is known, and if the variance in

the individual filter coefficients is negligible compared to  $\sigma_u^2$ , the variance of the elements of the filtered output ( $\sigma_f^2$ ) can be determined from [Ref. 12]

$$\sigma_f^2 = \sigma_u^2 \sum_{i=1}^N H_i^2 \quad (6-5)$$

where  $H_i$  are the filter coefficients, and the sum is over the  $N$  elements of the IRSTD output signal.

For the purpose of this thesis, all digital elements of the target and background distributions were either quantized or simulated to be quantized by a 13-bit A/D converter. Of these 13 bits, one bit is used to designate sign and 12 bits are used to specify magnitude. Therefore, the variance of the elements of the background distributions and target signals can be considered to be  $4.97 \times 10^{-9}$ . Since the target signals are imbedded into the background distributions to construct the unfiltered signal, the variance of the elements of the unfiltered signal must be represented as the sum of the variances of the elements of the background distributions and target signals, which is equal to  $9.94 \times 10^{-9}$ .

Using Equation (6-5), the variances of the elements of the filtered outputs for LMS1 through LMS15 were determined, and are listed in Table 3 on page 44. These variances give a measure of the noise amplification effect of the filtering process, which becomes more and more significant as the width of the filter increases.

**Table 3. VARIANCES OF ELEMENTS OF UNFILTERED AND FILTERED IRSTD OUTPUTS**

LMS Filter	$\sigma_u^2 \times 10^9$	$\sigma_f^2 \times 10^9$
LMS1	9.94	14.9
LMS2	9.94	19.3
LMS3	9.94	29.3
LMS4	9.94	39.3
LMS5	9.94	49.3
LMS6	9.94	59.3
LMS7	9.94	69.3
LMS8	9.94	79.2
LMS9	9.94	89.2
LMS10	9.94	99.2
LMS11	9.94	109.1
LMS12	9.94	119.0
LMS13	9.94	128.9
LMS14	9.94	138.8
LMS15	9.94	148.6

### C. FILTER OUTPUTS

Various selections of the 15 trial filters were used on BKDI, BKDII, and BKDIII. TGTI through TGTVI were embedded into each background, and the resultant output signals were filtered. The S/N ratios of both the filtered and unfiltered outputs were then determined, and are listed in Table 4 on page 45, Table 5 on page 45, and Table 6 on page 45.

**Table 4. S/N RATIOS FOR BKD I**

TGT	LMS Filter							
	raw	LMS8	LMS9	LMS10	LMS11	LMS12	LMS13	LMS14
I	0.932	29.0	29.7	29.1	27.9	26.4	24.8	23.2
II	0.936	29.0	29.8	29.2	28.0	26.5	24.9	23.3
III	0.934	28.3	29.2	28.8	27.7	26.4	24.9	23.3
IV	0.923	23.5	25.2	25.8	25.6	25.0	24.2	23.1
V	0.936	19.1	21.0	22.1	22.7	22.9	22.8	22.4
VI	0.959	18.7	20.4	21.4	22.0	22.4	22.5	22.4

**Table 5. S/N RATIOS FOR BKD II**

TGT	LMS Filter							
	raw	LMS8	LMS9	LMS10	LMS11	LMS12	LMS13	LMS14
I	0.909	31.5	32.2	31.5	29.9	28.0	26.1	24.1
II	0.913	31.5	32.3	31.6	30.0	28.1	26.2	24.2
III	0.911	30.8	31.7	31.1	29.7	28.0	26.1	24.3
IV	0.900	25.5	27.3	27.9	27.5	26.6	25.4	24.1
V	0.913	20.8	22.7	23.9	24.3	24.3	24.0	23.3
VI	0.936	20.3	22.1	23.1	23.6	23.7	23.7	23.3

**Table 6. S/N RATIOS FOR REAL BACKGROUND**

TGT	LMS Filter					
	raw	LMS2	LMS3	LMS4	LMS5	LMS6
I	1.89	11.2	12.7	11.9	10.3	8.8
II	1.89	11.2	12.7	11.9	10.3	8.9
III	1.89	10.8	12.5	11.8	10.4	8.9
IV	1.87	8.5	11.1	11.5	10.6	9.5
V	1.90	6.8	9.4	10.7	10.6	9.9
VI	1.95	6.7	9.1	10.6	10.9	10.3

These tables show that LMS9 through LMS13 yield the highest S/N ratios for the simulated backgrounds, and that LMS3 through LMS5 yield the highest S/N ratios for the real background. This difference between backgrounds is expected, because the real background was sampled at a rate three times slower than the simulated background. This increased sampling time corresponds directly to a reduction in the half-amplitude width to sampling time ratio ( $\frac{t_d}{t_s}$ ) by a factor of three. Therefore, taking the case of TGTI as an example, the change in the optimal filter from LMS9 for BKDI and BKDII to LMS3 for BKDIII is expected.

Additionally, as discussed by Nitzberg *et al.* [Ref. 3], an increase in the sampling time of a digital system leads to a sampling-effect loss of signal shape information in the system output. This loss of signal shape information can be considered as a source of high frequency noise, which will be amplified, along with the target signal, in the filtering process. Therefore, the increased sampling time of BKDIII accounts for the remarkable difference between the S/N ratios of the filtered outputs of the real and simulated backgrounds.

For purposes of comparison, the reduction of S/N ratio with increased sampling times for the LMS filter was studied by Nitzberg *et al.* in a white noise environment [Ref. 3]. This study showed a decrease in S/N ratio by a factor of approximately three, as the sampling time was increased by a factor of three. The results of this study compare well with the decrease in S/N ratio by a factor of approximately five in the present case. This comparison can be made, because the study by Nitzberg *et al.* considered only a white noise background, whereas the present case considers a background consisting of white noise as well as background clutter, both of which are known to be corrupted by quantization error due to digitization. These additional noise sources are amplified, along with the white noise, as the sampling time is increased from 0.10472 mrad sample to 0.31416 mrad sample, thereby causing additional degradation of the S/N ratio. Additionally, since the IRSTD DCU samples data at 0.10472 mrad sample, vice 0.31416 mrad sample, sampling time degradation is not expected from IRSTD outputs digitized by the system's DCU.

To illustrate the effectiveness of these filters, various filtered and unfiltered outputs are illustrated in Figure 26 on page 47 through Figure 35 on page 57 of this Chapter, as well as in Figure 36 on page 61 through Figure 61 on page 78 in Appendix A and Appendix B. The significance of these figures will be discussed in the following sections.



### 1. Unfiltered Outputs

Figure 26 on page 47, Figure 27 on page 48, and Figure 28 on page 48 are plots of the unfiltered outputs of BKDI, BKDII, and BKDIII with TGTI, TGTI, and TGTVI embedded, respectively. The targets are located at the center of the unfiltered outputs, and have a S/N ratio of approximately one in BKDI and BKDII, and a S/N ratio of approximately two in BKDIII. These plots are shown to illustrate the fact that extraction of the targets from the background by simple means, such as thresholding, would not be very effective.

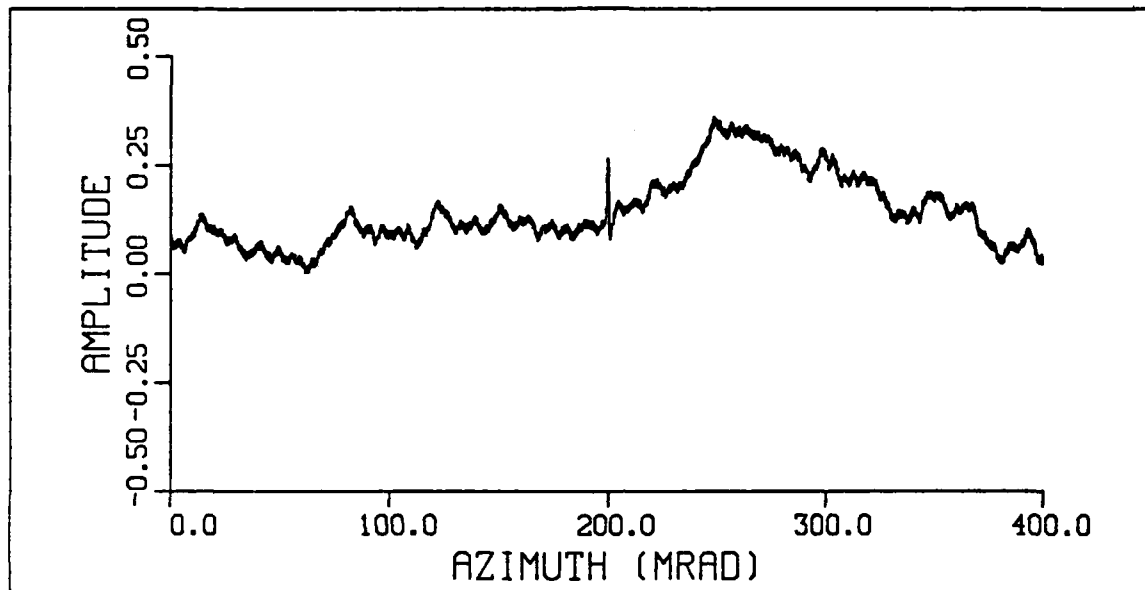


Figure 26. Unfiltered Output; BKDI, TGTI: TGTI embedded in BKDI;  
S/N = 0.932.

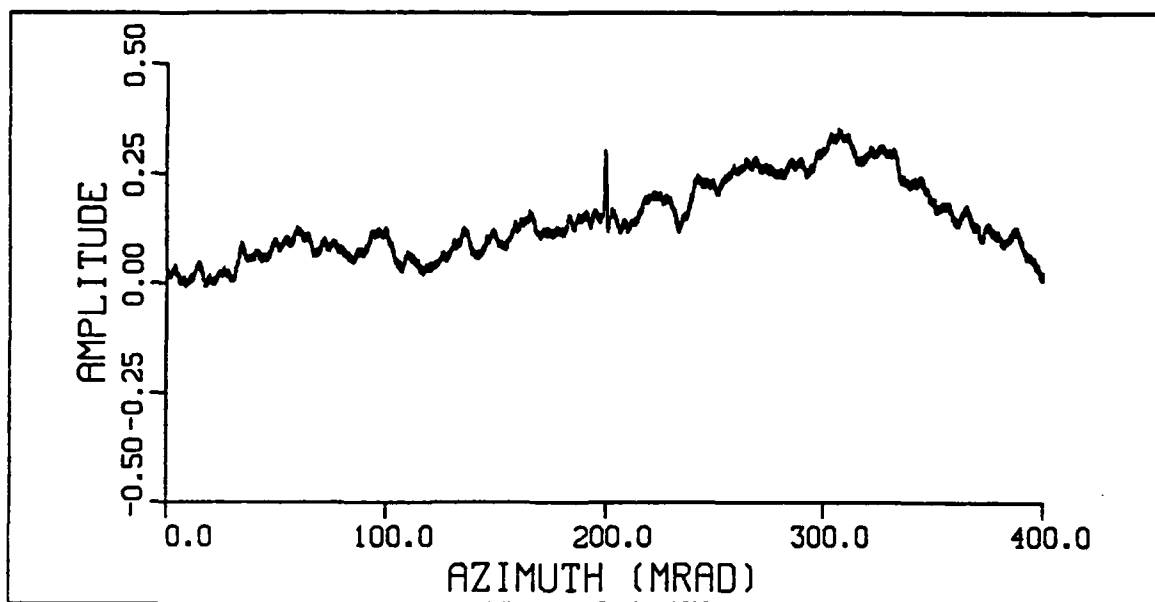


Figure 27. Unfiltered Output; BKDII, TGTI: TGTI embedded in BKDII;  
 $S/N = 0.909$ .

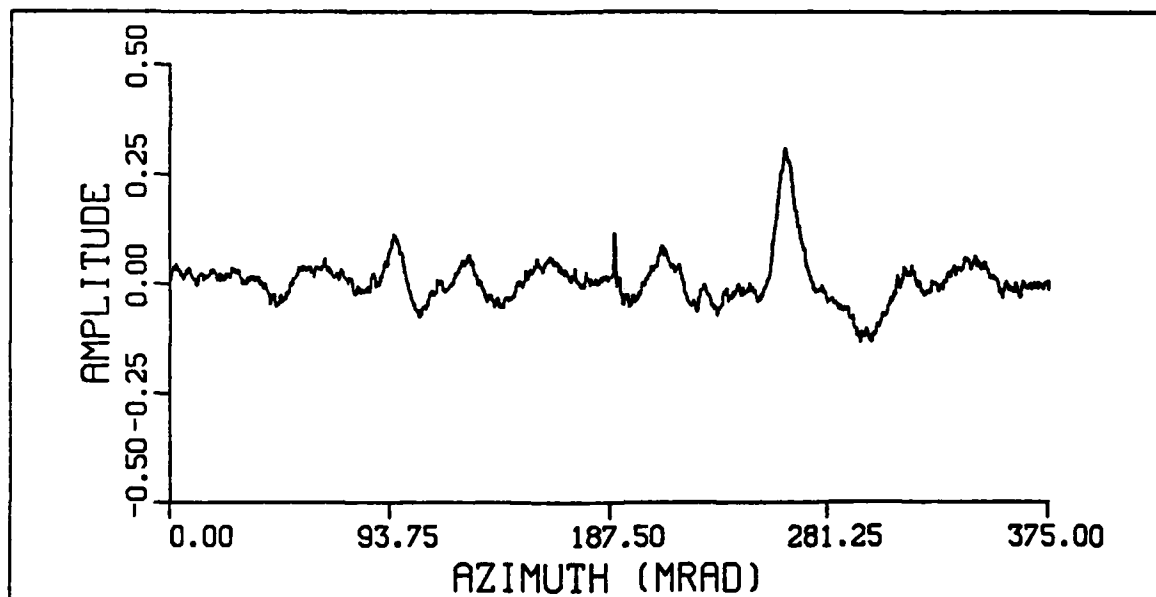


Figure 28. Unfiltered Output; BKDIII, TGTVI: TGTVI embedded in BKDIII;  
 $S/N = 1.95$ .

## 2. Filtered Outputs: Target Amplitude versus Noise Amplitude

Figure 29 on page 51 through Figure 32 on page 54 are plots of TGTI embedded in BKDI and filtered by LMS filters of increasing width; LMS6, LMS9, LMS12, and LMS15 respectively. It can be seen, by referring to the upper plot of each figure, that the amplitude of the target signal increases with filter width, as expected from the thresholding properties of the filters. However, the S/N ratio reaches a maximum when the filter's half-amplitude width most nearly matches the half-amplitude width of the target signal (Figure 30 on page 52).

Additionally, as the filter widens more and more noise is also allowed to pass, thereby reducing the S/N ratio. This increase in noise with filter width is displayed in the lower plot of each figure, which has been normalized to an amplitude of 1.0 to give a better illustration of the noise. It can be seen that the amplitudes of individual noise peaks begin to increase rapidly as the filter width increases past LMS9 (Figure 30 on page 52). Specifically, as the filter widths increase to LMS12 and LMS15 (Figure 31 on page 53 and Figure 32 on page 54), sharp peaks begin emerging from the background noise. These peaks are undesirable, in that they could be interpreted as false targets if the post-filter thresholding were set too low.

From studying these figures, it can be concluded that LMS9 results in the optimal output for BKDI. This filter not only amplifies TGTI to a level appropriate for detection and acquisition processing, but passes a minimal amount of noise, compared to filters of greater width.

Figure 36 on page 61 through Figure 39 on page 64, in Appendix A, are plots of TGTI embedded in BKDII and filtered by LMS6, LMS9, LMS12, and LMS15. Figure 40 on page 65 through Figure 43 on page 68, in Appendix A, are plots of TGTI embedded in BKDIII and filtered by LMS1, LMS3, LMS5, and LMS7. Using similar analysis on these figures, it can be concluded that LMS9 results in the optimal output for TGTI in BKDII, and LMS3 results in the optimal output for TGTI in BKDIII. However, before it is possible to consider LMS3 and LMS9 optimal filters for other targets in these backgrounds, it is necessary to look at the ability of these filters to amplify TGTII through TGTVI.

Referring back to Table 4 on page 45, Table 5 on page 45, and Table 6 on page 45, it can be seen that TGTI through TGTIII have optimal S/N ratios for LMS3 and LMS9, whereas TGTIV through TGTVI have optimal S/N ratios for LMS filters of greater width. However, the S/N ratios of TGTIV through TGTVI for LMS3 and LMS9 are very close in magnitude to the maximum S/N ratios for these targets, within

16% in the worst case. Therefore, it can be assumed that LMS3 and LMS9 will amplify all six targets to levels appropriate for post-filter processing.

To illustrate that this assumption is valid, plots of all target and background combinations, filtered with these proposed optimal filters, are included as Figure 44 on page 69 through Figure 61 on page 78 in Appendix B. As these plots illustrate, LMS3 and LMS9 effectively remove the DC offset and linear noise from the background clutter, and amplify the target signals for all background and target combinations. These resultant outputs can then be effectively used as inputs for target acquisition, designation, and tracking routines, for all target and background combinations similar to those used in this study.

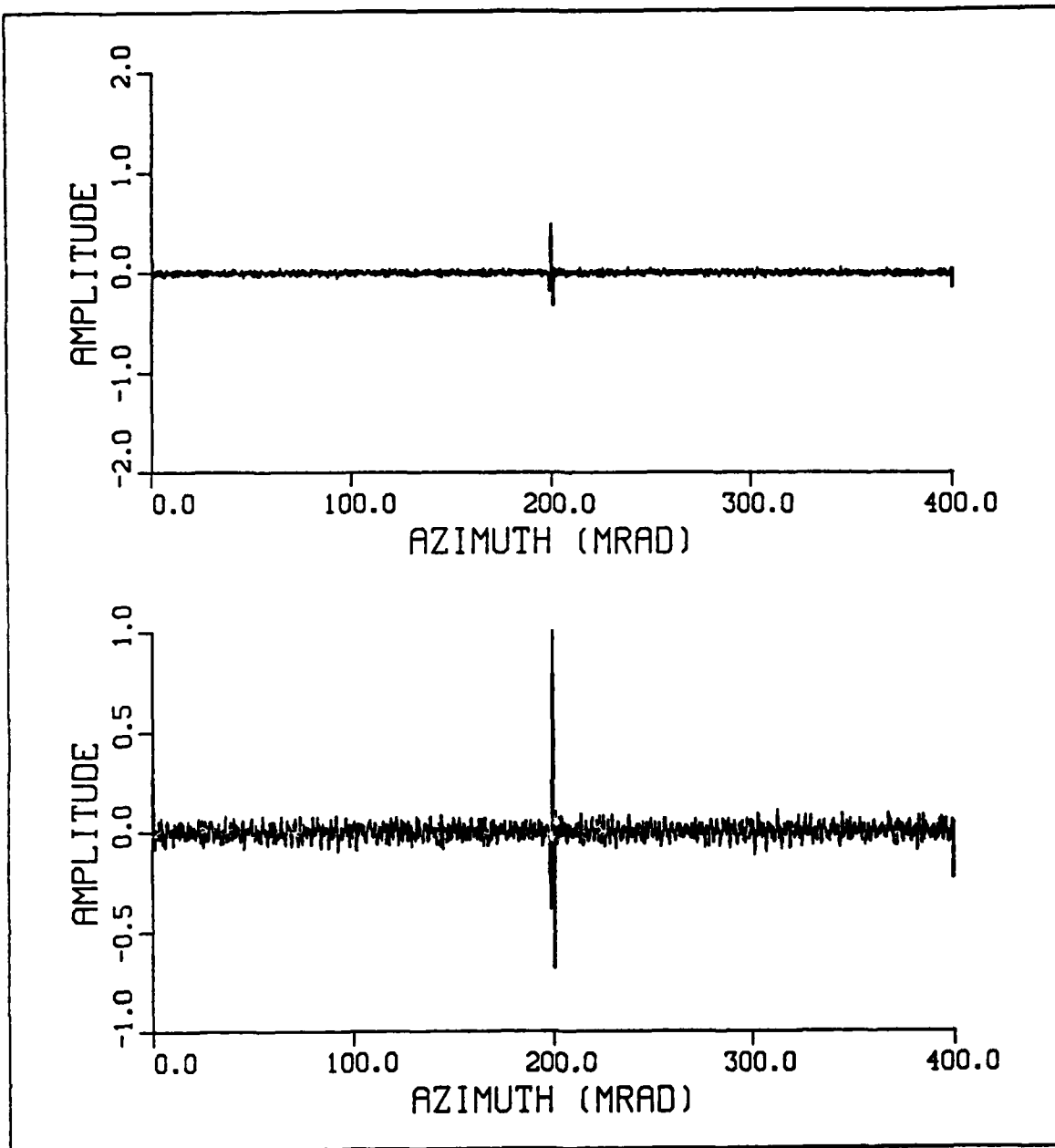


Figure 29. Filtered Output; BKDI, TGTI, LMS6: Upper plot, direct filter output; lower plot, normalized to peak amplitude of 1.0;  $S/N = 26.7$ .

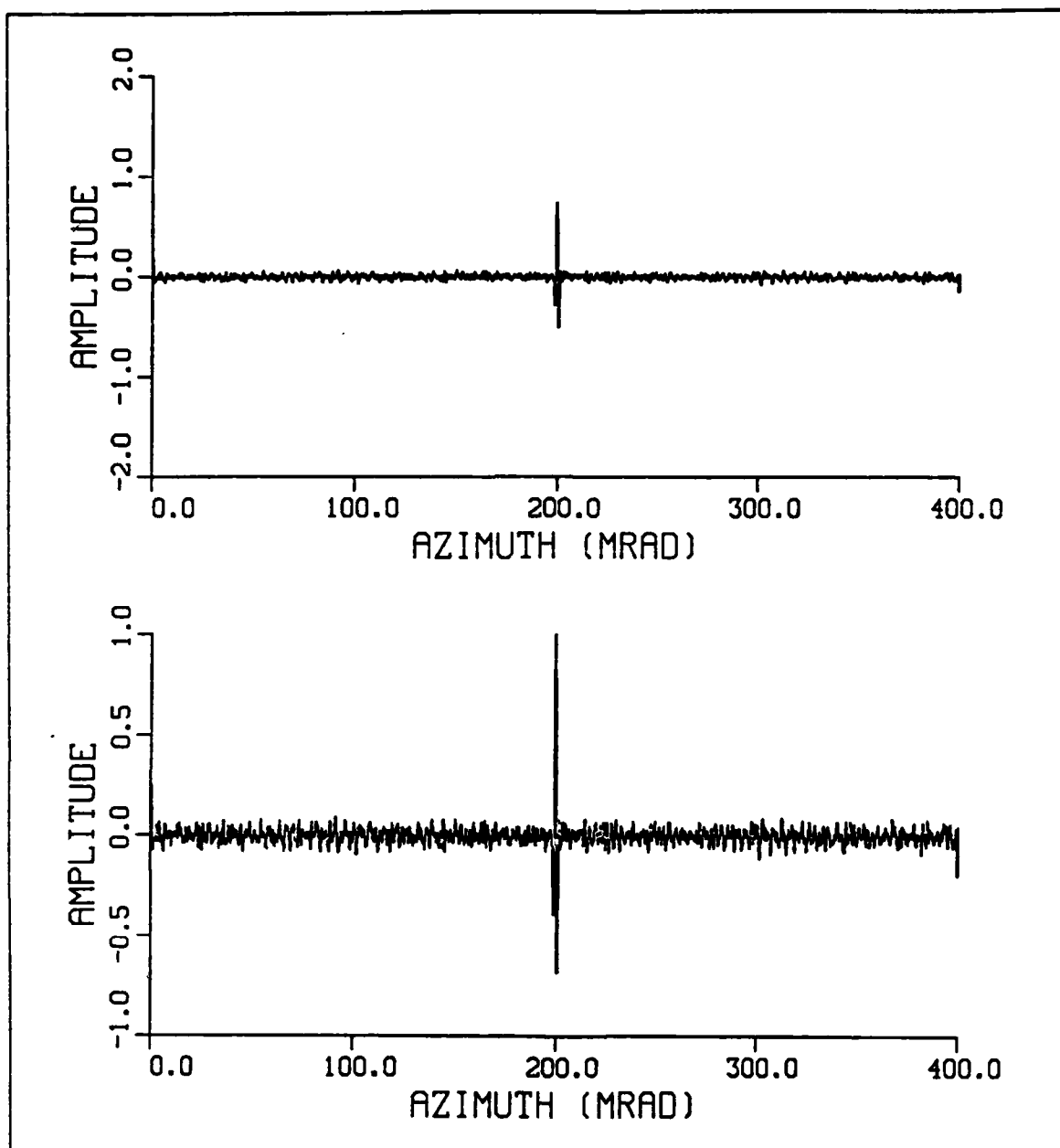


Figure 30. Filtered Output; BKDI, TGTI, LMS9: Upper plot, direct filter output; lower plot, normalized to peak amplitude of 1.0; S.N. = 29.7.

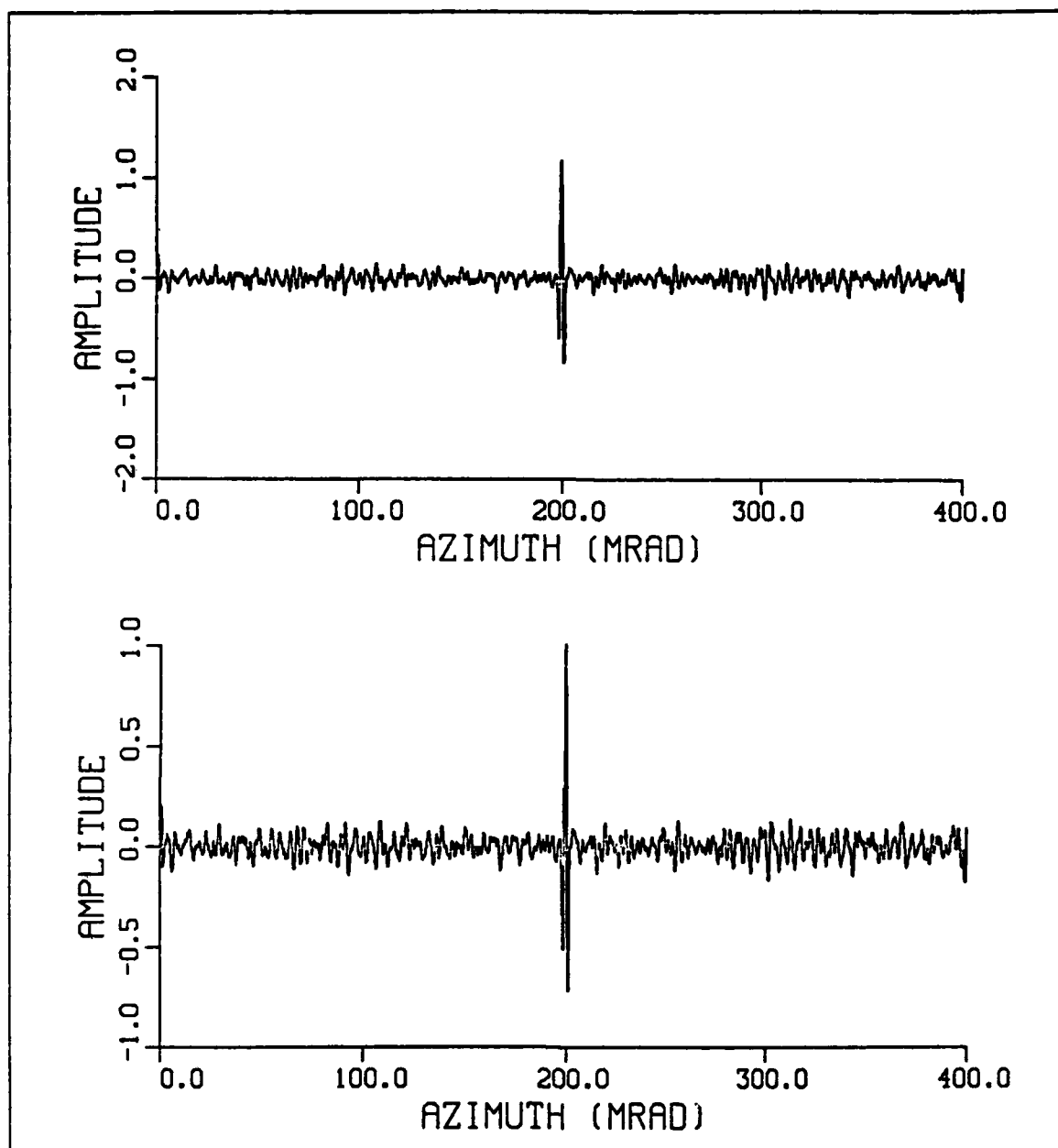
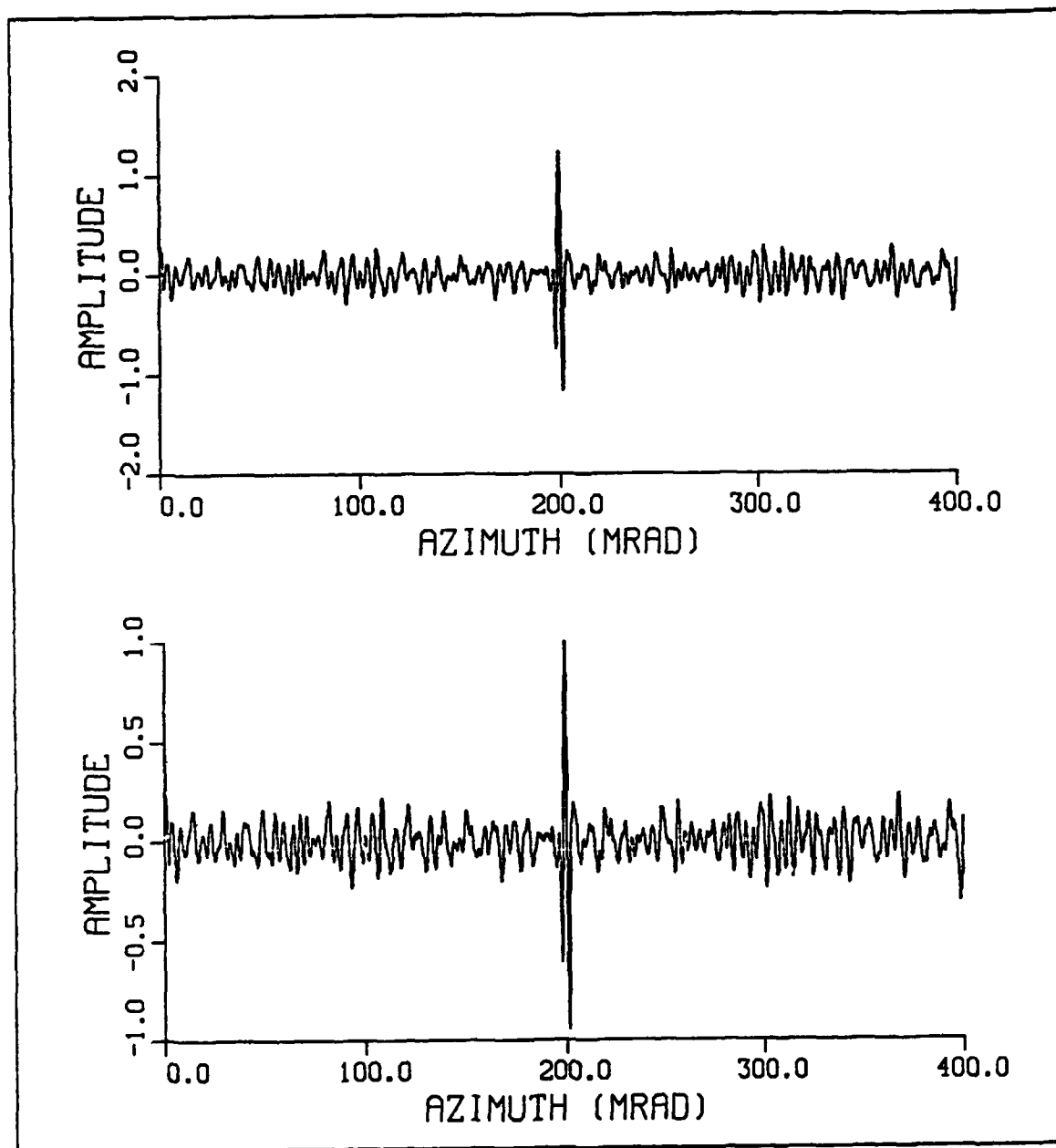


Figure 31. Filtered Output; BKDI, TGTI, LMS12: Upper plot, direct filter output; lower plot, normalized to peak amplitude of 1.0;  $S/N = 26.4$ .



**Figure 32.** Filtered Output; BKDI, TGTI, LMS15: Upper plot, direct filter output; lower plot, normalized to peak amplitude of 1.0;  $S/N = 21.6$ .



### 3. Filtered Outputs: Multiple Targets

Figure 33 is a plot of the filtered output of TGTI, TGTIV, and TGTV embedded in BKDI, and filtered with LMS9. Figure 34 on page 56 is a plot of the filtered output of TGTI, TGTIV, and TGTVI embedded in BKDIII, and filtered with LMS3. As these plots illustrate, LMS3 and LMS9 provide effective filtering of multiple targets of varying size, which is essential if they are to be used in a real environment.

### 4. Filtered Outputs: Real Background and Target

Figure 35 on page 57 is a plot of real IRSTD output data obtained during system calibration [Ref. 2]. The upper plot shows the unfiltered output as the system was scanned across the roof of Spanagel Hall at NPS Monterey. The lower plot shows the effect of LMS3 on the raw system output. As illustrated, the background contains many clutter sources, in addition to sky, and LMS3 proves to be extremely effective in removing them all, as well as filtering out the whip antenna target (TGTVI). This filtered output clearly illustrates the potential of the LMS filter as an effective signal processing filter for the IRSTD system.

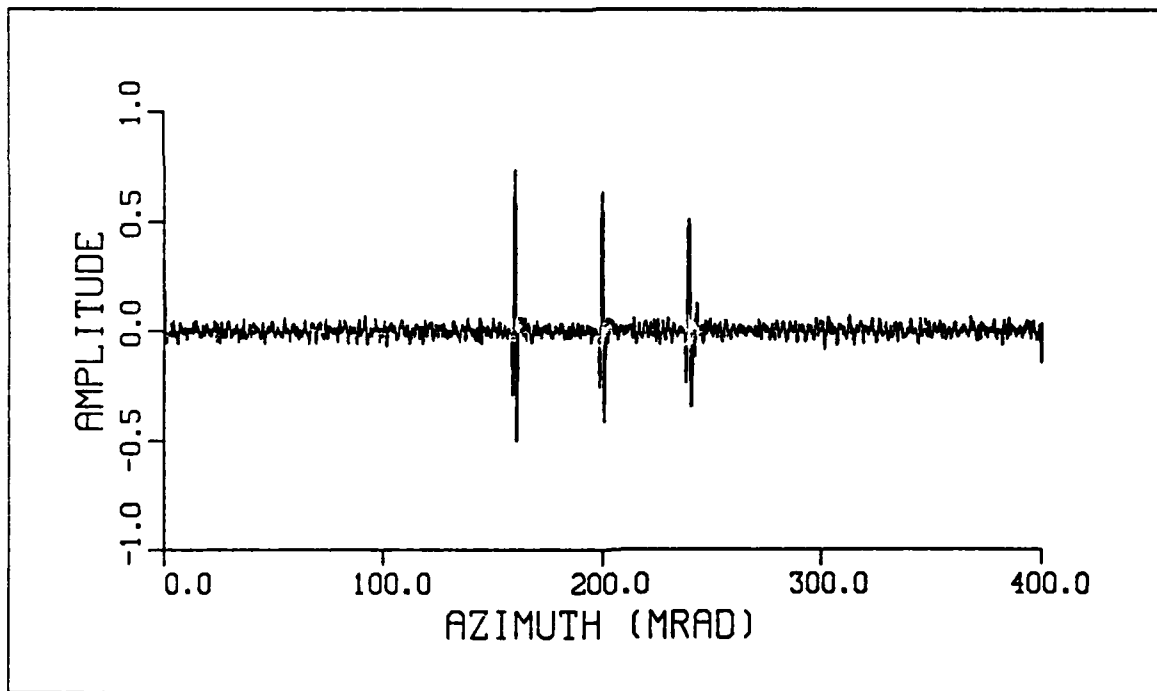


Figure 33. Filtered Output; Multiple Targets: TGTI, TGTIV, and TGTV embedded in BKDI and filtered with LMS9.

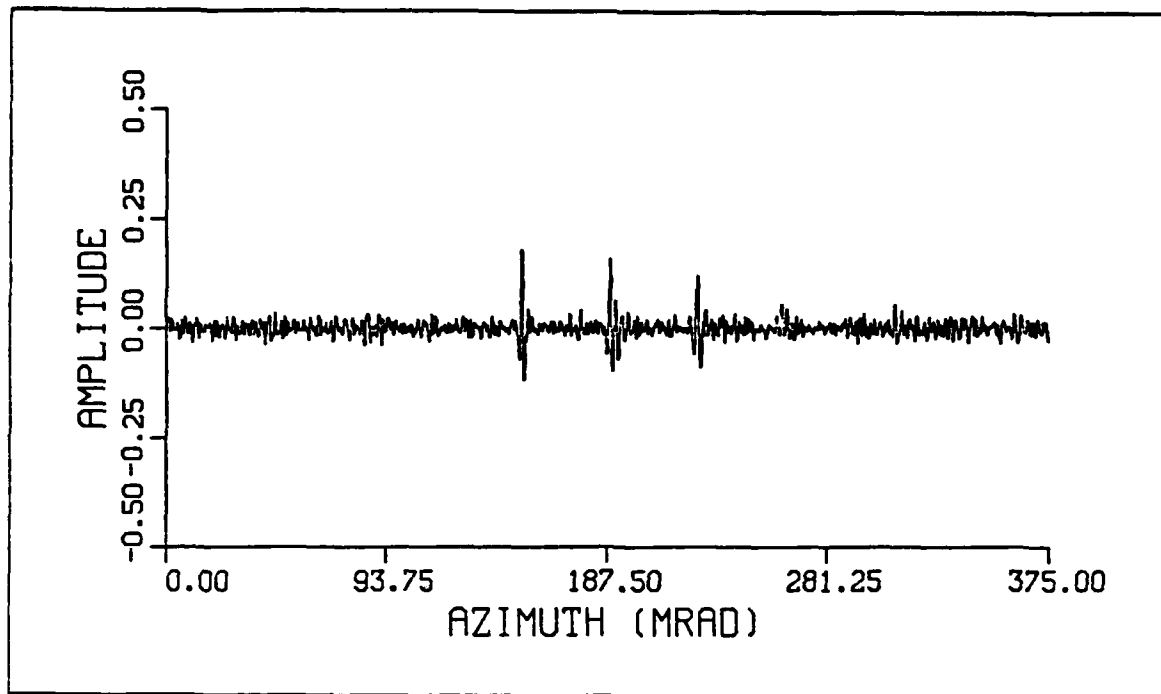


Figure 34. Filtered Output; Multiple Targets: TGTI, TGTIV, and TGTVI embedded in BKDIII and filtered with LMS3.

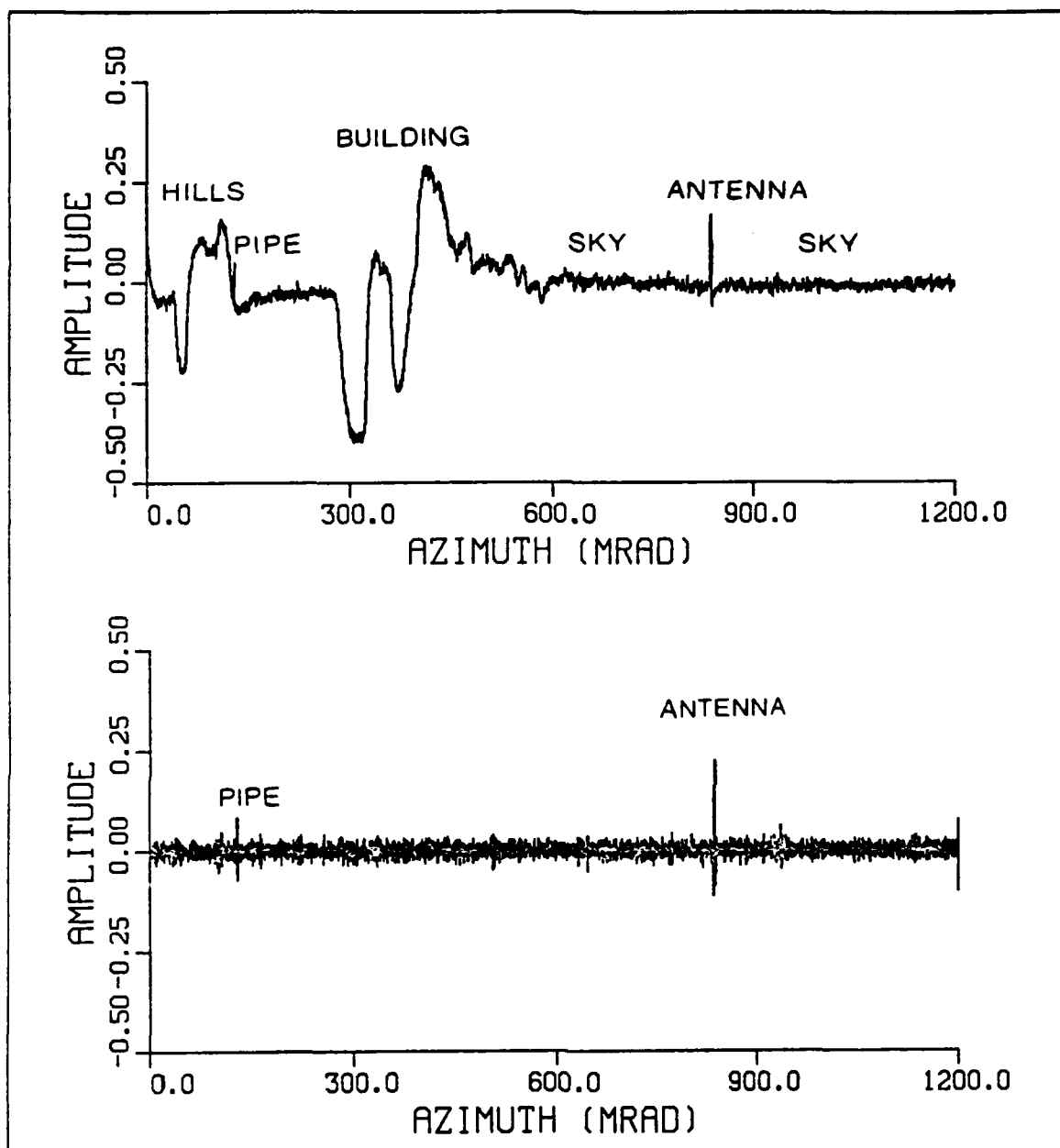


Figure 35. Real Output: Upper plot, unfiltered output; lower plot, filtered with LMS3.

## VII. CONCLUSIONS AND RECOMMENDATIONS

### A. CONCLUSIONS

From the results of Chapter VI, it can be assumed that LMS9 and LMS3 are the optimal LMS filters for extracting point and near-point targets from the simulated and real IR backgrounds respectively. This difference in optimal filters for the simulated and real backgrounds is due to the fact that the simulated background was sampled at 0.10472 mrad sample, whereas the real background was sampled at 0.31416 mrad sample. Therefore, these optimal filters were generated from a raised cosine function with a half-amplitude width of 0.9 mrad, sampled at 0.1 mrad sample for LMS9 and 0.3 mrad sample for LMS3. This result corresponds with prefiltering studies on the half-amplitude width of the target signals, and is an indication that the raised cosine target model is appropriate for these targets.

It should also be noted that the results of this investigation can be used with standard inputs, independent of the local background, whereas other approaches [Refs. 9, 13] require a priori knowledge of the background structure.

Since the LMS filter is very simple and takes minimal processing time, it is ideally suited for implementation as an initial filter for the NPS IRSTD system. Additionally, since the output of the IRSTD system consists of digitized detector outputs from an array of 90 detectors, it is natural to consider extending this filtering technique to two-dimensions. However, since the output signal is digitized at 0.10472 mrad per sample in the azimuth direction, and the detector dimensions are 2.0 mrad in the elevation direction, the resolution of the two-dimensional output signal can be considered to be 0.10472 mrad by 2.0 mrad per data point. Considering this order of magnitude difference in the resolution of the two directions of the two-dimensional signal, and the fact that the point and near-point targets studied have half-amplitude widths of approximately 0.9 mrad, it can be seen that filtering in the elevation direction would necessitate the use of an LMS filter generated from a model target function with a half-amplitude width to sampling time ratio of one ( $\frac{t_d}{t_s} = 1$ ). Therefore, a suitable two-dimensional LMS filter model target function would have to be developed from a two-dimensional Gaussian distribution or a raised Bessel function defined over its first period of oscillation. In addition, either model target function would have to be constructed in such a manner that  $\frac{t_d}{t_s} = 9$  in the azimuth direction and  $\frac{t_d}{t_s} = 1$  in the elevation direction.

Although developing and implementing such a filter is feasible, the processing time required for performing 90 one-dimensional filtering operations over  $N$  elements, is comparable with the processing time required for performing one two-dimensional filtering operation over 90 by  $N$  elements (2.14 vice 2.03 seconds respectively). Therefore, it is advisable to implement this filtering technique in its simplest, or one-dimensional, form.

## **B. RECOMMENDATIONS**

It is recommended that the following studies be conducted on the NPS IRSTD system:

- Incorporate LMS9 as an initial signal processing filter on the output of the lead detector array of the IRSTD system.
- Follow LMS9 with an automatic target acquisition routine.
- Study the outputs of this automatic target acquisition routine to optimize target false alarm rates.
- Study the outputs of various hypothesis testing techniques [Ref. 14 ], to further discriminate between true targets (missiles and aircraft), and false targets (birds, high frequency noise, background discontinuities, etc.).
- Develop a filtering technique for extracting extended targets ( $t_d > 1.5$  mrad) from background clutter.
- Incorporate this extended target filter into the IRSTD system, to filter the outputs from the lag detector array. This would give the system two different outputs for each scan.
- Study the potential for imaging the extended targets, with the intention of developing ship-type recognition techniques.

It is believed that much groundwork for further studies with the NPS IRSTD system has been laid by this thesis. Follow-on studies of the types listed above are both feasible and important, as the U.S. Navy has great need for an effective passive IR system capable of detecting and tracking air and surface targets.

## **APPENDIX A. FILTERED OUTPUTS: TARGET AMPLITUDE VERSUS NOISE AMPLITUDE**

Figure 36 on page 61 through Figure 43 on page 68 are plots of filtered outputs of TGTI embedded in BKDII and BKDIII. BKDII was filtered by LMS6, LMS9, LMS12, and LMS15, and BKDIII was filtered by LMS1, LMS3, LMS5, and LMS7. It can be seen, by referring to the upper plot of each figure, that the amplitude of the target signal increases with filter width, as expected from the thresholding properties of the filters. However, the S/N ratio reaches a maximum when the filter's half-amplitude width most nearly matches the half-amplitude width of the target signal (Figure 37 on page 62 and Figure 41 on page 66).

Additionally, as the filter widens more and more noise is also allowed to pass, thereby reducing the S/N ratio. This increase in noise with filter width is displayed in the lower plot of each figure, which has been normalized to an amplitude of 1.0 to give a better illustration of the noise. It is clear, from these figures, that the noise amplitude increases rapidly with filter width, and contains sharp peaks which could be interpreted as false targets if post-filter thresholding were set too low.

From studying these figures, it can be concluded that LMS9 results in the optimal output for BKDII, and LMS3 results in the optimal output for BKDIII. These filters not only amplify TGTI to levels appropriate for detection and acquisition processing, but pass a minimal amount of noise, compared to filters of greater width.

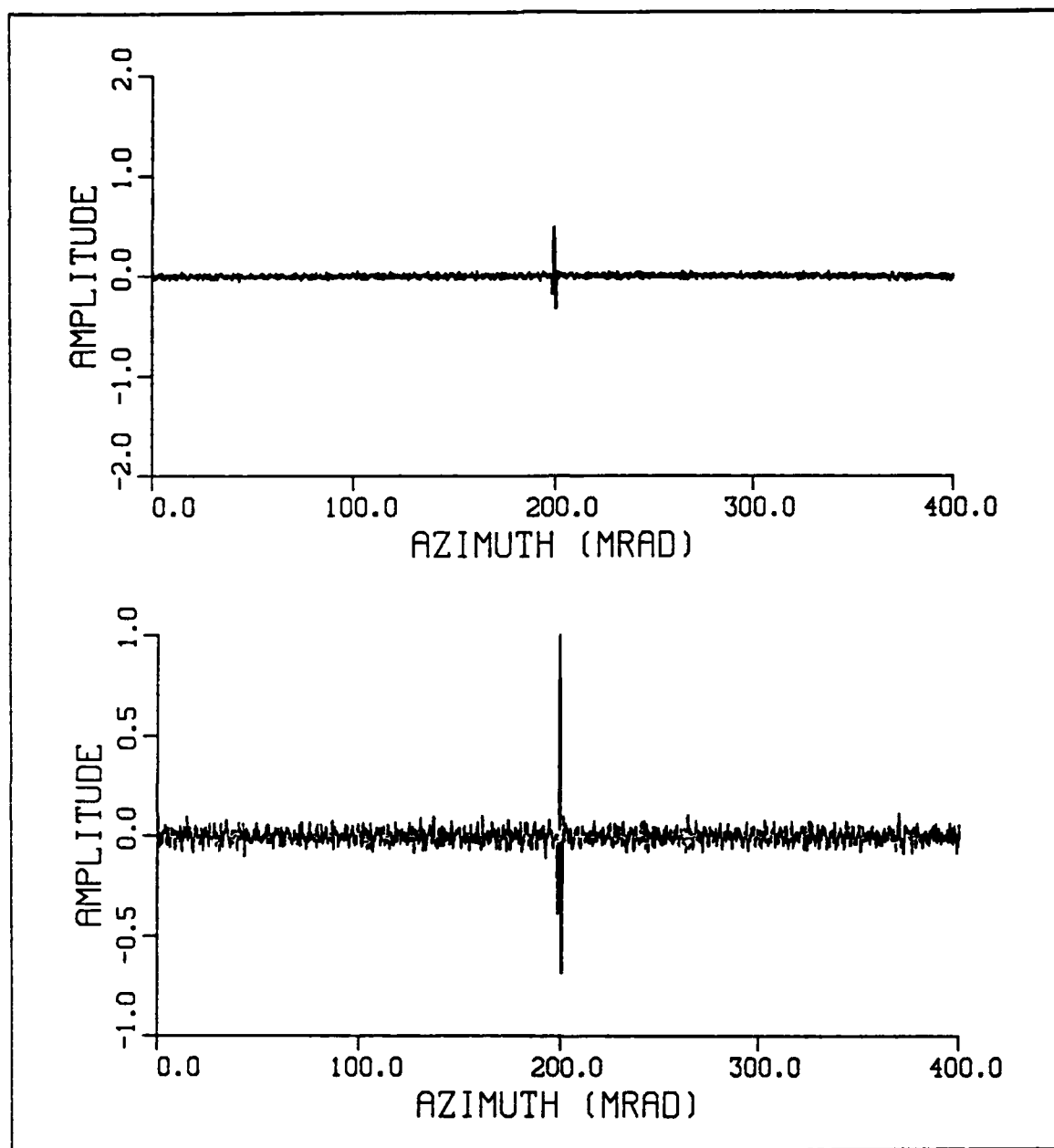


Figure 36. Filtered Output; BKDII, TGTI, LMS6: Upper plot, direct filter output; lower plot, normalized to peak amplitude of 1.0;  $S/N = 28.9$ .

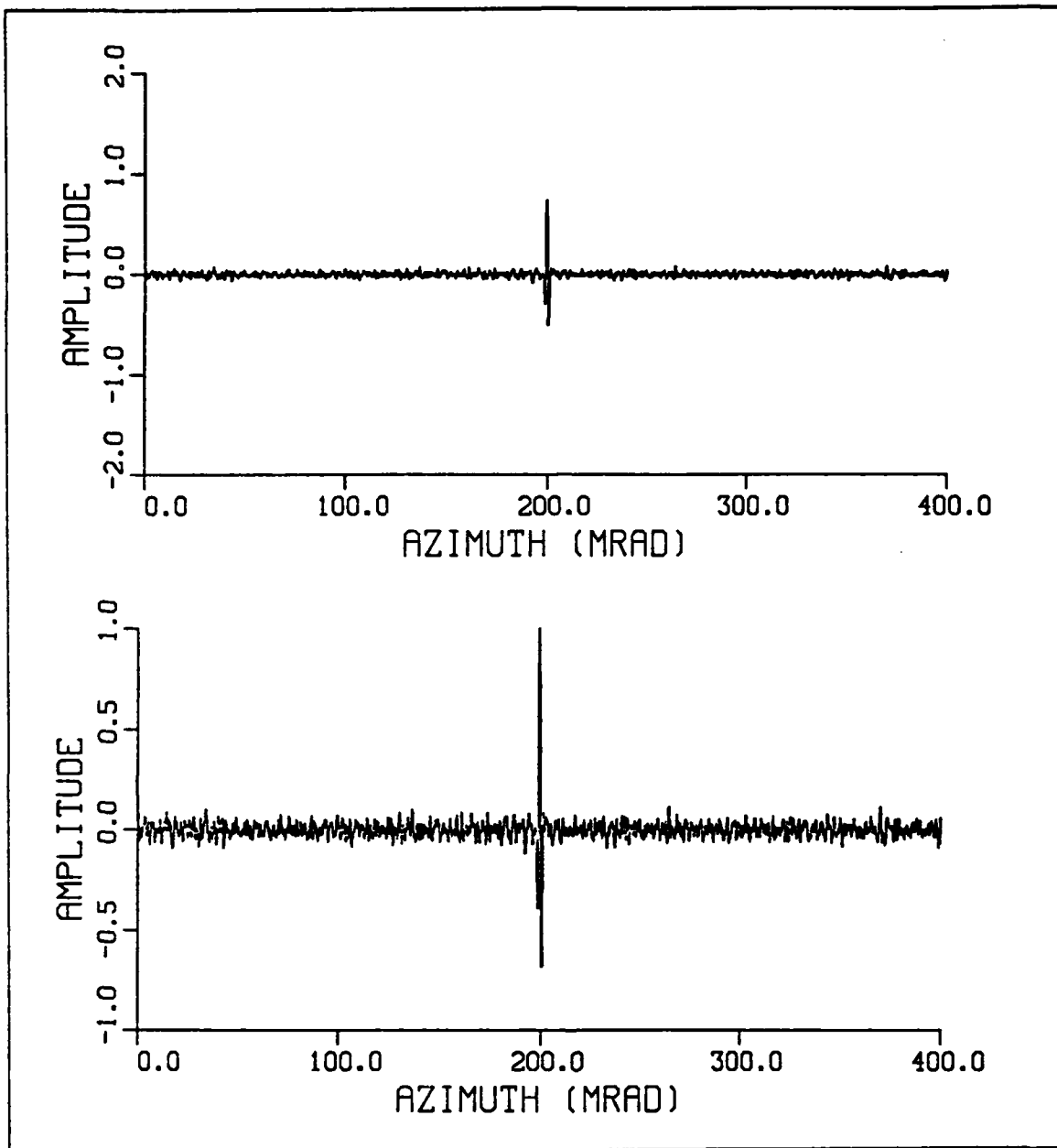


Figure 37. Filtered Output; BKDII, TGTI, LMS9: Upper plot, direct filter output; lower plot, normalized to peak amplitude of 1.0; S/N = 32.2.



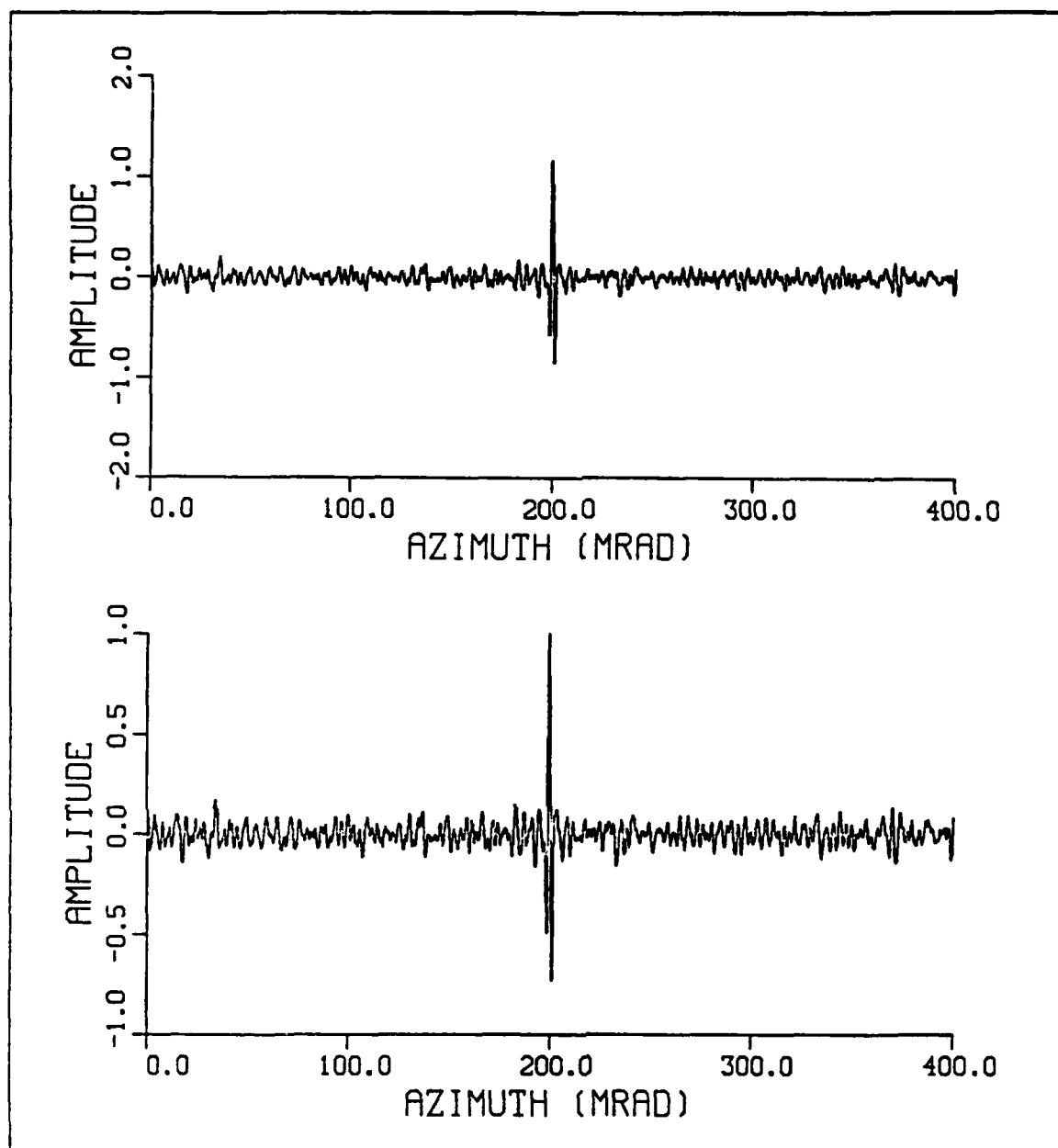


Figure 38. Filtered Output; BKDII, TGTI, LMS12: Upper plot, direct filter output; lower plot, normalized to peak amplitude of 1.0; S.N. = 28.0.

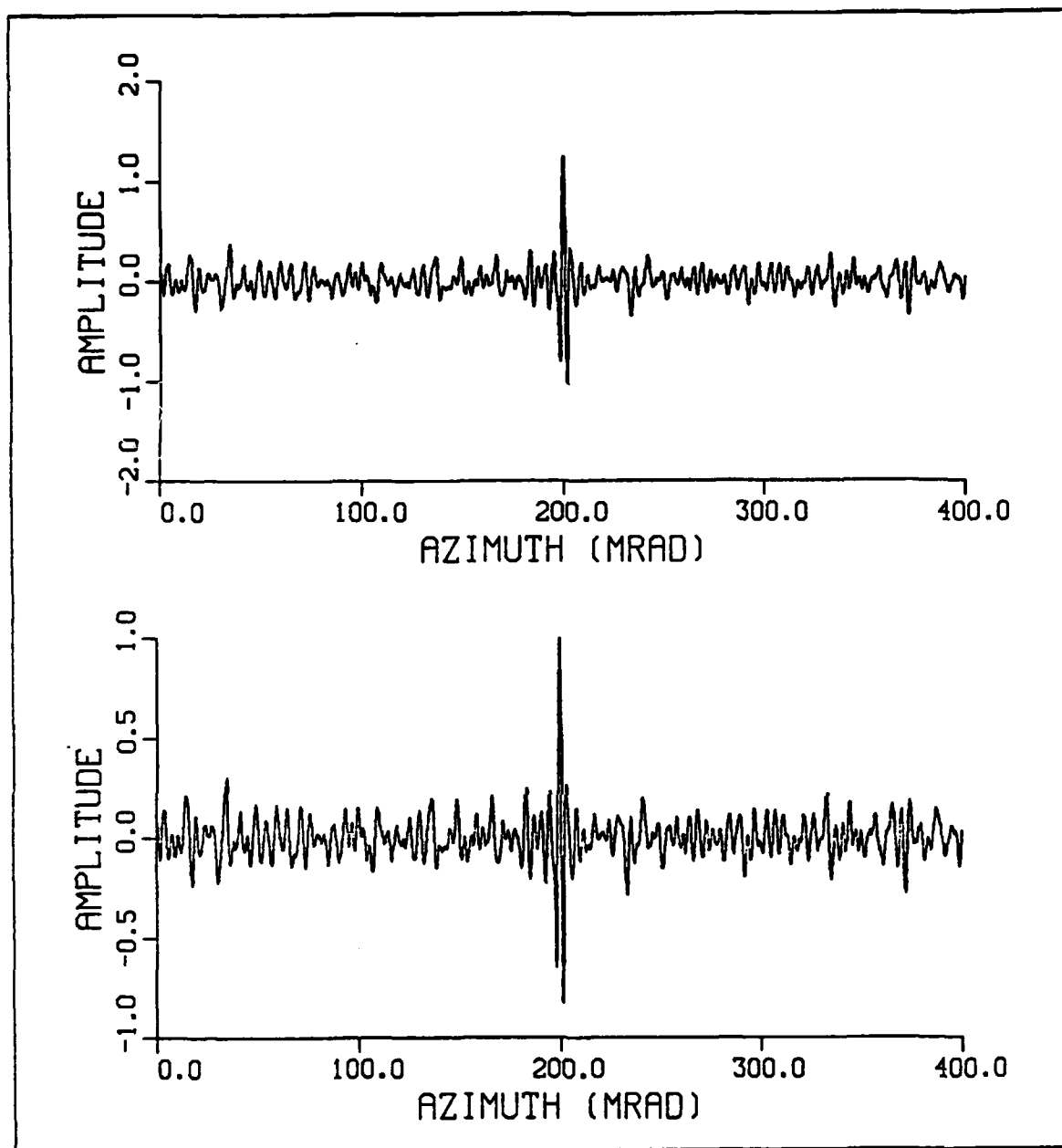


Figure 39. Filtered Output; BKDII, TGTI, LMS15: Upper plot, direct filter output; lower plot, normalized to peak amplitude of 1.0;  $S/N = 21.6$ .

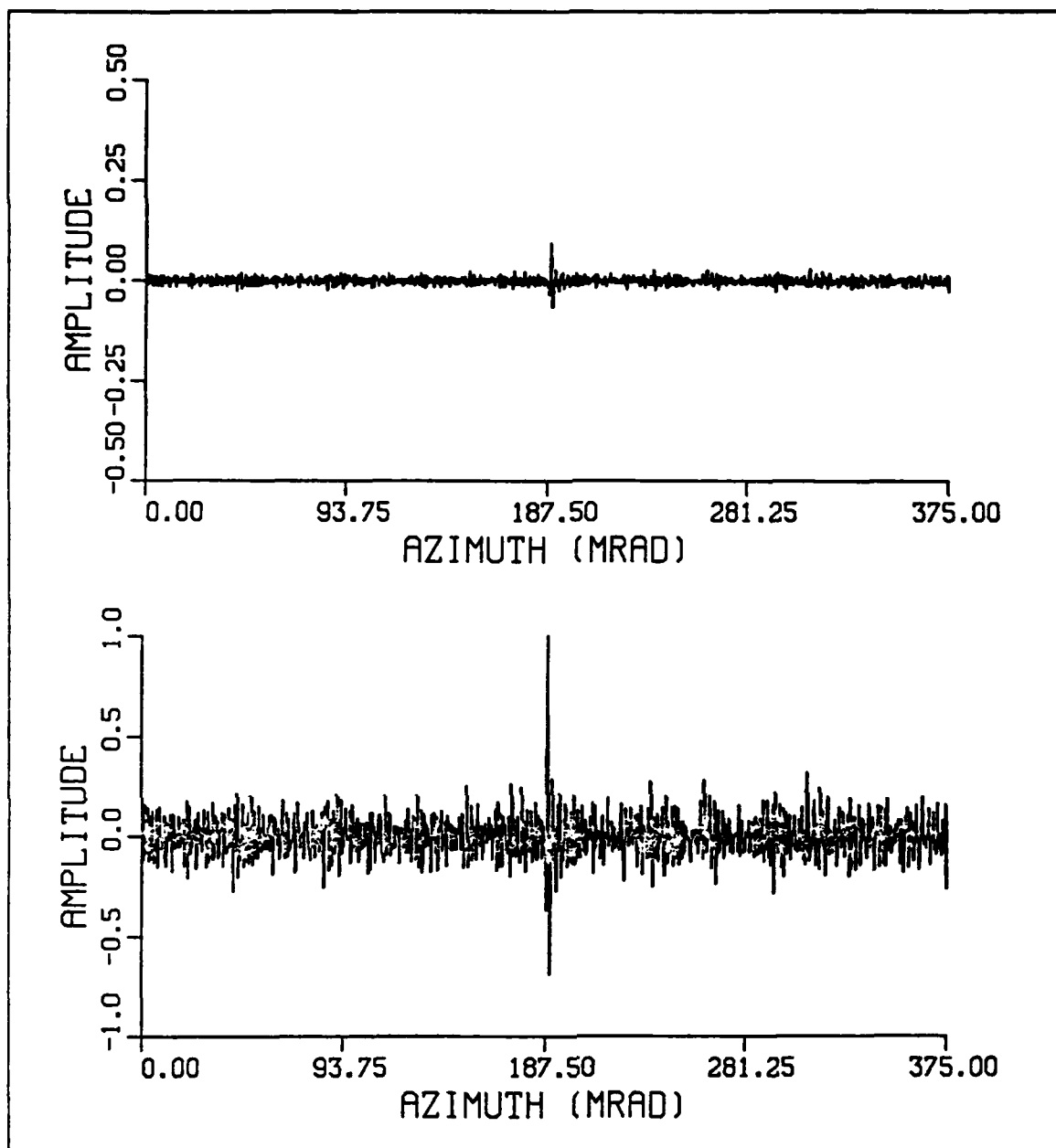


Figure 40. Filtered Output; BKDIII, TGTI, LMSI: Upper plot, direct filter output; lower plot, normalized to peak amplitude of 1.0;  $S/N = 8.1$ .

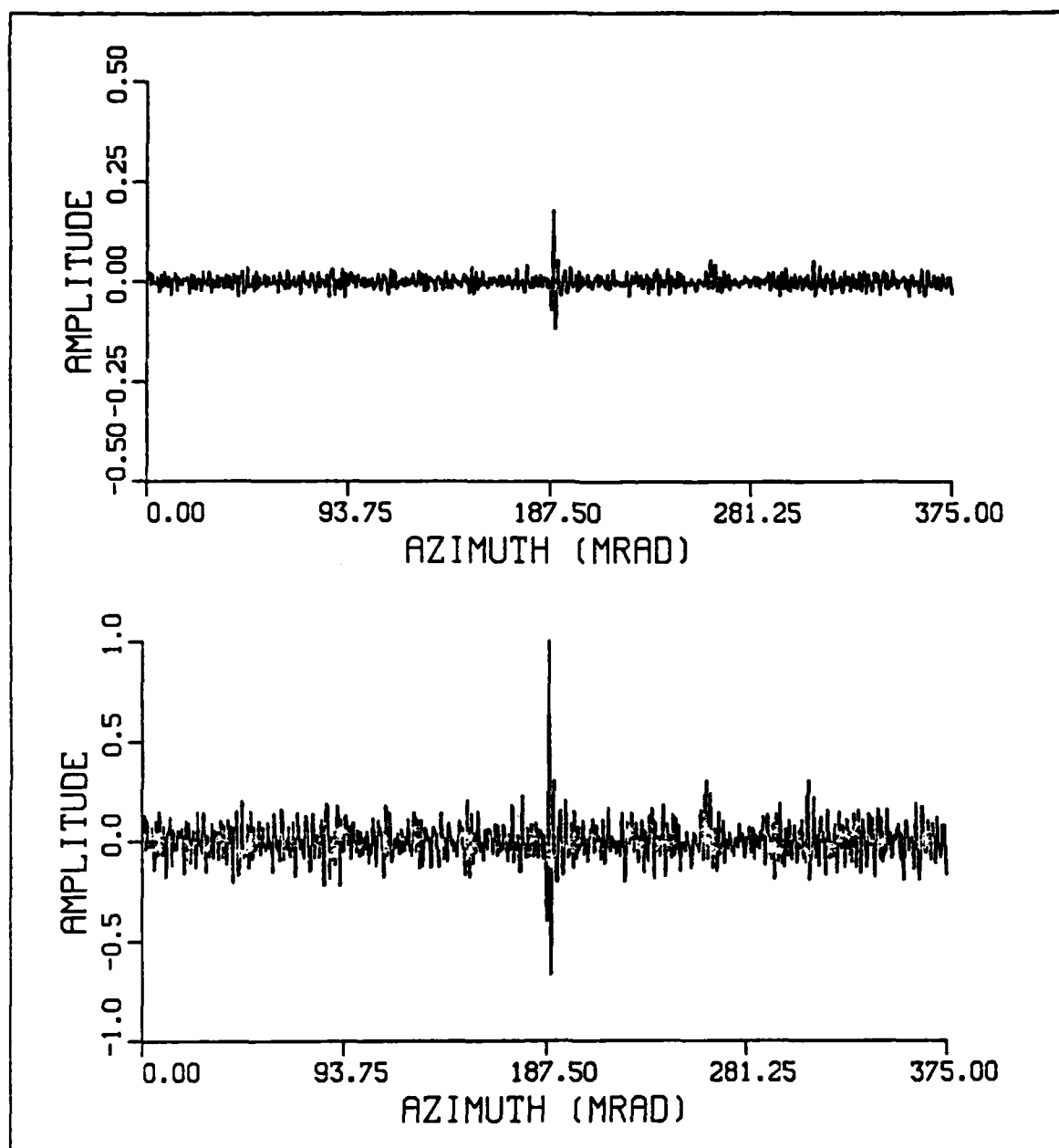


Figure 41. Filtered Output; BKDIII, TGTI, LMS3: Upper plot, direct filter output; lower plot, normalized to peak amplitude of 1.0;  $S/N = 12.7$ .

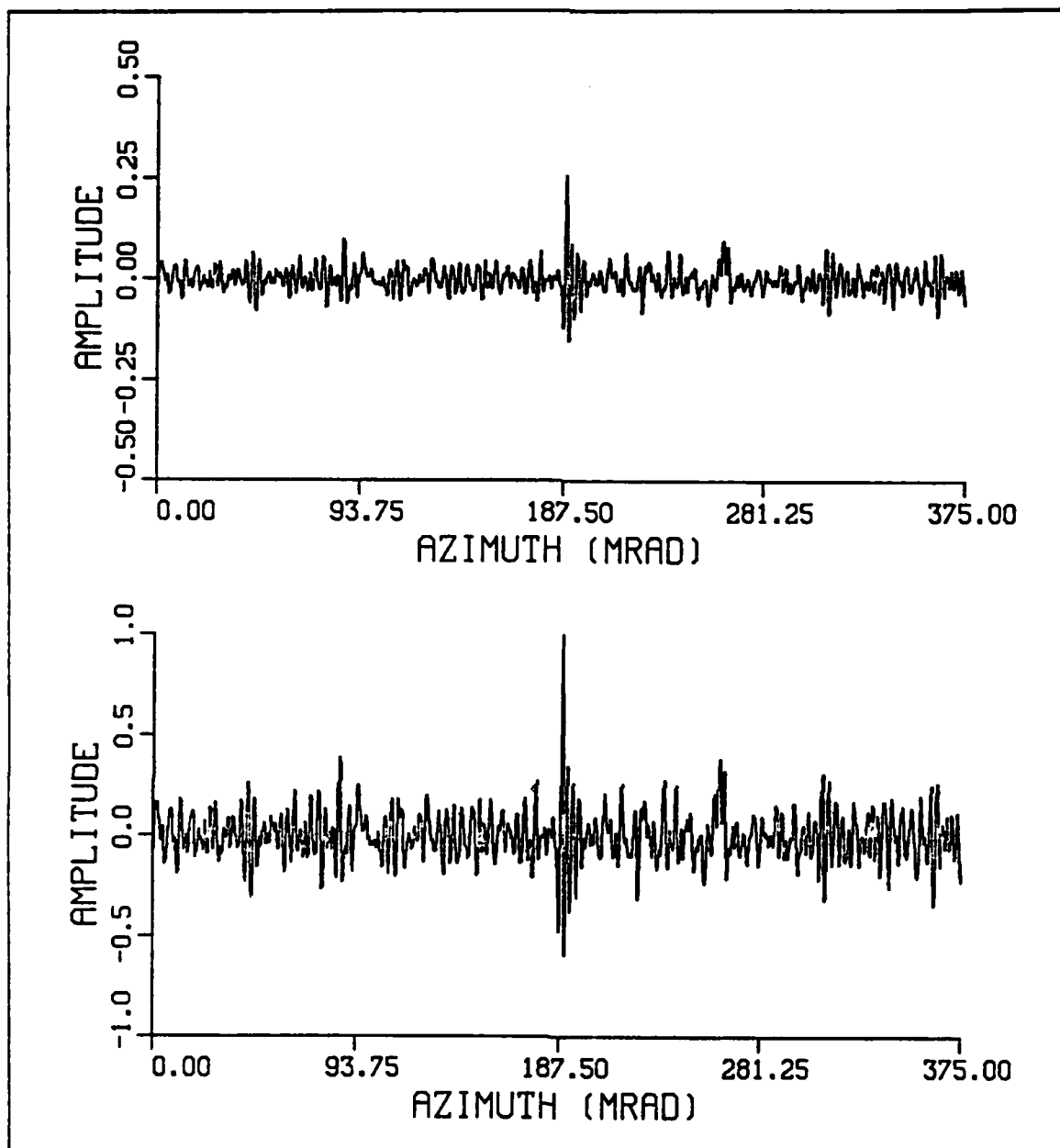


Figure 42. Filtered Output; BKDIII, TGTI, LMS5: Upper plot, direct filter output; lower plot, normalized to peak amplitude of 1.0;  $S/N = 10.3$ .

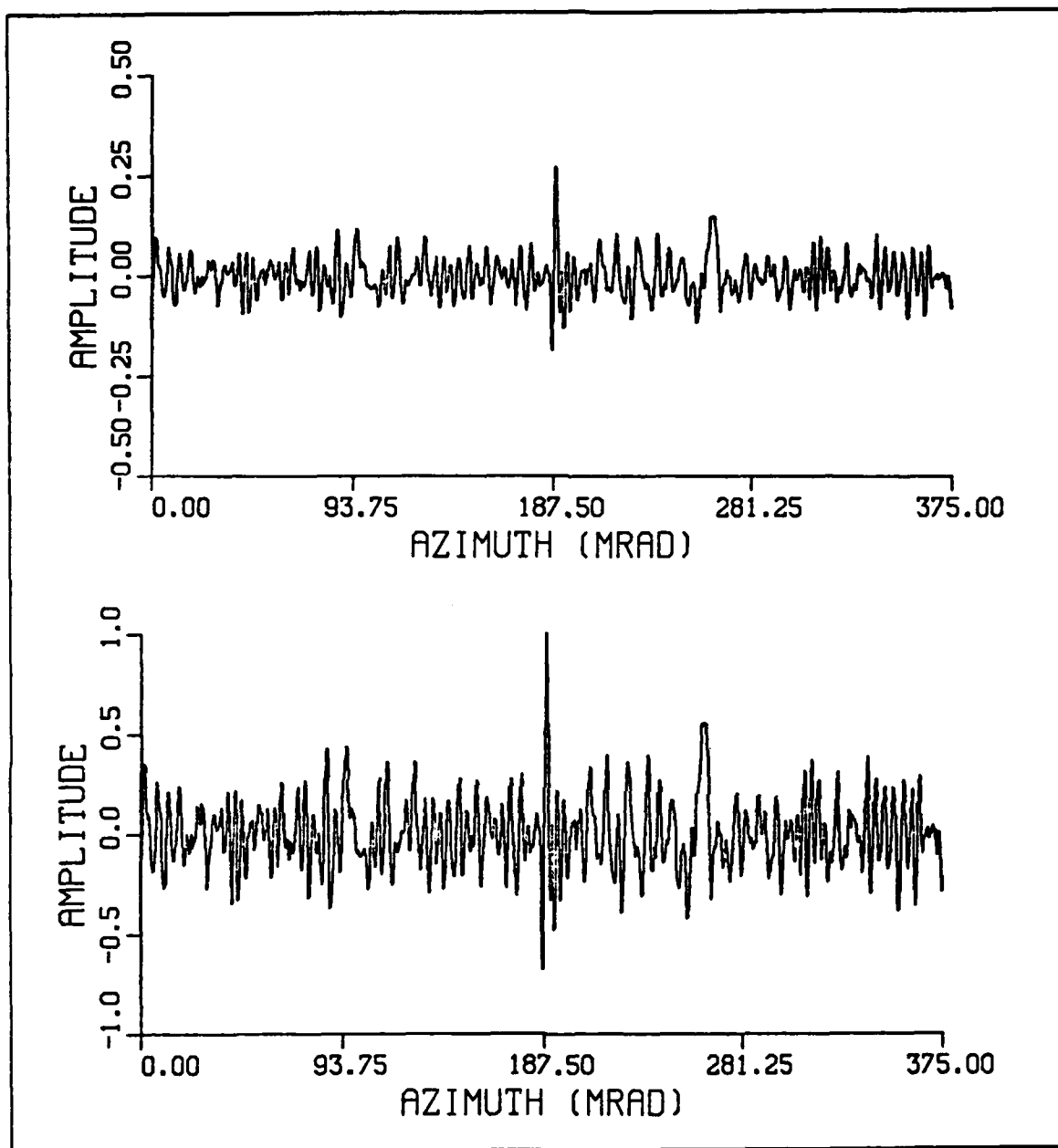


Figure 43. Filtered Output; BKDIII, TGTI, LMS7: Upper plot, direct filter output; lower plot, normalized to peak amplitude of 1.0;  $S/N = 7.6$ .

## APPENDIX B. FILTERED OUTPUTS: OPTIMAL LMS FILTERS

Figure 44 through Figure 61 on page 78 are plots of the filtered outputs of all background and target combinations filtered with their proposed optimal filters, LMS3 and LMS9. As these plots illustrate, these filters effectively remove the DC offset and linear noise from the background clutter, and amplify the target signals for all background and target combinations. These resultant outputs, can be effectively used as inputs for target acquisition, designation, and tracking routines.

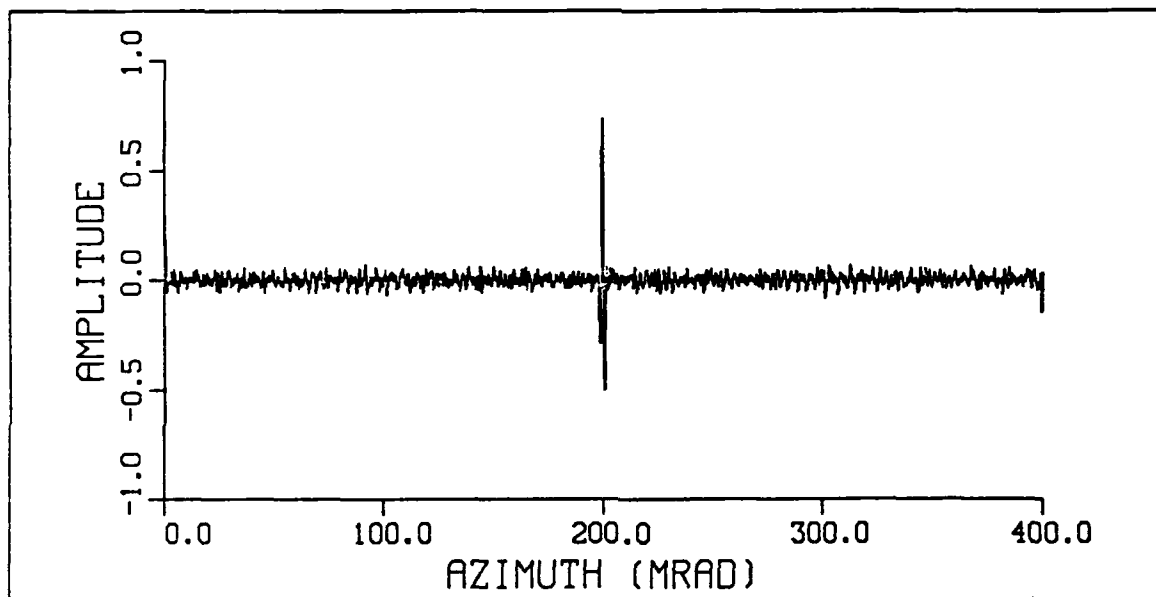


Figure 44. Filtered Output; BKDI, TGTI, LMS9: TGTI embedded in BKDI and filtered by LMS9; S/N = 29.7.

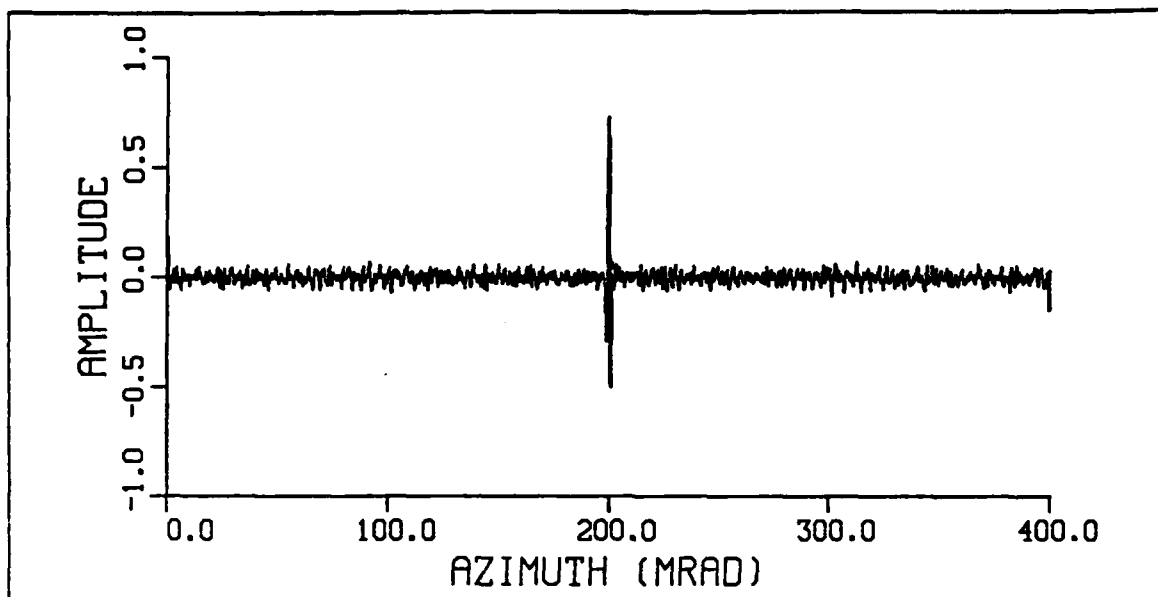


Figure 45. Filtered Output; BKDI, TGTII, LMS9: TGTII embedded in BKDI and filtered by LMS9;  $S/N = 29.8$ .

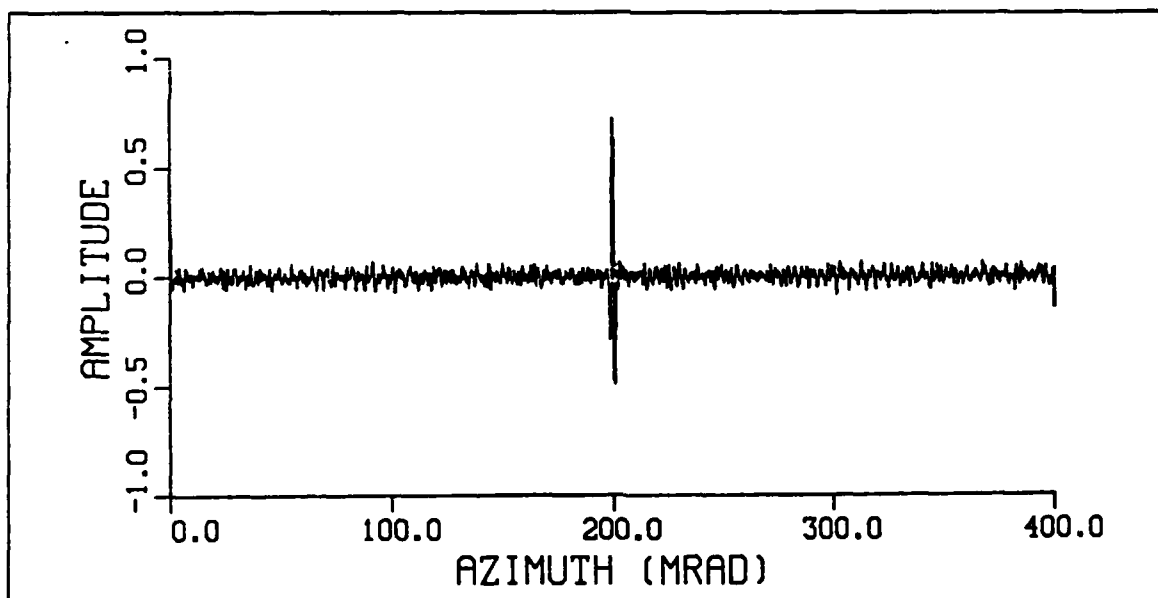


Figure 46. Filtered Output; BKDI, TGTIII, LMS9: TGTIII embedded in BKDI and filtered by LMS9;  $S/N = 29.2$ .



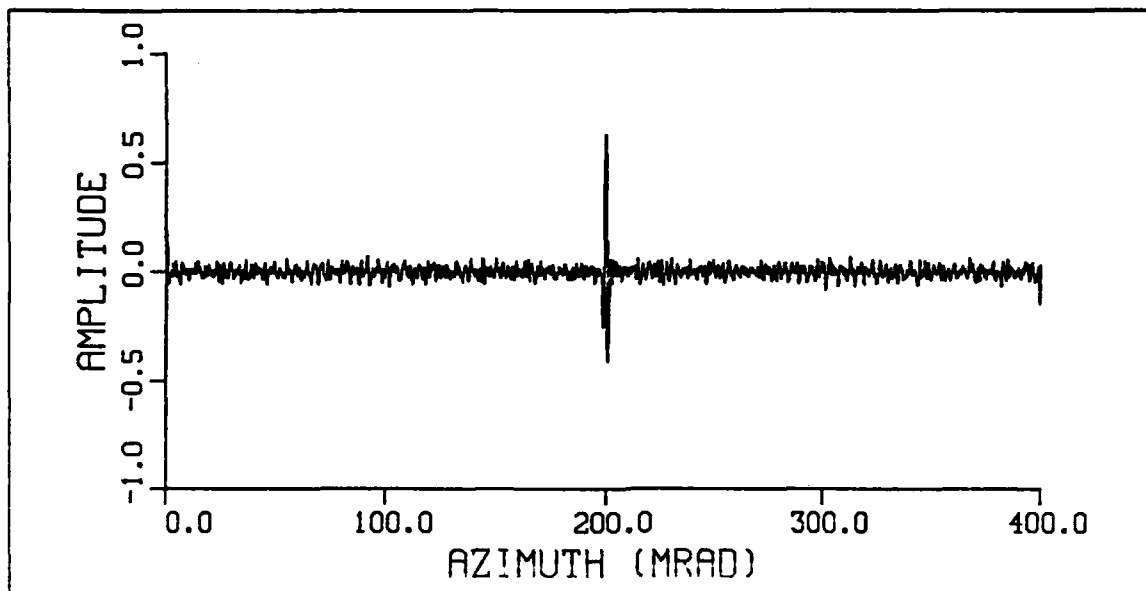


Figure 47. Filtered Output; BKDI, TGTIV, LMS9: TGTIV embedded in BKDI and filtered by LMS9;  $S/N = 25.2$ .

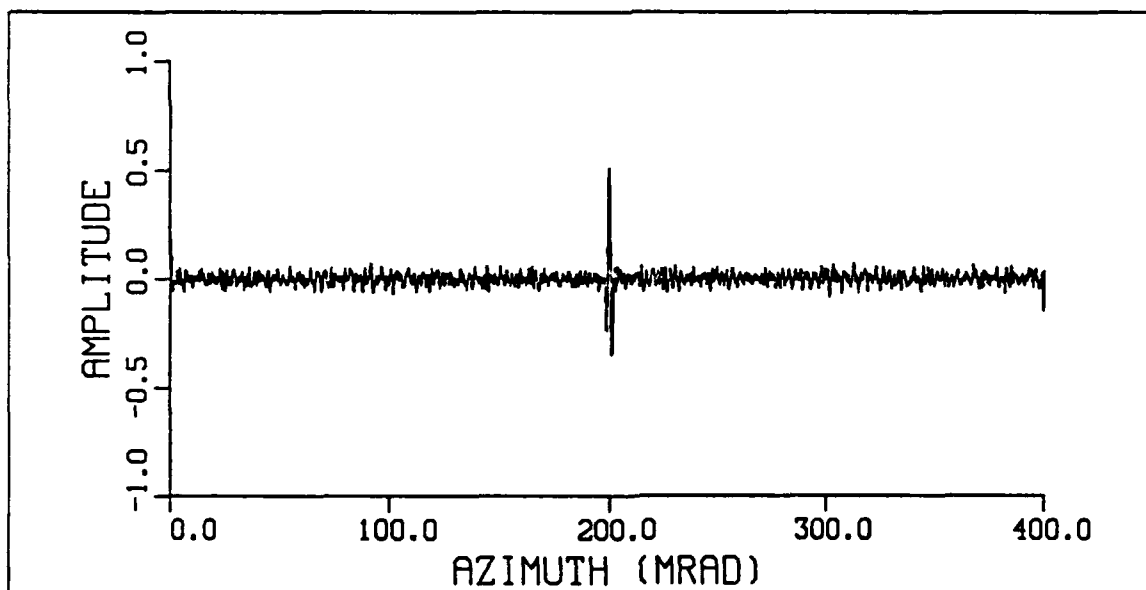


Figure 48. Filtered Output; BKDI, TGTIV, LMS9: TGTIV embedded in BKDI and filtered by LMS9;  $S/N = 21.0$ .

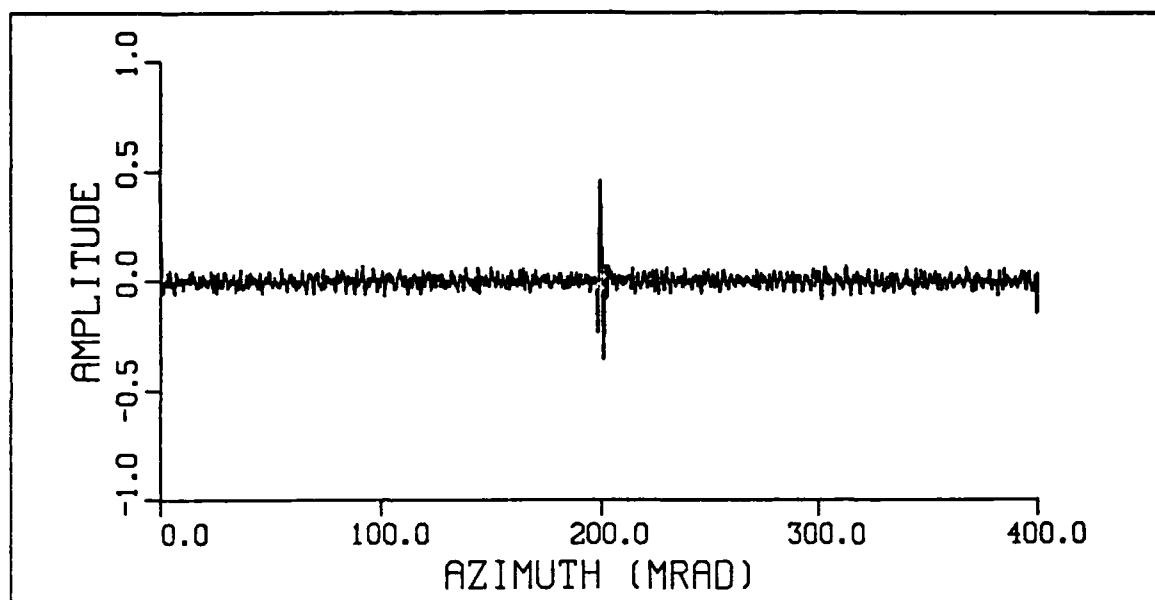


Figure 49. Filtered Output; BKDI, TGTVI, LMS9: TGTVI embedded in BKDI and filtered by LMS9;  $S/N = 20.4$ .

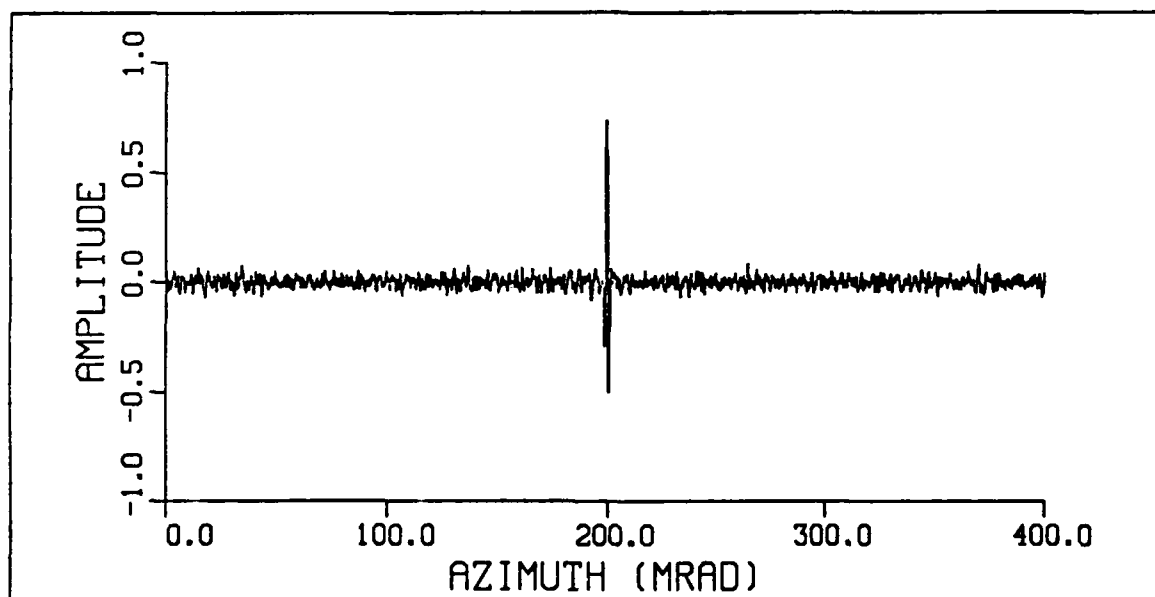


Figure 50. Filtered Output; BKDI, TGTI, LMS9: TGTI embedded in BKDI and filtered by LMS9;  $S/N = 32.2$ .

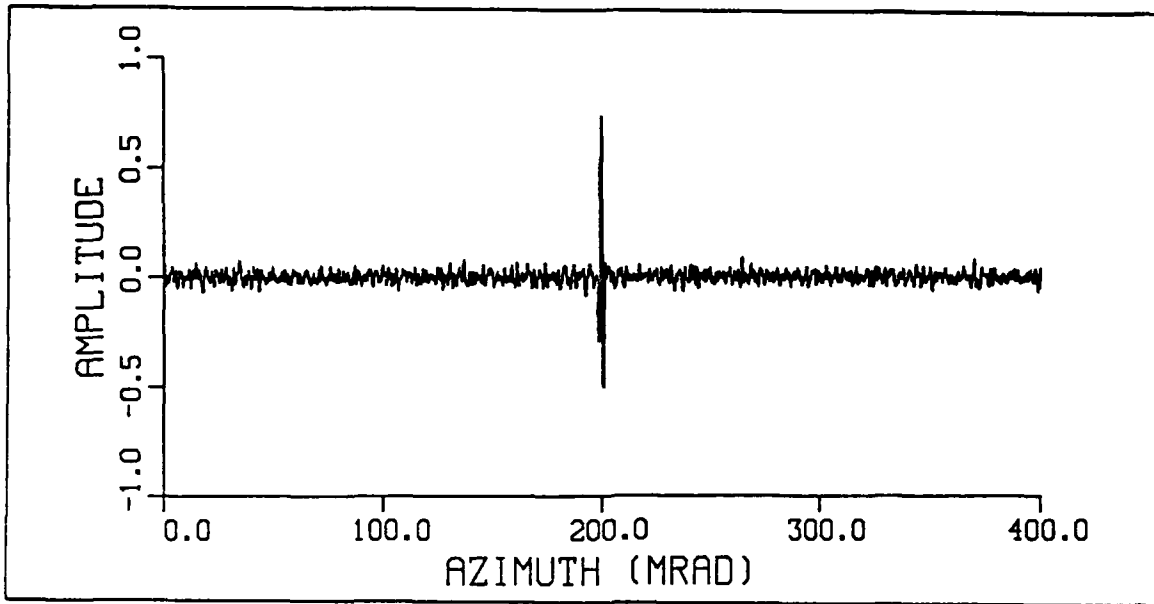


Figure 51. Filtered Output; BKDII, TGTII, LMS9: TGTII embedded in BKDII and filtered by LMS9;  $S/N = 32.3$ .

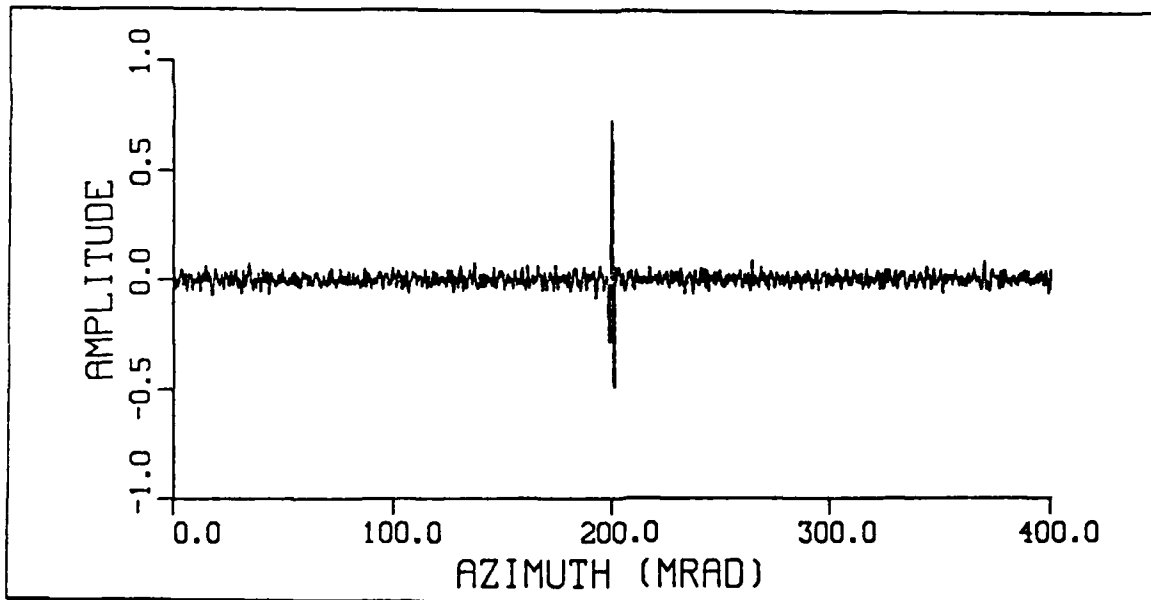


Figure 52. Filtered Output; BKDII, TGTIII, LMS9: TGTIII embedded in BKDII and filtered by LMS9;  $S/N = 31.7$ .

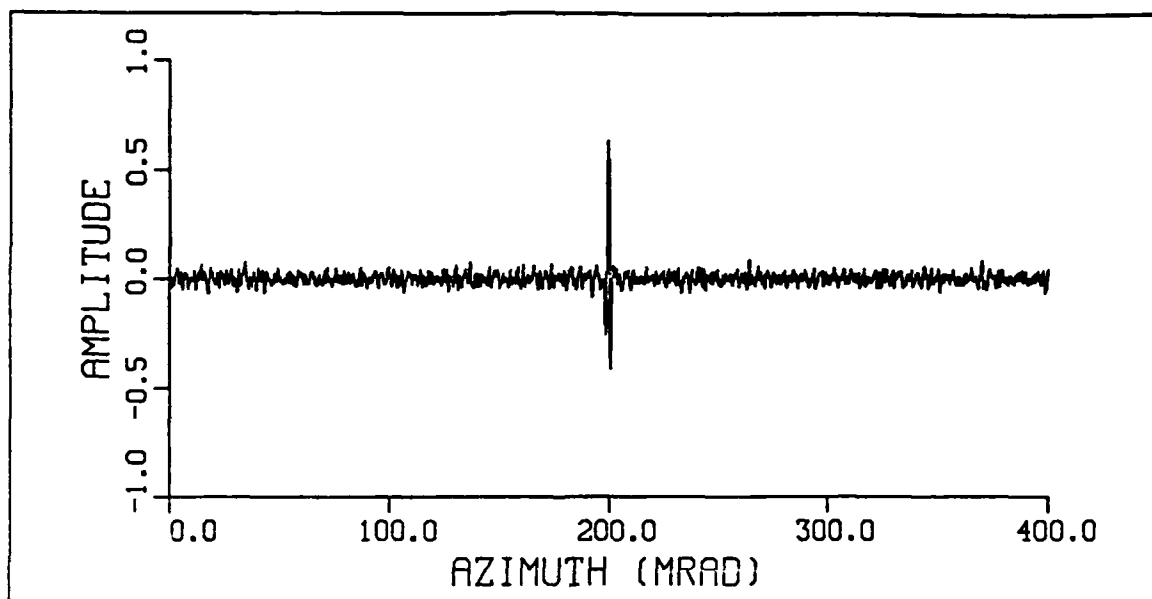


Figure 53. Filtered Output; BKDII, TGTIV, LMS9: TGTIV embedded in BKDII and filtered by LMS9; S/N = 27.3.

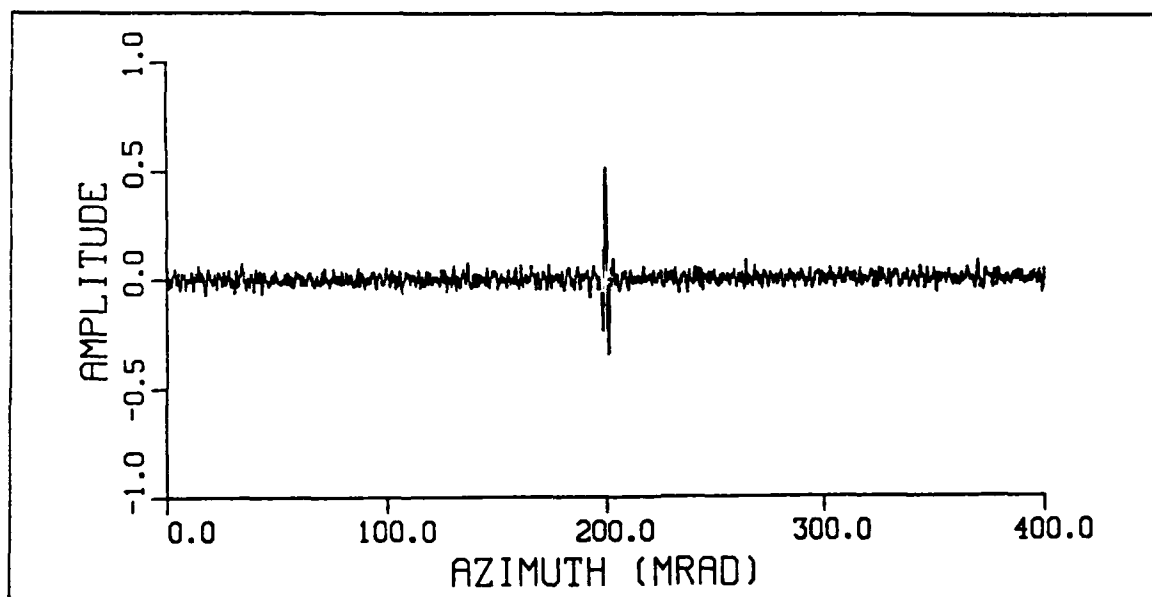


Figure 54. Filtered Output; BKDII, TGTIV, LMS9: TGTIV embedded in BKDII and filtered by LMS9; S/N = 22.7.

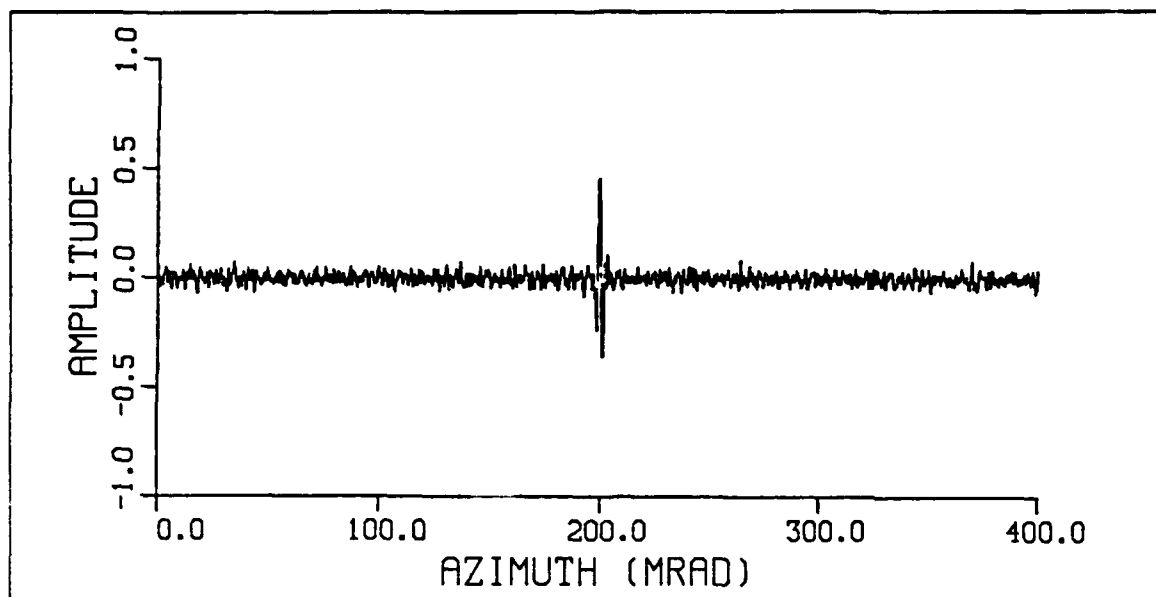


Figure 55. Filtered Output; BKDII, TGTVI, LMS9: TGTVI embedded in BKDII and filtered by LMS9;  $S/N = 22.1$ .

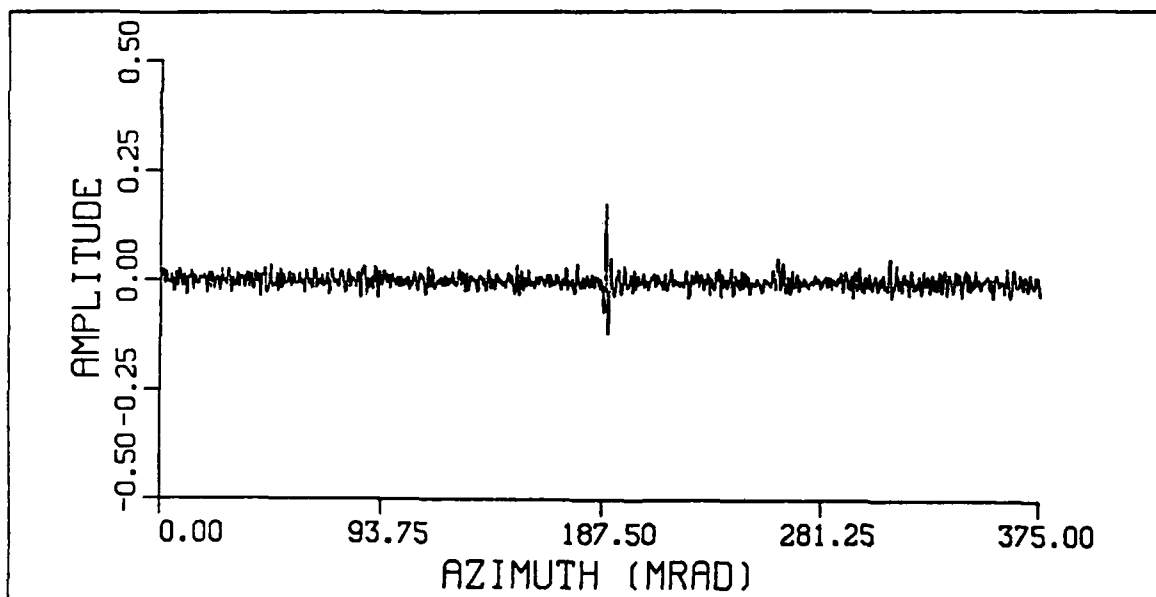


Figure 56. Filtered Output; BKDIII, TGTI, LMS3: TGTI embedded in BKDIII and filtered by LMS3;  $S/N = 12.7$ .

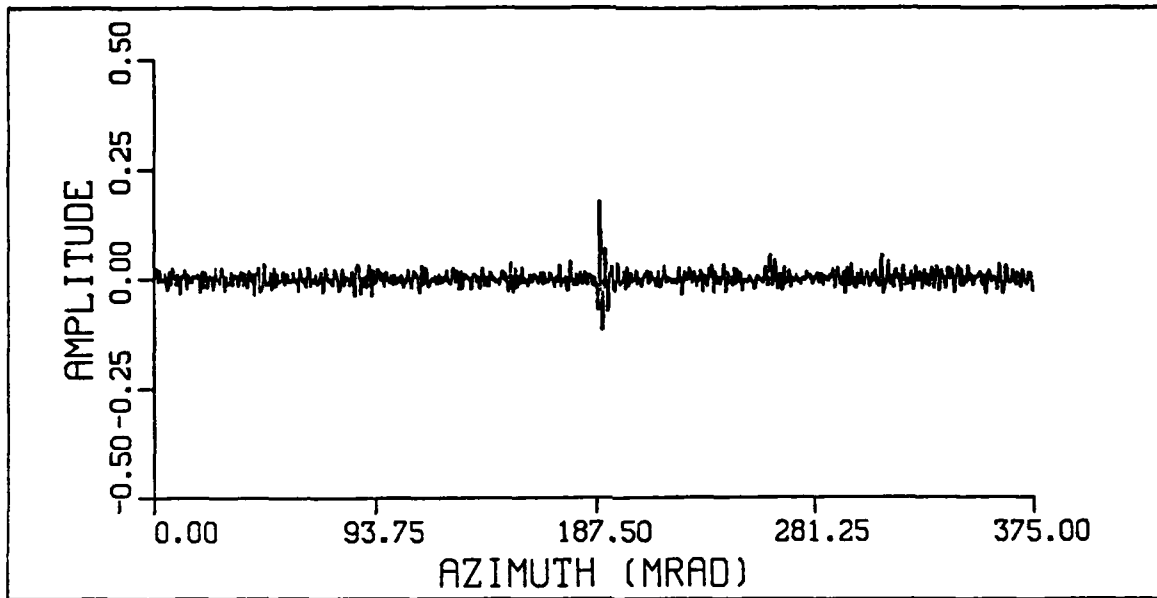


Figure 57. Filtered Output; BKDIII, TGTII, LMS3: TGTII embedded in BKDIII and filtered by LMS3;  $S/N = 12.7$ .

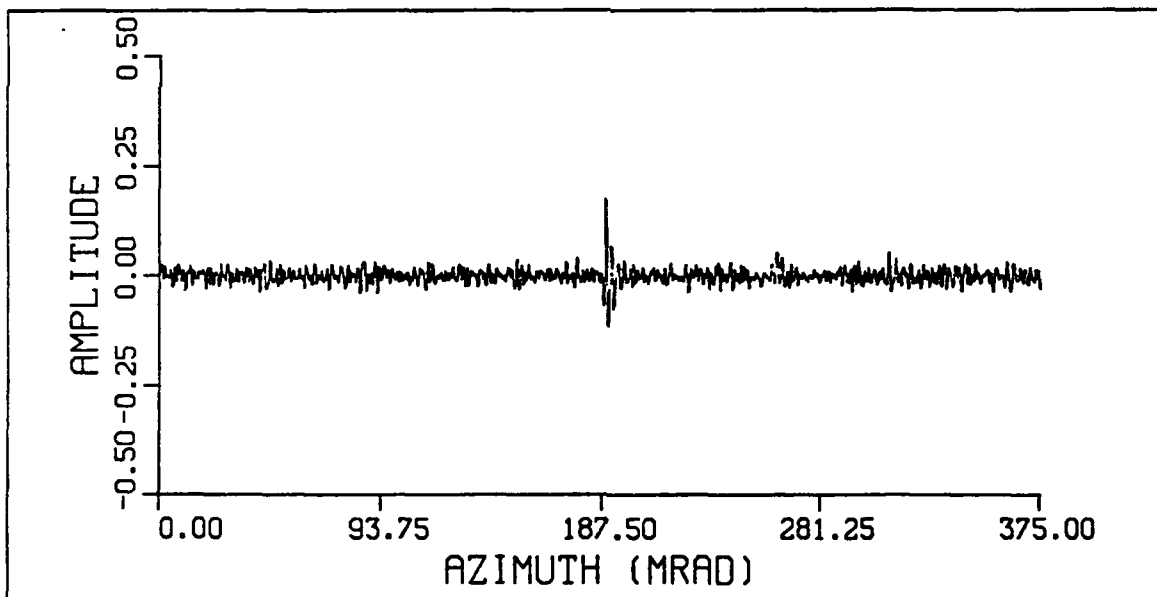


Figure 58. Filtered Output; BKDIII, TGTIII, LMS3: TGTIII embedded in BKDIII and filtered by LMS3;  $S/N = 12.5$ .

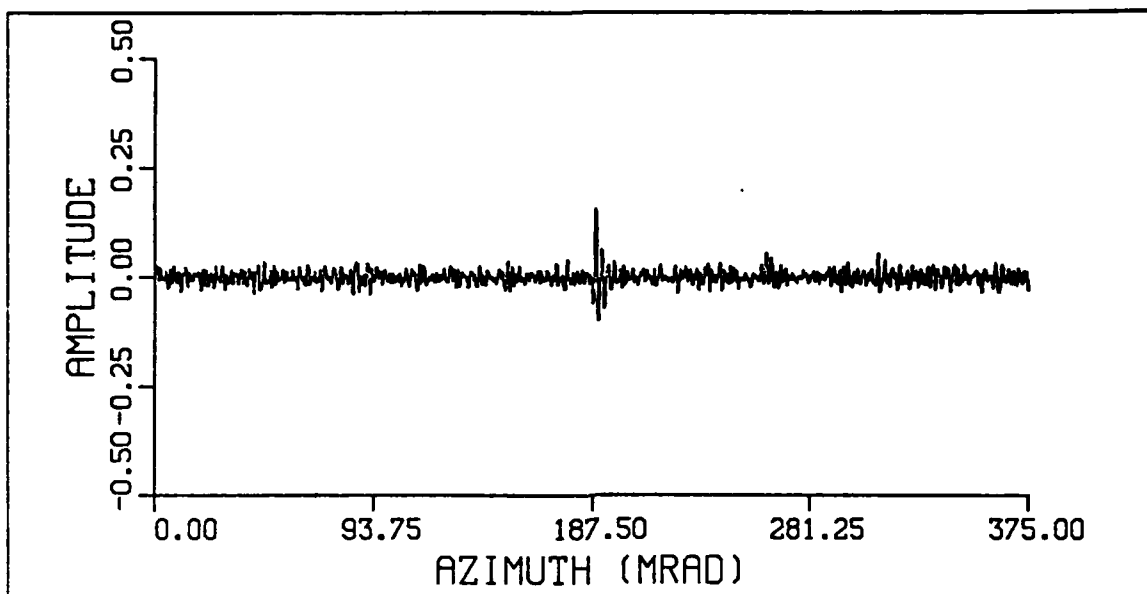


Figure 59. Filtered Output; BKDIII, TGTIV, LMS3: TGTIV embedded in BKDIII and filtered by LMS3;  $S/N = 11.1$ .

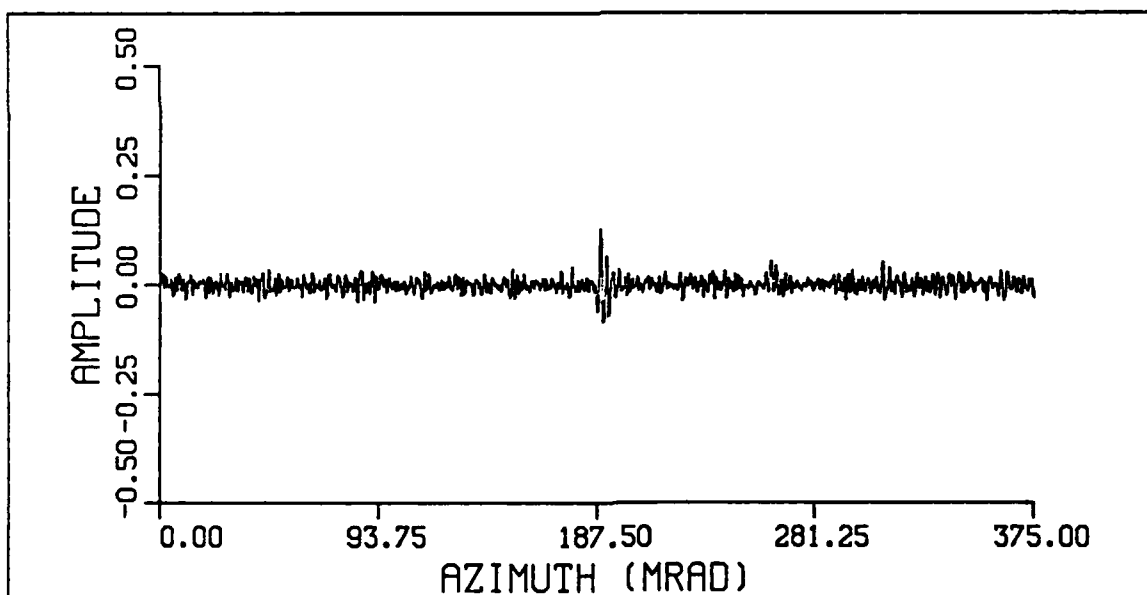


Figure 60. Filtered Output; BKDIII, TGTIV, LMS3: TGTIV embedded in BKDIII and filtered by LMS3;  $S/N = 9.4$ .

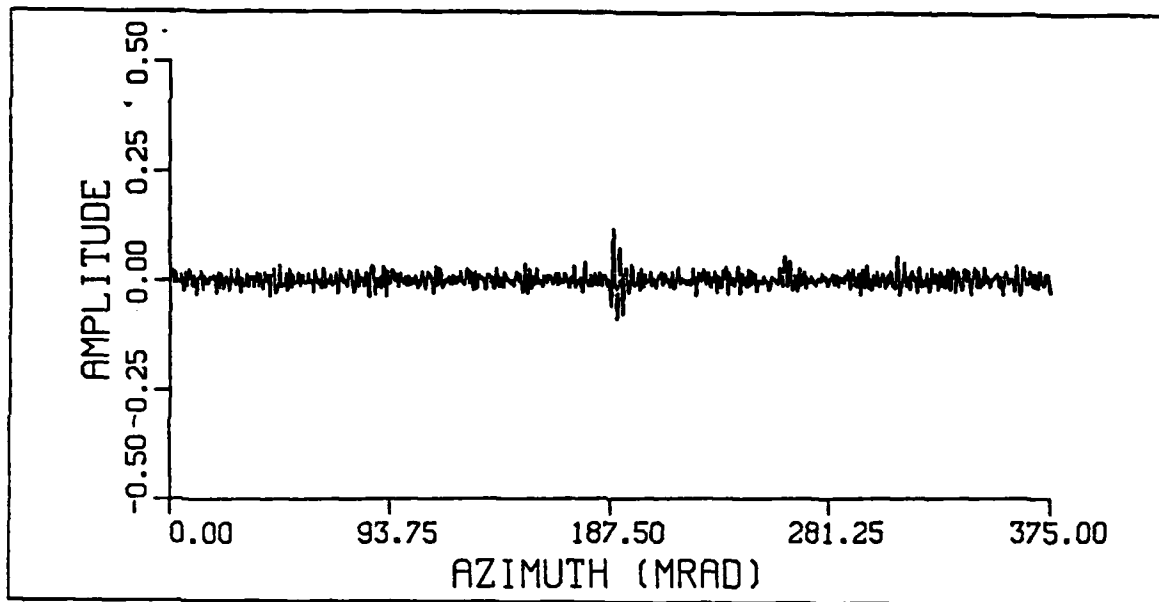


Figure 61. Filtered Output; BKDIII, TGTVI, LMS3: TGTVI embedded in BKDIII and filtered by LMS3; S/N=9.1.



## APPENDIX C. BACKGROUND MODEL FORTRAN PROGRAM

This appendix is included to present the FORTRAN code used for generating simulated background distributions. All comments and discussion of the parameters and functions of the program are included as comment lines in the program code.

This program was designed to be run on the NPS IBM 3033/4381 Mainframe Computer Network, using VS FORTRAN on the systems Virtual Machine. The output of this program contains the simulated IR background amplitude distribution in a 20 by 4000 element matrix.

```
C      PROGRAM BKD1
      DIMENSION U1(4000,20),U2(201),U3(4000),U4(101)
      DOUBLE PRECISION DSEED
      CHARACTER*80 T1$,XL$
      CHARACTER*40 CL$,SI$
      CALL SHERPA ('BKDPLOT2','A',3)
C
C      CONSTANTS AND VARIABLES
C
      M=4000
      M2=201
      M3=101
      N=20
      IT=1
      DSEED=414813567.DO
      CLEN=1667.
      SIGMA=0.15
      CL$='CORRELATION LENGTH = 166.7 MRAD$'
      SI$='SIGMA = 0.1$'
      IZ=INT(DSEED)
      ST=SQRT(2.)
      A1=-1./CLEN
      Z=EXP(A1)
      Z2=Z/(1.+(Z**ST))
      B1=1.-(Z*Z)
      B2=SQRT(B1)
      B3=1.-(2.*Z*Z)/(1.+(Z**ST))
      B4=SQRT(B3)
      DO 2 I=1,N
      DO 1 J=1,M
      U1(J,I)=0.
1 CONTINUE
2 CONTINUE
C
C      SET FIRST ELEMENT EQUAL TO ZERO
C
```

```

1000 U1(1,1)=0.
C
C   GENERATE RANDOM NUMBERS FOR FIRST ROW
C
C   CALL GGNML(DSEED,M,U3)
C
C   GENERATE ELEMENTS OF FIRST ROW
C
C   DO 20 I=2,M
C     I1=I-1
C     RN=U3(I1)
C     U1(I,1)=(SIGMA*B2*RN)+(Z*U1(I1,1))
20 CONTINUE
C
C   GENERATE REST OF BACKGROUND (ROW BY ROW)
C
C   DO 50 I=2,N
C
C   GENERATE RANDOM NUMBERS (ROW BY ROW)
C
C   CALL GGNML(DSEED,M,U3)
C   DO 40 J=1,M
C     I1=I-1
C     J1=J-1
C     RN=U3(J)
C
C   GENERATE ELEMENTS OF FIRST COLUMN
C
C   IF (J.EQ.1) U1(J,I)=(SIGMA*B2*RN)+(Z*U1(J,I1))
C
C   GENERATE REST OF ELEMENTS
C
C   U1(J,I)=(SIGMA*B4*RN)+(Z2*(U1(J,I1)+U1(J1,I)))
40 CONTINUE
50 CONTINUE
C
C   PLOT 3D BACKGROUND DISTRIBUTION
C
C   CALL PLOT32 (U1,M,N)
C
C   DETERMINE AMPLITUDE DISTRIBUTION
C
C   CALL DIST (U1,U2,U4,M,M2,M3,N,IT,CL$,SI$,IZ)
C   IF (IT.LE.1) THEN
C     IZ=INT(DSEED)
C     GO TO 1000
C   END IF
C   CALL DONEPL
C   STOP
C   END
C
C
C   SUBROUTINE DIST(U1,U2,U3,M,M2,M3,N,IT,CL$,SI$,IZ)
C   DIMENSION U1(M,N),U2(M2),U3(M3)
C   CHARACTER*40 CL$,SI$
C   DO 5 J=1,M2

```

```

      U2(J)=0.
5  CONTINUE
      DO 20 I=1,N
      DO 10 J=1,M
      II=INT(U1(J,I)*100. )+101.
      U2(II)=U2(II)+1.
10  CONTINUE
20  CONTINUE
      YMAX=0.
      DO 40 I=1,M2
      IF (U2(I).GT.YMAX) YMAX=U2(I)
40  CONTINUE
      DO 50 I=51,M2-50
      J=M2-50+1-I
      U3(J)=U2(I)
50  CONTINUE
      DO 60 I=1,M2
      U3(I)=U3(I)/YMAX
60  CONTINUE
C
C      PLOT AMPLITUDE DISTRIBUTION
C
      CALL PLOTIT(U3,M3)
      IT=IT+1
      RETURN
      END

      SUBROUTINE PLOTIT (Y,N)
      DIMENSION Y(N),X(101)
      REAL X,Y
      INTEGER IFIG
C      CALL PRTPLT(76,2)
C      CALL TEK618
      CALL PAGE (11.,8.5)
      CALL NOBRDR
      CALL HWROT('MOVIE')
      CALL AREA2D (4.8,2.6)
      CALL HEIGHT (0.15)
      CALL XNAME ('AMPLITUDE$',100)
      CALL YNAME ('OCCURANCES (NORMALIZED)$',100)
55  CALL GRAF (-.5,'SCALE',.5,0.,'SCALE',1.)
      DO 60 I=1,N
      X(I)=.01*FLOAT(I)-.51
60  CONTINUE
65  CALL CURVE (X,Y,N,0)
      CALL ENDPL(0)
      RETURN
      END
C
C      SUBROUTINE PLOT32(U1,M,N)
      DIMENSION U1(M,N)
      AN=REAL(N)*.1
      AM=REAL(M)*.1
      AN1=AN/2.

```

```

C      AM1=AM/4.
C      CALL PRTPLT(76,2)
C      CALL TEK618
      CALL PAGE (11.,8.5)
      CALL NOBRDR
      CALL HWROT('MOVIE')
      CALL AREA2D (5.,3.)
      CALL HEIGHT (0.15)
      CALL X3NAME ('AZIMUTH (MRAD)$',100)
      CALL Y3NAME ('ELEVATION (MRAD)$',100)
      CALL Z3NAME ('AMPLITUDE$',100)
      CALL VOLM3D (2.,2.,1.)
      CALL VUABS (5.,-5.,3.)
      CALL GRAF3D (0.,AM1,AM,0.,AN1,AN,-.5,.2,.5)
      CALL SURMAT (U1,M,M,0,N,0)
      CALL ENDPL(0)
      RETURN
      END
C

```

## APPENDIX D. IRSTD MODEL FORTRAN PROGRAM

This appendix is included to present the FORTRAN code used for generating simulated IRSTD detector outputs. All comments and discussion of the parameters and functions of the program are included as comment lines in the program code.

This program was designed to be run on the NPS IBM 3033 4381 Mainframe Computer Network, using VS FORTRAN on the systems Mutilple Virtual System. The output of this program contains the simulated IR detector output in a 4000 element array.

```
//GRIB1IRS JOB (3222,9999),'IR1D1MVS6',CLASS=G,REGION=3000K
//*FORMAT PR,DDNAME=GO.FT06F001,
//*FORMS=SEP1
// EXEC FORTVCLG,PARM.FORT='OPT(2)'
//FORT.SYSIN DD *
C
C  IRST MODEL - (4000,20) OBJECT PLANE
C
  IMPLICIT COMPLEX (C)
  DIMENSION U1(4000,20),U2(4000),U3(4000)
  DIMENSION U6(4000),U7(4000),U8(4000)
  DIMENSION C1(4000,20),C2(4000,20)
  DIMENSION IWK(25150),RWK(25150),CWK(20)
  DOUBLE PRECISION DSEED
  DSEED=765742451.D0
  M=4000
  N=20
  IRAN=13455
  KRAN=99947
C
C   GENERATE BACKGROUND DISTRIBUTION
C
  CALL BKGD1 (U1,U7,M,N,DSEED)
  DO 20 I=1,N
  DO 10 J=1,M
  C1(J,I)=CMPLX(U1(J,I),0.)
10 CONTINUE
20 CONTINUE
C
C   GENERATE SYSTEM PSF
C
  DO 40 I=1,N
  DO 30 J=1,M
  A1=REAL((J-(M/2))**2+(I-(N/2))**2)/40.
  IF (A1.GT.100.) A1=100.
  A2=1./EXP(A1)
```

```

      C2(J,I)=CMPLX(A2,0.)
30  CONTINUE
40  CONTINUE
C
C   GENERATE DETECTOR ARRAY DISTRIBUTION
C
      DO 50 J=1,M
      U2(J)=0.
50  CONTINUE
      J1=M/2
      J2=(M/2)+2
      DO 70 J=J1,J2
      U2(J)=1.
70  CONTINUE
C
C   GENERATE IMAGE PLANE DISTRIBUTION
C
      CALL FFT3D (C1,M,N,M,N,1,1,IWK,RWK,CWK)
      CALL FFT3D (C2,M,N,M,N,1,1,IWK,RWK,CWK)
      DO 120 I=1,N
      DO 110 J=1,M
      C1(J,I)=C1(J,I)*C2(J,I)
110  CONTINUE
120  CONTINUE
      CALL FFT3D (C1,M,N,M,N,1,-1,IWK,RWK,CWK)
      DO 140 I=1,N
      DO 130 J=1,M
      U1(J,I)=CABS(C1(J,I))
130  CONTINUE
140  CONTINUE
C
C   GENERATE IMAGE PLANE SLICES
C
      DO 180 J=1,M
      SUM1=0.
      DO 170 J1=1,20
      SUM1=SUM1+U1(J,J1)
170  CONTINUE
      U6(J)=SUM1
180  CONTINUE
      CALL CONVOL (U6,U2,U3,M)
      DO 230 J=1,M
      IRAN=IRAN*KRAN
      R=.002*(REAL(IRAN)*2.328306E-10)
      U3(J)=U3(J)+R
230  CONTINUE
C
C   AC COUPLED DETECTOR OUTPUTS
C
      DO 260 J=1,M
      A1=REAL(J)/1.3
      IF (A1.GT.100.) GO TO 250
      U7(J)=1./EXP(A1)
      GO TO 260
250  U7(J)=0.
260  CONTINUE

```

```

      CALL CONVOL (U3,U7,U8,M)
      WT1=0.
      DO 270 J=1,M
      U3(J)=U3(J)-U8(J)
      IF (ABS(U3(J)).GT.WT1) WT1=ABS(U3(J))
270  CONTINUE
      DO 290 J=1,M
      U3(J)=.35*(U3(J)/WT1)
290  CONTINUE

C
C      STORE DETECTOR OUTPUTS IN EXTERNAL FILE
C
      DO 310 J=1,M,10
      WRITE(6,9000)(U3(J+K),K=0,9)
9000  FORMAT (10F7.4)
      310  CONTINUE
      STOP
      END

C
      SUBROUTINE BKGD1(U1,U3,M,N,DSEED)
      DIMENSION U1(M,N),U3(M)
      DOUBLE PRECISION DSEED
      DO 2 I=1,N
      DO 1 J=1,M
      U1(J,I)=0.
1  CONTINUE
2  CONTINUE
      CLEN=1623.4
      SIGMA=0.1
C      CONSTANTS AND VARIABLES
      ST=SQRT(2.)
      A1=-1./CLEN
      Z=EXP(A1)
      Z2=Z/(1.+(Z**ST))
      B1=1.-(Z*Z)
      B2=SQRT(B1)
      B3=1.-(2.*Z*Z)/(1.+(Z**ST))
      B4=SQRT(B3)
1000 U1(1,1)=0.
      CALL GGNML(DSEED,M,U3)
      DO 20 I=2,M
      I1=I-1
      RN=U3(I1)
      U1(I,1)=(SIGMA*B2*RN)+(Z*U1(I1,1))
20  CONTINUE
      DO 50 I=2,N
      CALL GGNML(DSEED,M,U3)
      DO 40 J=1,M
      I1=I-1
      J1=J-1
      RN=U3(J)
      IF (J.EQ.1) U1(J,I)=(SIGMA*B2*RN)+(Z*U1(J,I1))
      U1(J,I)=(SIGMA*B4*RN)+(Z2*(U1(J,I1)+U1(J1,I)))
40  CONTINUE
50  CONTINUE
      RETURN

```

```

      END
C
      SUBROUTINE CONVOL(F,G,H,M)
      DIMENSION F(M),G(M),H(M)
      DO 10 I=1,M
      SUM=0.0
      DO 5 J=1,M
      K=MOD(I-J+M,M)+1
      SUM=SUM+F(J)*G(K)
5  CONTINUE
      H(I)=SUM
10  CONTINUE
      RETURN
      END
/*
//

```



## APPENDIX E. FILTER OUTPUT FORTRAN PROGRAM

This appendix is included to present the FORTRAN code used for filtering simulated and real background distributions. All comments and discussion of the parameters and functions of the program are included as comment lines in the program code.

This program was designed to be run on the NPS IBM 3033/4381 Mainframe Computer Network, using VS FORTRAN on the systems Virtual Machine. The output of this program contains the unfiltered and filtered detector outputs in 5000 element arrays, and the results of S/N ratio calculations.

```
C      PROGRAM FILT1
      IMPLICIT COMPLEX (C)
      DIMENSION U1(5000),U2(5000),U3(5000),XA(5000)
      DIMENSION T(100),F(50)
      DIMENSION C1(5000,1),C2(5000,1),C3(5000,1)
      DIMENSION IWK(30150),RWK(30150),CWK(1)
      CHARACTER*80 TITLE$,TIT$
      CHARACTER*20 FILN$
      CALL SHERPA ('OUTFILT2','A',3)

C
C      INITIALIZE CONSTANTS
C
      PI=3.1415926535897932
      IT=1
      N2=100
6000 DO 20 I=1,50
      F(I)=0.
      20 CONTINUE

C
C      SELECT BACKGROUND
C
      WRITE(*,*)'CHOOSE BACKGROUND (ENTER BKD NUMBER 1-5)'
      READ(*,*)IBKD
      IF (IBKD.EQ.1) FILN$='BKD1'
      IF (IBKD.EQ.2) FILN$='BKD2'
      IF (IBKD.EQ.3) FILN$='BKD3'
      IF (IBKD.EQ.4) FILN$='BKD4'
      IF (IBKD.EQ.5) FILN$='BKD5'
      N=4000
      IF (IBKD.EQ.3) N=1250
      CALL INPUT(U1,N,FILN$)

C
C      SELECT TARGET
C
      DO 10 I=1,N
      U2(I)=0.
```

```

10 CONTINUE
  WRITE(*,*) 'SELECT NUMBER OF TGTS'
  READ(*,*) NTGT
  DO 35 I=1,NTGT
    WRITE(*,*) 'CHOOSE TARGETS (ENTER TGT NUMBER 1-6)'
    READ(*,*) ITGT
    IF (IBKD.GE.3) GO TO 25
    IF (ITGT.EQ.1) FILN$='T1'
    IF (ITGT.EQ.2) FILN$='T2'
    IF (ITGT.EQ.3) FILN$='T3'
    IF (ITGT.EQ.4) FILN$='T4'
    IF (ITGT.EQ.5) FILN$='T5'
    IF (ITGT.EQ.6) FILN$='T6'
    GO TO 26
25 IF (ITGT.EQ.1) FILN$='T1A'
    IF (ITGT.EQ.2) FILN$='T2A'
    IF (ITGT.EQ.3) FILN$='T3A'
    IF (ITGT.EQ.4) FILN$='T4A'
    IF (ITGT.EQ.5) FILN$='T5A'
    IF (ITGT.EQ.6) FILN$='T6A'
26 CALL INPUT(T,N2,FILN$)
    IF (NTGT.EQ.1) ITL=N/2
    IF (NTGT.NE.1) THEN
      WRITE(*,*) 'ENTER TARGET LOCATION (PIXELS IN INTEGER)'
      READ(*,*) ITL
      END IF
      TL=0.1*REAL(ITL)
      WRITE(*,*) 'ENTER INTENSITY FACTOR OF TARGET (REAL)'
      WRITE(*,*) 'FOR S/N=1: 0.15 BKDI AND BKDII; 0.09 BKDIII'
      READ(*,*) TFAC
      K1=ITL-N2/2+1
      K2=K1+N2-1
      DO 30 J=K1,K2
        L=J-K1+1
        U2(J)=U2(J)+(TFAC*T(L))
        XA(J)=U2(J)+U1(J)
        IF (XA(J).GT.0.4095) U2(J)=0.4095-U1(J)
        IF (XA(J).LT.-0.4095) U2(J)=-0.4095-U1(J)
30 CONTINUE
35 CONTINUE
    DO 40 J=1,N
      C1(J,1)=CMPLX(U1(J),0.)
40 CONTINUE
    DO 50 J=1,N
      C2(J,1)=CMPLX(U2(J),0.)
50 CONTINUE
C
C
C
    SELECT FILTER
    DO 60 J=1,N
      C3(J,1)=CMPLX(0.,0.)
60 CONTINUE
    WRITE(*,*) 'SELECT FILTER (ENTER WIDTH-TO-SAMPLE RATIO)'
    READ(*,*) IFILT
    SUM=0.
    IFIL=(2*IFILT)+1

```

```

    IFIL2=IFILT+1
    DO 70 I=1,IFIL
    II=I-IFIL2
    ARG=(PI*REAL(II))/REAL(IFILT)
    F(I)=COS(ARG)+1.
    SUM= SUM+F(I)
70  CONTINUE
    AVE=SUM/REAL(IFIL)
    AMAX=0.
    DO 80 I=1,IFIL
    F(I)=F(I)-AVE
    IF (F(I).GT.AMAX) AMAX=F(I)
80  CONTINUE
    DO 90 I=1,IFIL
    F(I)=(F(I)/AMAX)
90  CONTINUE
    DO 150 I=1,IFIL
    II=I-IFIL2
    K=N/2+II
    C3(K,1)=CMPLX(F(I),0.)
150 CONTINUE
C
C    FFT OF BKD, TGT, AND FILTER
C
    CALL FFT3D (C1,N,1,N,1,1,1,IWK,RWK,CWK)
    CALL FFT3D (C2,N,1,N,1,1,1,IWK,RWK,CWK)
    CALL FFT3D (C3,N,1,N,1,1,1,IWK,RWK,CWK)
C
C    DATA REDUCTION
C
    V=1./(12.*(2.**24))
    VAR=2.*V
    AS1=0.
    AN1S=0.
    AS2=0.
    AN2S=0.
    DO 160 I=1,N
    A1=CABS(C1(I,1))
    A2=CABS(C2(I,1))
    A3=CABS(C3(I,1))
    AS1=AS1+A2
    AN1S=AN1S+(A1**2)
    AS2=AS2+(A2*A3)
    AN2S=AN2S+((A1*A3)**2)
160 CONTINUE
    AN1=SQRT(AN1S)
    AN2=SQRT(AN2S)
    SN1=AS1/AN1
    SN2=AS2/AN2
    SH=0.
    DO 165 I=1,IFIL
    SH=SH+(F(I)**2)
165 CONTINUE
    VARF=VAR*SH
C

```

```

C      EMBED TARGET
C
      KK=0
      DO 170 I=1,N
      IF (U2(I).EQ.0.) THEN
      U1(I)=U1(I)+U2(I)
      GO TO 170
      END IF
      IF (KK.EQ.1) GO TO 166
      IF (U2(I).NE.0.) THEN
      KK=1
      BL=U1(I)
      END IF
166  U1(I)=U2(I)+BL
170  CONTINUE
      DO 180 J=1,N
      C1(J,1)=CMPLX(U1(J),0.)
180  CONTINUE
C
C      FFT OF TGT AND BACKGROUND
C
      CALL FFT3D (C1,N,1,N,1,1,1,IWK,RWK,CWK)
C
C      CONVOLVE OUTPUT WITH FILTER
C
      DO 190 J=1,N
      C2(J,1)=C1(J,1)*C3(J,1)
190  CONTINUE
C
C      IFT OF FILTERED OUTPUT
C
      CALL FFT3D (C2,N,1,N,1,1,-1,IWK,RWK,CWK)
C
C      UNWRAP OUTPUT
C
      DO 200 J=1,N/2
      K=J+N/2
      U3(J)=REAL(C2(K,1))
      U3(K)=REAL(C2(J,1))
200  CONTINUE
      TITLE$=': DETECTOR OUTPUT - BKD $'
      WRITE(*,*) 'ENTER 1 IF PLOT OF UNFILTERED OUTPUT DESIRED'
      READ(*,*) IOUT
      IF (IOUT.NE.1) GO TO 210
      CALL PLOTIT (U1,XA,N,IT,TITLE$,IBKD,ITGT,TL,SN1,VAR)
      IT=IT+1
210  TIT$='FILTERED OUTPUT $'
      CALL PLOTI2 (U3,XA,N,IT,TITLE$,TIT$,IBKD,ITGT,IFILT,TL,SN2,VARF)
      IT=IT+1
      WRITE(*,*) 'ENTER 1 IF ANOTHER RUN IS DESIRED'
      READ(*,*) IBREP
      IF (IBREP.EQ.1) GO TO 6000
      CALL DONEPL
      STOP

```

```

END
C
C
SUBROUTINE INPUT(RE,N,FILN$)
DIMENSION RE(N)
CHARACTER*20 FILN$
CLOSE (2)
OPEN(2,FILE=FILN$,STATUS='OLD')
DO 1 J = 1,N,10
    READ(2,'(10F7.4)')(RE(J+K),K=0,9)
1 CONTINUE
RETURN
END
C
C
SUBROUTINE PLOTIT (Y,X,N,IFIG,TITLE$,IB,IT,TL,SN,VAR)
DIMENSION Y(N),X(N)
CHARACTER*80 TITLE$
REAL X,Y,STD
INTEGER IFIG
IF (IB.LE.2) AN=0.1*REAL(N)
IF (IB.GT.2) AN=0.3*REAL(N)
ANS=AN/4.
C
C
CALL PRTPLT(76,2)
CALL TEK618
CALL PAGE (11.,8.5)
CALL NOBRDR
CALL HWROT('MOVIE')
CALL AREA2D (5.,2.5)
CALL HEIGHT (0.15)
CALL YNAME ('AMPLITUDE$',100)
CALL XNAME ('AZIMUTH (MRAD)$',100)
CALL MESSAG ('FIGURE $',100,1.,5.6)
CALL INTNO (IFIG,'ABUT','ABUT')
CALL MESSAG (TITLE$,100,'ABUT','ABUT')
CALL INTNO (IB,'ABUT','ABUT')
CALL MESSAG ('TARGET NUMBER $',100,2.48,5.4)
CALL INTNO (IT,'ABUT','ABUT')
CALL MESSAG ('TARGET LOCATION = $',100,2.48,5.2)
CALL REALNO (TL,1,'ABUT','ABUT')
CALL MESSAG (' MRAD $',100,'ABUT','ABUT')
CALL MESSAG ('S/N = $',100,2.48,5.0)
CALL REALNO (SN,5,'ABUT','ABUT')
CALL MESSAG ('VARIANCE = $',100,2.48,4.8)
CALL REALNO (VAR,10,'ABUT','ABUT')
55 CALL GRAF (0.,ANS,AN,-.5,.25,.5)
    DO 60 I=1,N
        IF (IB.LE.2) X(I)=.1*REAL(I)
        IF (IB.GT.2) X(I)=.3*REAL(I)
60 CONTINUE
65 CALL CURVE (X,Y,N,0)
CALL ENDPL(0)
RETURN
END
C
C

```

```

SUBROUTINE PLOTI2 (Y,X,N,IFIG,TITLE$,TIT$,IB,IT,IFL,TL,SN,VAR)
DIMENSION Y(N),X(N)
CHARACTER*80 TITLE$,TIT$
REAL X,Y,STD
INTEGER IFIG
999 WRITE(*,*)'SELECT DISPLAY'
WRITE(*,*)'          1 = FIXED'
WRITE(*,*)'          2 = ADJUST'
WRITE(*,*)'          3 = NORMALIZED'
READ(*,*)IAD
YMAX=1.0
IF (IAD.EQ.1) THEN
WRITE(*,*)'SELECT YMAX (REAL)'
READ(*,*)YMAX
YMIN=-YMAX
DO 10 I=1,N
IF (Y(I).GT.YMAX) Y(I)=YMAX
IF (Y(I).LT.YMIN) Y(I)=YMIN
10 CONTINUE
END IF
IF (IAD.EQ.1) GO TO 111
YN=0.
DO 15 I=1,N
IF (Y(I).GT.YN) YN=Y(I)
15 CONTINUE
IF (IAD.EQ.2) YMAX=YN
IF (IAD.EQ.3) THEN
DO 20 I=1,N
Y(I)=Y(I)/YN
20 CONTINUE
END IF
111 IF (IB.LE.2) AN=0.1*REAL(N)
IF (IB.GT.2) AN=0.3*REAL(N)
ANS=AN/4.
C CALL PRTPLT(76,2)
C CALL TEK618
CALL PAGE (11.,8.5)
CALL NOBRDR
CALL HWROT('MOVIE')
CALL AREA2D (5.,2.5)
CALL HEIGHT (0.15)
CALL YNAME ('AMPLITUDE$',100)
CALL XNAME ('AZIMUTH (MRAD)$',100)
CALL MESSAG ('FIGURE $',100,1.,5.6)
CALL INTNO (IFIG,'ABUT','ABUT')
CALL MESSAG (TITLE$,100,'ABUT','ABUT')
CALL INTNO (IB,'ABUT','ABUT')
CALL MESSAG ('TARGET NUMBER $',100,2.48,5.4)
CALL INTNO (IT,'ABUT','ABUT')
CALL MESSAG (TIT$,100,2.48,5.2)
CALL INTNO (IFL,'ABUT','ABUT')
CALL MESSAG ('TARGET LOCATION = $',100,2.48,5.0)
CALL REALNO (TL,1,'ABUT','ABUT')
CALL MESSAG (' MRAD $',100,'ABUT','ABUT')
CALL MESSAG ('S/N = $',100,2.48,4.8)
CALL REALNO (SN,4,'ABUT','ABUT')

```

```

      CALL MESSAG ('VARIANCE = $',100,2.48,4.6)
      CALL REALNO (VAR,10,'ABUT','ABUT')
55  CALL GRAF (0.,ANS,AN,-YMAX,'SCALE',YMAX)
      DO 60 I=1,N
      IF (IB.LE.2) X(I)=.1*REAL(I)
      IF (IB.GT.2) X(I)=.3*REAL(I)
60  CONTINUE
65  CALL CURVE (X,Y,N,0)
      CALL ENDPL(0)
      WRITE(*,*)'ENTER 1 FOR ANOTHER PLOT'
      READ(*,*)IPLT
      IF (IPLT.EQ.1) GO TO 999
      RETURN
      END

```

## LIST OF REFERENCES

1. Parker, Gary W., *Optical Performance Implications of Naval Postgraduate School Modifications to the AN/SAR-8 Infrared Search and Target Designation System*, Master's Thesis, Naval Postgraduate School, Monterey, CA, September 1986.
2. Ayers, Gary R., *Calibration and Initialization of the NPS Modified Infrared Search and Target Designation (IRSTD) System*, Master's Thesis, Naval Postgraduate School, Monterey, CA, December 1987.
3. Nitzberg, R., Takken, E.H., Friedman, D., and Milton, A.F., "Spatial Filtering Techniques for Infrared (IR) Sensors," *SPIE*, v. 178, p. 40, 1979.
4. General Electric Company, *Description of the Electronics Processing Equipment for the IRST Program*, Syracuse, NY, 1977.
5. *The Infrared Handbook*, Office of Naval Research, Department of the Navy, Washington, DC, 1978.
6. Itakura, Y., Tsutsumi, S., and Takagi, T., "Statistical Properties of the Background Noise for the Atmospheric Windows in the Intermediate Infrared Region," *Infrared Physics*, v. 14, p. 203, 1974.
7. Ben-Yosef, N., Rahat, B., and Feigin, G., "Simulation of Infrared Background Scenes," *Applied Optics*, v. 22, p. 190, 1983.
8. International Mathematical and Statistical Libraries Incorporated, *IMSL User's Manual*, Houston, TX, 1984.
9. Scribner, D.A., and Peters, W.N., "Analytic Sensor Model for Evaluating Scanning Focal Plane Array Performance," unpublished paper held by NACIT, written on 14 May 1985.



10. Lloyd, J.M., *Thermal Imaging Systems*, Plenum Press, New York, NY, 1975.
11. Bose, N.K., *Digital Filters; Theory and Applications*, Elsevier Science Publishing Company, New York, NY, 1985.
12. Hamming, R.W., *Digital Filters*, Prentice Hall Inc., Englewood Cliffs, NJ, 1977.
13. Peters, W.N., "One- and Two-Dimensional Matched Filter for Scanning Electro-Optic Systems," *Journal of the Optical Society of America*, v. 3, no. 3, p. 347, 1986.
14. Peters, W.N., *An Adaptive Decision Process Utilizing Hypothesis Testing Techniques*, SWL Inc., McLean, VA, 1981.

## INITIAL DISTRIBUTION LIST

		No. Copies
1.	Defense Technical Information Center Cameron Station Alexandria, VA 22304-6145	2
2.	Library, Code 0142 Naval Postgraduate School Monterey, CA 93943-5002	2
3.	Professor K.E. Woehler, Code 61Wh Chairman, Department of Physics Naval Postgraduate School Monterey, CA 93943-5000	2
4.	Professor A.W. Cooper, Code 61Cr Naval Postgraduate School Monterey, CA 93943-5000	3
5.	Professor C.W. Therrien, Code 62Ti Naval Postgraduate School Monterey, CA 93943-5000	1
6.	CAPT J.A. Paine, PMS-421 Naval Sea Systems Command Washington, DC 20362-5101	1
7.	S.K. Petropoulos, Code R42 White Oak Laboratory Naval Surface Weapons Center Detachment Silver Spring, MD 20903-5000	1
8.	R. Bloedel Manager, Signal Processing Technology Boeing Company P.O. Box 3999 Seattle, WA 98124-2499	1
9.	M.W. Zurasky, Code G74 Naval Surface Weapons Center Dahlgren, VA 22448-5000	1
10.	Dr. D.A. Scribner, Code 6552 Naval Research Laboratory Washington, DC 20375	1

- |     |  |   |
|-----|--|---|
| 11. | Dr. R. Steinberg<br>Applied Physics Laboratory<br>Johns Hopkins University<br>Laurel, MD 20707 | 1 |
| 12. | LT S.J. Smith<br>Naval Ship Weapon Systems Engineering Station<br>Port Hueneme, CA 93043-5007  | 1 |
| 13. | Professor D.L. Walters, Code 61We<br>Naval Postgraduate School<br>Monterey, CA 93943-5000      | 1 |
| 14. | Mr. W.J. Lentz, Code 61Lz<br>Naval Postgraduate School<br>Monterey, CA 93943-5000              | 1 |
| 15. | Dr. P.L. Walker Code 61<br>Naval Postgraduate School<br>Monterey, CA 93943-5000                | 1 |
| 16. | LT M.L. Gribaudo<br>2914 70th S.E.<br>Mercer Island, WA 98040                                  | 2 |